Numerical Reaction-Transport Model of Lake Dynamics and Their Eutrophication Processes

Severin Stojanovic

Thesis submitted to the
Faculty of Graduate and Postdoctoral Studies
in partial fulfilment of the requirements
for the M.Sc. degree in Physics

Department of Physics
Faculty of Science
University of Ottawa

Contents

Acknowledgements

I would like to thank Professor Ivan L'Heureux of the Department of Physics, Faculty of Science, University of Ottawa as supervisor to this research.

Abstract

A 1D numerical reaction-transport model (RTM) that is a coupled system of partial differential equations is created to simulate prominent physical and biogeochemical processes and interactions in limnological environments. The prognostic variables considered are temperature, horizontal velocity, salinity, and turbulent kinetic energy of the water column, and the concentrations of phytoplankton, zooplankton, detritus, phosphate (H_3PO_4), nitrate $\left(NO_3^-\right)$, ammonium $\left(NH_4^+\right)$, ferrous iron $\left(Fe^{2+}\right)$, iron(III) hydroxide $\left(Fe\left(OH\right)_3\left(s\right)\right)$, and oxygen ($O_2$) suspended within the water column. Turbulence is modelled using the $k-\varepsilon$ closure scheme as implemented by *Gaspar et al.* (1990) for oceanic environments. The RTM is used to demonstrate how it is possible to investigate limnological trophic states by considering the problem of eutrophication as an example. A phenomenological investigation of processes leading to and sustaining eutrophication is carried out. A new indexing system that identifies different trophic states, the so-called *Self-Consistent Trophic State Index* (SCTSI), is proposed. This index does not rely on empirical measurements that are then compared to existing tables for classifying limnological environments into particular trophic states, for example, the concentrations of certain species at certain depths to indicate the trophic state, as is commonly done in the literature. Rather, the index is calculated using dynamic properties of only the limnological environment being considered and examines how those properties affect the sustainability of the ecosystem. Specifically, the index is calculated from a ratio of light attenuation by the ecosystem's primary biomass to that of total light attenuation by all particulate species and molecular scattering throughout the entire water column. The index is used to probe various simulated scenarios that are believed to be relevant to eutrophication: nutrient loading, nutrient limitation, overabundance of phytoplankton, solar-induced turbulence, and wind-induced turbulence.

Statement of Originality

The following two points highlight the major unique contributions by the author towards the academic advancement in knowledge and understanding of the matters presented in the thesis:

- The computer program used to perform simulations and obtain results was implemented independently by the author based on the model presented and developed in the thesis. In other words, it was written from 'scratch' and contains several thousand lines of code. The name of the program is *LakeSIM RTM* and is available for download at: http://code.google.com/p/lakesim-rtm/

- Proposal of the so-called *Self-Consistent Trophic State Index* (SCTSI). This is a new index that can be used to classify the trophic states of limnological environments.

- Development of a numerical reaction-transport model global in scope sufficient for phenomenological investigations, as opposed to developing a limited and context-specific model as often done in the literature to reproduce the behaviours of a particular limnological environment.

- The consideration of two iron species as prognostic variables with respective rate equations alongside phosphorus and nitrate species.

- The consideration of iron as an uptake pathway (in competition with phosphorus and nitrate species pathways) for the growth of phytoplankton.

List of Symbols

Symbol	Definition	Units
c_k	constant of proportionality for K_u	–
c_p	specific heat capacity of water	$\mathrm{J} \cdot (\mathrm{kg} \cdot \mathrm{K})^{-1}$
c_ε	constant of proportionality for ε	–
e	turbulent kinetic energy	$\mathrm{m}^2 \cdot \mathrm{s}^{-2}$
f	Coriolis parameter	s^{-1}
$f\,(w_{10})$	oxygen exchange coefficient	$\mathrm{m} \cdot \mathrm{s}^{-1}$
g	acceleration due to gravity	$\mathrm{m} \cdot \mathrm{s}^{-2}$
I	light intensity	$\mathrm{W} \cdot \mathrm{m}^{-2}$
I_0	light intensity at air-water interface	$\mathrm{W} \cdot \mathrm{m}^{-2}$
I_L	light intensity at water-sediment interface	$\mathrm{W} \cdot \mathrm{m}^{-2}$
k_1	light extinction coefficient (molecular scattering)	m^{-1}
k_2	light extinction coefficient (biogeochemical absorption)	$\big([\,] \cdot \mathrm{m}\big)^{-2}$
K_e	turbulent kinetic energy eddy diffusion coefficient	$\mathrm{m}^2 \cdot \mathrm{s}^{-1}$
K_S	saline eddy diffusion coefficient	$\mathrm{m}^2 \cdot \mathrm{s}^{-1}$
K_T	thermal eddy diffusion coefficient	$\mathrm{m}^2 \cdot \mathrm{s}^{-1}$

K_u	horizontal velocity eddy diffusion coefficient	$\mathrm{m}^2 \cdot \mathrm{s}^{-1}$
K_Σ	saline molecular diffusion coefficient	$\mathrm{m}^2 \cdot \mathrm{s}^{-1}$
l_b	buoyancy length scale	m
l_d	distance travelled downward to convert e to potential energy	m
l_k	turbulent mixing length scale	m
l_u	distance travelled upward to convert e to potential energy	m
l_ε	turbulent dissipative length scale	m
p	pressure exerted on water	Pa
$\mathrm{Pr_t}$	turbulent Prandtl number	–
Q_b	solar backradiation	$\mathrm{W} \cdot \mathrm{m}^{-2}$
Q_e	latent heat of evaporation	$\mathrm{W} \cdot \mathrm{m}^{-2}$
Q_s	sensible heat flux	$\mathrm{W} \cdot \mathrm{m}^{-2}$
S	salinity of water	–
t	time	s
T	temperature of water	°C
$\mathbf{u}$	horizontal velocity of water, $\mathbf{u} = \left(v_x, v_y\right)$	$\mathrm{m} \cdot \mathrm{s}^{-1}$
z	depth	m
α	thermal expansion coefficient	K^{-1}
β	saline contraction coefficient	–
γ	zooplankton excretion fraction	–
ε	dissipation rate of e	$\mathrm{m}^2 \cdot \mathrm{s}^{-3}$
ζ	zooplankton growth efficiency	–

λ	latitude	$^\circ$
μ	zooplankton grazing half-saturation coefficient	–
ρ	water density	$\mathrm{kg} \cdot \mathrm{m}^{-3}$
ρ_0	reference water density	$\mathrm{kg} \cdot \mathrm{m}^{-3}$
ω	relative zooplankton palatability for detritus compared to phytoplankton	–
Ω	angular velocity of Earth's rotation	$\mathrm{rad} \cdot \mathrm{s}^{-1}$

Chapter 1

Introduction

Water is essential for life on Earth and for human survival. It is imperative for humankind, therefore, to study everything that negatively affects the quality of water required for our survival; humans depend on freshwater for survival.

The most common and largest natural sources of freshwater are lakes, rivers, and estuaries (i.e., *limnological* or inland waters). These bodies of water contain ecosystems of organisms that live and thrive within the water. A particular process known as *eutrophication* (defined below) devastates the quality of water with disastrous effects on human survival, which include the inabilities to drink the water and obtain nourishment from water-dwelling organisms and vegetation. The process of eutrophication involves a very prominent and widespread organism found all over the world's water supplies known as *algae* or *phytoplankton*. The most visible sign of a change in water quality as a result of eutrophication is an overabundance of algae such that the water itself assumes a color tint of green, yellow, brown, or red. Eutrophication was studied because of the potential devastation it can induce in the vitality of limnological ecosystems, for example, Lake Biwa in Japan (*Okuda et al.* (1995)).

The research presented in this thesis attempts to numerically model the interactions of the most important organisms and chemical compounds encountered in freshwater

ecosystems by utilizing a reaction-transport approach. Chapters 1 and 2 focus on developing and verifying the model. The model is then used in Chapters 3 and 4 in a preliminary attempt to phenomenologically investigate the eutrophication process of freshwater ecosystems. The aim of Chapters 3 and 4 is more to demonstrate how the model of Chapters 1 and 2 can be used to investigate specific scenarios such as the eutrophication process, rather than providing an exhaustive treatment on the matter; given the extent of the computer program and limits on research scope and initiative, emphasis has been placed on developing the model and program with subsequent investigation as demonstration of the use of the model.

Broad concensus (*Wetzel* (2001)) characterizes the eutrophication of a limnological ecosystem as consisting of the following coexisting events:

- Excessive nutrient loading;
- Overabundance of the ecosystem's primary biomass (for example, phytoplankton);
- Formation of an anoxic region in the lower portion of the water column that extends towards the sediment; and
- Severe reduction in animal populations (for example, zooplankton).

Excessive Nutrient Loading

Nutrients are the food-like substances required for the growth and sustenance of an ecosystem's primary biomass. In the present model, the primary biomass is phytoplankton and its corresponding nutrients are phosphorus, nitrogen, and iron.

Nutrient loading is the dynamical relationship between an ecosystem's primary biomass and its nutrients. Excessive nutrient loading occurs when nutrients are available to the primary biomass such that growth of this biomass is in excess of what the ecosystem can healthily support. An overabundance in the primary biomass eventually leads to

devastation of the ecosystem and possibly a significant increase in toxicity (for example, the overabundance of cyanobacteria).

Overabundance of the Ecosystem's Primary Biomass

Eutrophic limnological environments have an overabundance of the primary biomass in the upper portions of the water column. The overabundance of this biomass can occur in two ways: i) excessive nutrient loading, and ii) redistribution of the biomass through physical mixing processes. Wind-induced turbulence at the air-water interface can act as a mixing mechanism to redistribute the biomass in the upper portion of the water column.

Formation of an Anoxic Region

The overabundance of the primary biomass saturates the upper portion of the water column and significantly limits light penetration at greater depths. Since phytoplankton require light in order to undergo the photosynthetic process to grow, the phytoplankton at greater depths away from the air-water interface will have difficulty in proliferating. Moreover, oxygen is required for zooplankton respiration, for the degradation of dead and decaying phytoplankton, and the oxidation and nitrification processes. Without phytoplankton present to replenish this oxygen, an anoxic region will form in the lower portions of the water column.

Severe Reduction in Animal Populations

All animals require oxygen for respiration in order to survive. The animals in the present model are zooplankton. In addition to their requirement for oxygen, zooplankton also require phytoplankton in order to survive; zooplankton graze on phytoplankton to obtain nourishment.

Despite an overabundance of phytoplankton in the upper portion of the water column,

an overall decline in the zooplankton population will occur as a result of deoxygenation and lack of phytoplankton at greater depths. Even though certain species of zooplankton have their own mobility mechanisms to follow phytoplankton, for example, a flagellum or physical adaptation to alter buoyancy, their mobility is severly limited since they mostly restrict themselves to the thermocline[1] region of the water column. The distribution of zooplankton outside of the thermocline region can be accounted for if turbulent mixing is considered.

The results and discussion of Chapter 5 attempt to provide theoretical insight into how to approach answering three fundamental questions related to the eutrophication process of freshwater ecosystems:

1. *What mechanisms cause and sustain freshwater eutrophication?*

2. *Is it possible to predict when freshwater eutrophication will occur?*; and

3. *Can a single variable be used to reasonably characterize eutrophication?*

The reaction-transport model that has been developed was used to simulate various scenarios of biogeochemical interactions and physical forcing mechanisms affecting these interactions in an attempt to induce the eutrophication process. An example of the former is the effect of nutrient limitation on phytoplankton growth. An example of the latter is the effect of wind-induced turbulence distributing phytoplankton throughout the water column. The purpose of these simulations was not to model a particular limnological environment *per se*, but rather to probe the biogeochemical and physical effects on the eutrophication process of a general and non-specific limnological environment.

A new variable is proposed, i.e., the so-called *Self-Consistent Trophic State Index* (SCTSI), which makes it possible to identify and describe the trophic state of freshwater

[1] A region in the water column that is characterized by a non-zero temperature gradient.

ecosystems in a self-consistent manner with respect to the reaction-transport model developed. The trophic state is an arbitrary classification scheme based on the productivity of an ecosystem's primary biomass. It recognizes three distinct trophic states:

- Oligotrophic (relatively poor availability of nutrients and virtually non-existent ecosystem; little presence of primary biomass);
- Mesotrophic (abundance of nutrients and a sustainable ecosystem; sustainable amount of primary biomass); and
- Eutrophic (excessive nutrients and an unsustainable ecosystem; overabundance of primary biomass).

The SCTSI can be used as a supplement to the numerical, empirically-based classification schemes often encountered in the literature, for example, 1 g chlorophyll per liter typifying eutrophic environments (*Wetzel* (2001)). Since eutrophication is a process, the SCTSI is defined to be a quantity that exhibits a particular behaviour in time rather than a quantity for which absolute values are defined *a priori*, of which the latter are often arbitrarily imposed in the literature. The SCTSI is defined such as to remain in accordance with the standard practice of classifying trophic states with respect to the production and depletion of the primary biomass.

The SCTSI is meant to supplement the *Trophic State Index* (TSI) proposed by *Carlson* (1977), which is still readily used in the literature, e.g., *Wetzel* (2001). The so-called Secchi Disk, chlorophyll concentration of the primary biomass, and phosphorus concentration are used by *Carlson* (1977) as the basis for calculating the TSI. The approach of *Carlson* (1977) relies on experimentally-obtained values to produce a static indicator of the trophic states. The benefit of the SCTSI is that it additionally considers the dynamics of primary biomass production and consumption. This allows us to probe the biogeochemical and physical mechanisms determining a particular trophic state and to predict future trophic tendencies. The SCTSI can also be used as an aid to test and

compare the accuracies of different numerical models (for example, model output).

The Model

The model is segmented into two components: i) the 'physical' submodel and ii) the 'ecological' submodel. When coupled together, these two submodels directly affect one another as they become intricately linked to each other through feedback mechanisms.

The Physical Submodel

The physical submodel is concerned with the following properties of the water column:

- Temperature;
- Horizontal Velocity of Fluid Layers (resolved into two components);
- Salinity[1]; and
- Turbulent Kinetic Energy.[2]

The Ecological Submodel

The ecological submodel consists of only the interactions and reactions between biological species and chemical quantities. Specifically, the ecological submodel is concerned with the concentrations of:

- Plankton;
  - Phytoplankton; and
  - Zooplankton;

[1]Even though this thesis is concerned with freshwater, salinity is included for completeness since many limnological environments are appreciably saline.

[2]Turbulent Kinetic Energy is a scalar representation of the degree to which turbulence is present in the system. Hydrodynamic equations representing turbulence are used due to the statistical nature of fluid flow in limnological environments.

- Detritus;
- Nutrients
  - Phosphate, H_3PO_4;
  - Nitrogen;
    - Nitrate, NO_3^-;
    - Ammonium, NH_4^+;
  - Iron
    - Ferrous Iron, Fe^{2+};
    - Ferric Iron, $Fe(OH)_3$ (s); and
- Oxygen, O_2.

In attempting to answer the three fundamental questions posited above with regards to eutrophication, two physical forcing mechanisms (i.e., mechanisms by which turbulence is induced) are considered: (1) solar heating, and (2) wind at the air-water interface. It will be demonstrated in Chapter 5 that solar-induced turbulence is not capable of sustaining long-term eutrophic states and its ability to produce eutrophication are negligible compared to wind-induced turbulence. Furthermore, it will be demonstrated that wind-induced turbulence (in the absence of solar heating) is able to produce and sustain eutrophication. It will also be demonstrated that wind-induced turbulence can create distinct mixing zones in the upper regions of the water column; the depth of these zones directly correlate to the strength of the wind. These zones significantly inhibit the biogeochemical quantities from advecting out of the zones and into the sediment, thereby allowing the biogeochemical interactions promoting algal growth to persist for greater lengths of time, which eventually result in persistent eutrophic states. The reason why wind-induced turbulence significantly dominates solar-induced heating as the primary mechanism to produce eutrophic states and as the only mechanism of the two to allow

eutrophic states to persist will become apparent when examining the rate equation for the production of turbulent kinetic energy. Essentially, the production of turbulent kinetic energy relies on the presence of temperature gradients (resulting from solar heating) and velocity gradients (resulting from shear stresses as a result of wind) of the water. Considering reasonable values for solar insolation and wind speeds at the air-water interface, the resulting temperature gradients are negligible compared to the velocity gradients.

Model Development

The model presented herein was developed with the purpose of phenomenologically investigating the particular problem of eutrophication. The motivation for developing this model differs from what is often encountered in the literature in that we are not attempting to probe or reproduce the behaviours of a particular limnological environment in the real world.

It is not possible to use previously-developed models for the purpose of phenomenological investigations. Those models are incomplete and inadequate, and were developed to study specific problems for specific, narrow contexts that does not permit them to be extended to be useful for a more global, phenomenological study. For example, it is not possible to phenomenologically investigate eutrophication without considering a physical submodel. Yet, some models neglect the use of a physical submodel because the primary purpose is to understand biogeochemical interactions in isolation. Other models are interested strictly in the physics of turbulent mixing and disregard biogeochemical quantities altogether. This staggering of models in the literature result from the diversification and specialization in interests such as physics, biology, chemistry, and geology. Therefore, the model we propose does not build upon a single, existing model that we have extended or refined in complexity. Rather, elements of existing models have been used, modified, and enhanced where deemed necessary. Also, elements of models that were not considered appropriate or rigorous in treatment were discarded in their

original implementations, and the ideas were completely reintroduced in more coherent and rigorous manners.

Computational Resources

The computer program implementing the model was developed in standard C++ as defined by version 4 of the GNU Compiler Collection ('gcc') and will compile with any compiler on any operating system that implements this standard. The code is also being ported to C# and WinForms for the Windows operating system in order to provide a graphical user interface and to improve the reuseability of the code through the use of 'namespaces' and 'properties'.

Motivation from a Discipline Perspective

Studying the problem of eutrophication provides the opportunity to become acquainted with and utilize the methods of investigation encountered in the various scientific disciplines of physics, mathematics, chemistry, biology, and geology. Considering a problem of this scope allows the researcher to broaden his/her awareness of other scientific disciplines as well as to develop the ability to consider problems in broader contexts. Given that the water column of limnological environments is a fluid, physicists have a direct interest in studying how physical forcing mechanisms and couplings to ecosystems affect this fluid and its dynamics.

Chapter 2

Theory

When modeling the water column dynamics of limnological environments, it is pedagogically beneficial to conceptually subdivide the water column model, or *ecological* model, into two distinct submodels: *physical* and *biogeochemical*. This subdivision also greatly aids in the testing and debugging of the numerical implementation of the model.

The physical submodel describes the properties and characteristics of the water and its flow using the theories of classical fluid mechanics of turbulent incompressible Newtonian fluids. The submodel proposed herein is based largely on the models developed by *Gaspar et al.* (1990), *Therry and Lacarrère* (1983), and *Bougeault and Lacarrère* (1989). The model of *Gaspar et al.* (1990) was developed for oceanic modeling of the water column based on the atmospheric boundary layer circulation models of *Therry and Lacarrère* (1983) and *Bougeault and Lacarrère* (1989). These three models are inadequate as ecological models because they do not consider biogeochemical species and the effects that the respective biogeochemical kinetic interactions exert on the fluid's properties and flow; coupling physical and biogeochemical submodels allows feedback mechanisms between the two submodels.

The prognostic variables of the physical submodel are the *horizontal velocity*, *turbulent kinetic energy*, *temperature*, and *salinity* of the water. The water is considered to be an

incompressible Newtonian fluid, except in the framework of the so-called Boussinesq approximation. This approximation relates vertical changes of water density to vertical changes in temperature and salinity multiplied by the acceleration of gravity (*Monin and Yaglom* (1971)).

The biogeochemical submodel describes the kinetic interactions between particulate and dissolved species within the water column. The particulate species considered are: *phytoplankton*, *zooplankton*, *detritus*, and *iron(III) hydroxide* $\left(\mathrm{Fe\,(OH)_3\,(s)}\right)$. The dissolved species considered are: *phosphate* (H_3PO_4), *nitrate* $\left(NO_3^-\right)$, *ammonium* $\left(NH_4^+\right)$, *ferrous iron* $\left(Fe^{2+}\right)$, and *oxygen* (O_2). The prognostic variables of the submodel are the respective concentrations of the mentioned species. This submodel is not exclusively based on any particular existing model, but substantially borrows from *Soetaert et al.* (2001), *Omlin et al.* (2001), and *Edwards et al.* (2001). While *Soetaert et al.*'s physical submodel is based on *Gaspar et al.*'s model, the latter two models do not couple their respective biogeochemical submodels to a physical submodel. The submodel presented herein adapts some features of *Soetaert et al.*'s physical submodel not explicitly mentioned by *Gaspar et al.*, for example, the boundary conditions at the water-sediment interface. However, the numerical implementation by *Soetaert et al.* is computationally unsatisfactory in rigour and is, therefore, not considered. A new contribution presented herein that is lacking in the literature is the consideration of iron as a full-fledged prognostic variable with a corresponding rate equation coupled on par to other biogeochemical prognostic variables and their respective rate equations. Even though iron in organic matter composition is present only in trace amounts, and hence its general absence from existing models, it is an essential nutrient for organic matter production (*Reynolds* (2006), *Kalff* (2002), and *Wetzel* (2001)).

All prognostic variables of the ecological model are modeled using rate equations resolved explicitly in two independent variables: time (t) and depth (z) within the water column. Using a Cartesian coordinate system with the origin located at the air-water

interface, the convention used is the following: the positive x-coordinate is taken to be in the westward direction, the positive y-coordinate in the northward direction, and the positive z-coordinate in the vertical direction downwards from the air-water interface. The values of the prognostic variables in the $x - y$ plane are considered as projections onto a single point at the given depth z as a result of cross-sectional averages in this plane.

2.1 The Physical Submodel

2.1.1 Reynolds' Decomposition

Due to the chaotic and statistical nature of turbulence (*Monin and Yaglom* (1971)), Reynolds' decomposition is applied to the continuity, Navier-Stokes, and temperature rate equations for incompressible Newtonian fluids in order to simplify the study of turbulent behaviour.

Given a prognostic variable, Reynolds' decomposition, or *ansatz*, rewrites this variable as the sum of a time-averaged, or mean, part and a random fluctuation about this average. For example, consider a smooth, continuous function $f(\mathbf{r}, t)$ that is at least differentiable as required by the differential rate equation in which it appears. This function is rewritten as

$$f(\mathbf{r}, t) = \overline{f}(\mathbf{r}, t) + f'(\mathbf{r}, t) \tag{2.1}$$

where

$$\overline{f}(\mathbf{r}, t) \equiv \frac{1}{\Delta T} \int_{t-\frac{\Delta T}{2}}^{t+\frac{\Delta T}{2}} f(\mathbf{r}, \tau)\, d\tau \tag{2.2}$$

such that ΔT is large compared to the characteristic timescale of f', but small compared to the characteristic timescale of $\overline{f}$ (*Monin and Yaglom* (1971)). By definition, we require

that

$$\overline{f'}(\mathbf{r},t)=0. \tag{2.3}$$

Given two correlated variables, $f(\mathbf{r},t)$ and $g(\mathbf{r},t)$ (where $g(\mathbf{r},t)$ can also be rewritten using Reynolds' decomposition), the interpretation of the non-trivial term:

$$\overline{f'g'}=\overline{g'f'}\neq 0 \quad \text{(in general)} \tag{2.4}$$

is of central importance in modeling turbulence and will be discussed in the *Turbulence Closure Scheme* subsection (2.1.6).

2.1.2 The Continuity Equation

The general form of the continuity equation for a fluid is:[1]

$$\frac{\partial(\rho\phi)}{\partial t}+\nabla\cdot(\rho\phi\mathbf{v})=\nabla\cdot\left(K_\phi\nabla\phi\right)+S_\phi \tag{2.5}$$

where ρ represents a mass density and ϕ represents a quantity proportional to the prognostic variable so that $\rho\phi$ is the amount of this quantity changing per unit volume, $\mathbf{v}$ is the convective velocity of $\rho\phi$, K_ϕ is the molecular diffusion coefficient of ϕ, and S_ϕ is a source/sink term.

Applying Reynolds' decomposition to the quantity ϕ, i.e., $\phi(\mathbf{r},t)=\overline{\phi}(\mathbf{r},t)+\phi'(\mathbf{r},t)$, the time-averaged general form of the incompressible continuity equation (in Cartesian coordinates) is:

$$\frac{\partial\left(\rho\overline{\phi}\right)}{\partial t}+\nabla\cdot\left(\rho\overline{\phi\mathbf{v}}\right)=\nabla\cdot\left(K_\phi\nabla\overline{\phi}\right)+\overline{S}_\phi+\nabla\cdot\left(-\rho\overline{\mathbf{v}'\phi'}\right). \tag{2.6}$$

The additional so-called Reynolds' turbulent correlations, $-\rho\overline{\mathbf{v}'\phi'}$, are determined by

[1] The derivation is shown in Appendix A.

either solving corresponding rate equations (derived from the Navier-Stokes equation, below), or parametrizing according to a particular turbulence closure scheme. Additional rate equations and parametrizations are required due to the increase in the number of variables appearing in the original equation simply resulting from Reynolds' decomposition. An attempt to write rate equations for the Reynolds' turbulent correlation terms will generate third-order moments, for example, $-\rho\overline{\mathbf{v}'\mathbf{v}'\phi'}$, that then need to be parametrized or determined by corresponding rate equations. The system of equations must be truncated at some desired level by using an adequate parametrization scheme. Higher-order closure schemes are thought to produce greater numerical accuracy, but increase computation time significantly.

2.1.3 The Navier-Stokes Equation

The Navier-Stokes equation is obtained by applying the conservation of momentum (Newton's second law of motion) to a fluid particle. The forces acting on a fluid particle that are considered are *surface* forces, such as pressure and viscous forces, and *body* forces, such as gravitational, centrifugal, Coriolis, and electromagnetic forces. The Navier-Stokes equation for an incompressible fluid is:[1]

$$\frac{\partial(\rho\mathbf{v})}{\partial t} + \nabla\cdot(\rho\mathbf{v}\mathbf{v}) = \nabla\cdot(\eta\nabla\mathbf{v}) - \nabla p + S_{\mathbf{v}} \tag{2.7}$$

where η is the dynamic viscosity of the fluid, p is the pressure acting on the fluid, and the source term, $S_{\mathbf{v}}$, represents body forces.

Applying Reynolds' decomposition to the Navier-Stokes equation, i.e., $\mathbf{v}(\mathbf{r},t) = \overline{\mathbf{v}}(\mathbf{r},t) + \mathbf{v}'(\mathbf{r},t)$, the time-averaged incompressible Navier-Stokes equation (also referred to as Reynolds' equation) is:

$$\frac{\partial(\rho\overline{\mathbf{v}})}{\partial t} + \nabla\cdot(\rho\overline{\mathbf{v}}\overline{\mathbf{v}}) = \nabla\cdot(\eta\nabla\overline{\mathbf{v}}) - \nabla\overline{p} + \overline{S}_{\mathbf{v}} + \nabla\cdot\left(-\rho\overline{\mathbf{v}'\mathbf{v}'}\right). \tag{2.8}$$

[1]The derivation is shown in Appendix A.

Expressing the prognostic variable for the water's horizontal velocity as $\overline{\mathbf{u}} = \left(\overline{v}_x, \overline{v}_y\right)$, the time-averaged rate equations follows directly from equation (2.8), taking into account the fact that the velocity field depends only on z and $\overline{v}_z \cong 0$:

$$\boxed{\frac{\partial\left(\rho\overline{\mathbf{u}}\right)}{\partial t} = \rho f\left(\hat{\mathbf{z}} \times \overline{\mathbf{u}}\right) + \frac{\partial\left(-\rho\overline{u'_z\mathbf{u}'}\right)}{\partial z}}. \tag{2.9}$$

Since the water column is in a rotating frame of reference, i.e. the Earth, the Coriolis force is accounted for by the term $f\left(\hat{\mathbf{z}} \times \overline{\mathbf{u}}\right)$, where f is the Coriolis parameter. It is given by:

$$f = 2\Omega \sin\lambda \tag{2.10}$$

where Ω is the angular velocity of the Earth's rotation and λ is the latitude.

The molecular viscous term $\nabla\cdot(\eta\nabla\overline{\mathbf{u}})$ has been dropped since it is negligible compared to the Reynolds' (turbulent) stress term $\frac{\partial\left(-\rho\overline{u'_z\mathbf{u}'}\right)}{\partial z}$.

2.1.4 The Turbulent Kinetic Energy and Temperature Equations

We consider the contribution to a fluid's total energy per unit mass, $E\left(\mathbf{r}, t\right)$, to be the sum of two sources:

i) kinetic energy per unit mass resulting from macroscopic movement of the fluid, $E_k\left(\mathbf{r}, t\right) = \frac{1}{2}\|\mathbf{v}\|^2 = \frac{1}{2}v^2 = \frac{1}{2}\left(v_x^2 + v_y^2 + v_z^2\right)$, and

ii) internal energy per unit mass, $E_i\left(\mathbf{r}, t\right)$, resulting from the movement of microscopic particles making up the fluid.

• **Turbulent Kinetic Energy, $\overline{e}$**

Using Reynolds' decomposition, the macroscopic kinetic energy per unit volume is rewritten as:

$$\rho E_k\left(\mathbf{r},t\right)=\rho\left(\frac{1}{2}\overline{v}^2+\frac{1}{2}v'^2+\mathbf{v}'\cdot\overline{\mathbf{v}}\right). \tag{2.11}$$

Turbulent kinetic energy is defined as the *time-average* of the random fluctuating velocity terms appearing in the above Reynolds' decomposition, $\overline{e}\equiv\frac{1}{2}\left(\overline{v_x'^2}+\overline{v_y'^2}+\overline{v_z'^2}\right)$. It is a scalar representation of the degree of turbulence.

The time-averaged rate equation for the turbulent kinetic energy of an incompressible Newtonian fluid can be derived from the Navier-Stokes equation, again taking into account the fact that the velocity field depends only on z and $\overline{v}_z\cong 0$:[1]

$$\boxed{\frac{\partial\overline{e}}{\partial t}=-\frac{\partial}{\partial z}\left(\overline{v_z'e}+\frac{\overline{v_z'p'}}{\rho_0}\right)-\overline{v_z'\mathbf{u}'}\cdot\frac{\partial\overline{\mathbf{u}}}{\partial z}+\overline{v_z'b'}-\varepsilon} \tag{2.12}$$

where ρ_0 is a reference density, b is the buoyancy, and ε is the rate of dissipation of turbulent kinetic energy. The buoyancy is expressed as $b=g\left(\frac{\rho}{\rho_0}-1\right)$, where g is the acceleration of gravity.

The term $\overline{v_z'b'}$ is present in the framework of the so-called Boussinesq approximation, where density fluctuations must be taken into account when they are multiplied by g:

$$\begin{aligned}\overline{v_z'b'}&=\overline{v_z'g\frac{\rho'}{\rho_0}}=\overline{v_z'g\frac{\rho_0}{\rho_0}\left[1-\alpha\left(T\left(z,t\right)-T_0\right)+\beta\left(S\left(z,t\right)-S_0\right)\right]'}\\&=-g\alpha\overline{v_z'T'}+g\beta\overline{v_z'S'}\end{aligned} \tag{2.13}$$

where α and β are thermal expansion and saline contraction coefficients, respectively, T and S are the temperature and salinity, respectively, and T_0 and S_0 are reference temperatures and salinities, respectively.

Once again, the molecular viscous terms have been dropped since they are negligible

[1]The derivation is shown in Appendix A.

compared to the Reynolds' turbulent correlation terms.

• **Temperature, $\overline{T}$**

In order to obtain the rate equation for temperature, we begin with the rate equation for the internal energy, E_i, of an incompressible Newtonian fluid:

$$\frac{\partial\left(\rho E_i\right)}{\partial t}+\nabla\cdot\left(\rho E_i\mathbf{v}\right)=\nabla\cdot\left(\chi\nabla T\right)+\frac{\eta}{2}\sum_{ij}\left(\frac{\partial v_i}{\partial x_j}+\frac{\partial v_j}{\partial x_i}\right)^2+S_{E_i} \tag{2.14}$$

where T is the temperature of the fluid, χ is the coefficient of thermal conductivity, and S_{E_i} is a source term.

Since E_i is due to microscopic sources, it is a thermodynamic property of the fluid on macroscopic scales. As such, we can rewrite it in terms of other thermodynamic properties, for example, the temperature:

$$\rho E_i=\rho c_p T \tag{2.15}$$

where c_p is the specific heat capacity of the fluid.

Making this substitution into the above equation for E_i gives:

$$\frac{\partial\left(\rho c_p T\right)}{\partial t}+\nabla\cdot\left(\rho c_p T\mathbf{v}\right)=\nabla\cdot\left(\chi\nabla T\right)+\frac{\eta}{2}\sum_{ij}\left(\frac{\partial v_i}{\partial x_j}+\frac{\partial v_j}{\partial x_i}\right)^2+S_{E_i}. \tag{2.16}$$

Using Reynolds' decomposition for the temperature,

$$\rho c_p T\left(z,t\right)=\rho c_p\left(\overline{T}\left(z,t\right)+T'\left(z,t\right)\right) \tag{2.17}$$

we arrive at the time-averaged rate equation for the temperature, again taking into

account the fact that the velocity field depends only on z and $\overline{v}_z \cong 0$:

$$\boxed{\frac{\partial \overline{T}}{\partial t} = -\frac{1}{\rho_0 c_p}\frac{\partial I}{\partial z} + \frac{\partial\left(-\overline{v_z' T'}\right)}{\partial z}} \tag{2.18}$$

where ρ has been rewritten as a reference density ρ_0 and $-\frac{1}{\rho_0 c_p}\frac{\partial I}{\partial z}$ is a sink term accounting for the attenuation of light intensity, I. The light attenuation is given by the expression (*Omlin et al.* (2001)):

$$I(z) = I_0 e^{\left(-\int_0^z \left(k_1 + k_2 \cdot [\mathrm{BGC}]\right) dz'\right)} \tag{2.19}$$

where I_0 is the light intensity at the air-water interface, k_1 is an empirical coefficient accounting for light scattering and molecular absorption by water particles, and $k_2 \cdot [\mathrm{BGC}]$ accounts for light absorbed by biogeochemical matter and organisms, such as plankton and detritus, through photosynthetic uptake or blockage; [BGC] refers to the concentration of biogeochemical matter and organisms.

The molecular viscous and heat conductivity terms are dropped since they are negligible compared to the Reynolds' turbulent correlation term $\frac{\partial\left(-\overline{v_z' T'}\right)}{\partial z}$.

2.1.5 Salinity

We define salinity following what *Wetzel* (2001) has identified to be the most useful definition of many: considering total ion concentration of certain cations and anions, we express salinity as the mass total ions per mass of solution ($\mathrm{g} \cdot \mathrm{kg}^{-1}$). Specifically, the cations of interest are calcium $\left(\mathrm{Ca}^{++}\right)$, magnesium $\left(\mathrm{Mg}^{++}\right)$, sodium $\left(\mathrm{Na}^{+}\right)$, and potassium $\left(\mathrm{K}^{+}\right)$. The anions of interest are hydrocarbonate $\left(\mathrm{HCO}_3^{-}\right)$, carbonate $\left(\mathrm{CO}_3^{-}\right)$, sulphate $\left(\mathrm{SO}_4^{-}\right)$, and chlorine $\left(\mathrm{Cl}^{-}\right)$.

However, salinity is included here simply for completeness, since some limnological environments have been observed to be appreciably saline (*Wetzel* (2001)). The results presented in this thesis, however, are concerned exclusively with freshwater. It is only in

anticipation of future considerations of how salinity may be incorporated into the model that a broader mathematical consideration is proposed.

In analogy with equation (2.18), *Gaspar et al.* (1990) writes the time-averaged rate equation for salinity as:

$$\boxed{\frac{\partial \overline{S}}{\partial t} = \nabla \cdot \left(K_\Sigma \nabla \overline{S} \right) + \frac{\partial \left(-\overline{u'_z S'} \right)}{\partial z}} \tag{2.20}$$

where K_Σ is the molecular saline diffusivity.

2.1.6 Turbulence Closure Scheme

Reynolds' decomposition and a statistical approach are employed in developing the relevant prognostic rate equations in order to properly account for the physical transport mechanism of turbulent flow. However, this approach produces more unknown variables than known equations, i.e., the Reynolds' turbulent correlation terms. If we attempt to write equations for the additional variables, then the problem is further multiplied in that another generation of unknown variables are produced, the problem propagating *ad infinitum*. The infinite production of more unknown variables than known equations is known as the *closure* problem. The only way to "close" the scheme so that the number of unknown variables is equal to the number of known equations is to parametrize the additional unknown variables.

In order to close the set of time-averaged rate equations for the prognostic variables, a classical closure scheme based on turbulent vertical flux parametrization is used. The fluctuating correlated terms arising as a result of Reynolds' decomposition are parametrized using the classical concept of large-scale eddy diffusivity (*Gaspar et al.*

(1990)):

$$-\overline{v_z'\mathbf{u}'} = \overline{K}_u \frac{\partial \overline{\mathbf{u}}}{\partial z} \tag{2.21}$$

$$-\left(\overline{v_z' e} + \frac{\overline{v_z' p'}}{\rho_0}\right) = \overline{K}_e \frac{\partial \overline{e}}{\partial z} \tag{2.22}$$

$$-\overline{v_z' T'} = \overline{K}_T \frac{\partial \overline{T}}{\partial z} \tag{2.23}$$

$$-\overline{v_z' S'} = \overline{K}_S \frac{\partial \overline{S}}{\partial z} \tag{2.24}$$

Here, $\overline{K}_u$, $\overline{K}_e$, $\overline{K}_T$, and $\overline{K}_S$ are appropriate eddy diffusivity coefficients (in units of length$^2 \cdot$ time^{-1}).

The above parametrizations immediately yield the following equalities in the turbulent kinetic energy rate equation:

$$-\overline{v_z'\mathbf{u}'} \cdot \frac{\partial \overline{\mathbf{u}}}{\partial z} = \overline{K}_u \frac{\partial \overline{\mathbf{u}}}{\partial z} \cdot \frac{\partial \overline{\mathbf{u}}}{\partial z} \tag{2.25}$$

$$\overline{v_z' b'} = g\alpha \overline{K}_T \frac{\partial \overline{T}}{\partial z} - g\beta \overline{K}_S \frac{\partial \overline{S}}{\partial z}. \tag{2.26}$$

Similarly to *Gaspar et al.* (1990), *Therry and Lacarrère* (1983), and *Monin and Yaglom* (1971), the present model parametrizes $\overline{K}_u$ in terms of the turbulent kinetic energy and a turbulent mixing length:

$$\overline{K}_u = c_k l_k \sqrt{\overline{e}} \tag{2.27}$$

where c_k is an empirical constant and l_k is a turbulent mixing length scale (determined below).

The other eddy diffusivities are then related to $\overline{K}_u$ via the so-called turbulent Prandtl number, $\mathrm{Pr_t} \approx 1$ (*Bougeault and Lacarrère* (1989), *Gaspar et al.* (1990)):

$$\overline{K}_e = \overline{K}_T = \overline{K}_S \equiv \frac{\overline{K}_u}{\mathrm{Pr_t}}. \tag{2.28}$$

The fluxes appearing in the continuity, Navier-Stokes, and temperature equations due to molecular diffusivity are orders of magnitude smaller than those of eddy diffusivity. Therefore, only fluxes due to the latter are retained in the prognostic rate equations.

The dissipation rate of turbulent kinetic energy, ε, is parametrized in terms of the turbulent kinetic energy and a turbulent dissipation length, l_ε, following *Kolmogorov* (1941b) and *Gaspar et al.* (1990):

$$\varepsilon = \frac{c_\varepsilon \overline{e}^{\frac{3}{2}}}{l_\varepsilon} \tag{2.29}$$

where c_ε is an empirical constant.

To complete the closure scheme, one can either write a rate equation for ε, as is often done for higher-order closure schemes, or parametrize the turbulent length scales l_k and l_ε. Parametrization of the turbulent length scales give reasonable results compared to rate equations for ε and experimental data for the planetary boundary layer (*Therry and Lacarrère* (1983)). An added advantage in parametrizing the turbulent length scales is the increase in computational efficiency in comparison to solving an additional rate equation. As a result, the present model implements a parametrization scheme for the turbulent length scales.

The specific parametrization of the turbulent length scales in the present model is that of *Gaspar et al.* (1990) and *Bougeault and Lacarrère* (1989), with a slight modification in notation and representation:

$$\overline{e}\,(z_0) = \int_{z_0}^{z_0 - l_u} g\left(\alpha\Big[\overline{T}\,(z_0) - \overline{T}\,(z)\Big] - \beta\left[\overline{S}\,(z_0) - \overline{S}\,(z)\right]\right) dz \tag{2.30}$$

$$\overline{e}\,(z_0) = \int_{z_0}^{z_0 + l_d} g\left(\alpha\Big[\overline{T}\,(z_0) - \overline{T}\,(z)\Big] - \beta\left[\overline{S}\,(z_0) - \overline{S}\,(z)\right]\right) dz \tag{2.31}$$

$$l_k = \min\left(l_u, l_d\right) \tag{2.32}$$

$$l_\varepsilon = \sqrt{l_u l_d}. \tag{2.33}$$

The physical interpretations of the primary length scales l_u and l_d (pertinent turbulent length scales at all depths) are simple and straightforward: "they are the distances traveled upward (l_u) or downward (l_d) by a fluid particle in converting all of its original turbulent kinetic energy, $\overline{e}\left(z_0\right)$, into potential energy" (*Gaspar et al.* (1990)).

The above definitions for l_u and l_d take into account the most general case of variable density stratifications, encompasing both stable and non-stable situations. In the case of a stable situation with constant positive density gradient, l_u and l_d are directly proportional to the so-called buoyancy length scale, l_b (*Gaspar et al.* (1990)):

$$l_u = l_d = \sqrt{2} l_b \equiv \frac{\sqrt{2\overline{e}}}{N} \tag{2.34}$$

where N is the Brunt-Väisälä frequency, $N = \sqrt{\frac{g}{\rho_0}\frac{\partial \overline{\rho}}{\partial z}}$.

On the other hand, for unstable situations, l_u and l_d will be the length of the unstable region until either reaching a stably stratified region or until reaching the physical boundaries.

As in *Gaspar et. al.* (1990), a countergradient term appearing in the parametrization of the vertical flux of temperature in convective cases, used by *Therry and Lacarrère* (1983) and *Bougeault and Lacarrère* (1989), is disregarded since stable density gradients have not been oberved for convective oceanic mixed layers (and assumed in the present model to also be true for limnological environments), even though they have been observed in convective atmospheric boundary layers (*Gaspar et. al.* (1990)).

2.1.7 Boundary Conditions

The following boundary conditions are taken (with slight modifications) from *Soetaert et al.* (2001) and *Cummings* (1926).

Horizontal Velocity, $\overline{\mathbf{u}} = \left(\overline{v}_x, \overline{v}_y\right)$

At the air-water interface ($z = 0$) there is a Neumann (flux) boundary condition; at the water-sediment interface ($z = L$) there is a mixed diffusive boundary condition. They represent wind-induced and water-movement induced shear stresses at the air-water and water-sediment surfaces, respectively:

$$-\overline{K}_u \frac{\partial\left(\rho_0 \overline{v}_x\right)}{\partial z}\bigg|_{z=0} = \rho_a \tau_{10} w_{10} \cdot w_{10} \cos\theta \tag{2.35}$$

$$-\overline{K}_u \frac{\partial\left(\rho_0 \overline{v}_y\right)}{\partial z}\bigg|_{z=0} = \rho_a \tau_{10} w_{10} \cdot w_{10} \sin\theta \tag{2.36}$$

$$-\overline{K}_u \frac{\partial\left(\rho_0 \overline{v}_x\right)}{\partial z}\bigg|_{z=L} = \rho_0 \tau_L \overline{v}_{x,\delta} \sqrt{\overline{v}_{x,\delta}^2 + \overline{v}_{y,\delta}^2} \tag{2.37}$$

$$-\overline{K}_u \frac{\partial\left(\rho_0 \overline{v}_y\right)}{\partial z}\bigg|_{z=L} = \rho_0 \tau_L \overline{v}_{y,\delta} \sqrt{\overline{v}_{x,\delta}^2 + \overline{v}_{y,\delta}^2} \tag{2.38}$$

where τ_{10} and τ_L are the corresponding surface drag coefficients at the air-water and water-sediment interfaces, respectively, with τ_{10} conventionally taken 10 m above the air-water interface, θ is the horizontal wind angle (measured positively clockwise from the westward direction) conventionally taken 10 m above the interface, and $\overline{\mathbf{u}}_\delta$ is the velocity close to the water-sediment interface (taken to be at 1 m above the sediment bed in *Soataert et al.* (2001)). It is given by the expression:

$$\overline{\mathbf{u}}_\delta = \frac{\overline{\mathbf{u}}_h}{1 + \frac{\sqrt{\tau_L}}{\kappa} \ln\left(\frac{h}{\delta_u}\right)} \tag{2.39}$$

where κ is the so-called Kármán constant and $\overline{\mathbf{u}}_h$ is the horizontal velocity of the water at a height h above the water-sediment interface located as close as possible within the numerical discretization scheme to the edge of the water's velocity boundary layer thickness δ_u.

The expression for $\overline{\mathbf{u}}_\delta$ is based on boundary layer theory whereby the effects of friction-inducing physical boundaries need to be considered since the shear stresses they induce in the fluid cause noticeable gradient deviations in the fluid's prognostic quantity profiles up to a certain distance, δ, from the physical boundary (*Schlichting* (1979), *Young* (1989)).

The velocity boundary layer thickness can be calculated as (*Schlichting* (1979), *Young* (1989)):

$$\delta_u = \int_0^h \left(1 - \frac{u}{u_\delta}\right) dz \tag{2.40}$$

where u_δ denotes the velocity at the boundary layer's edge.[1]

It is standard practice (*Schlichting* (1979)) to numerically approximate the boundary layer thickness to be the distance from the physical boundary where the fluid's velocity immediately within the boundary layer differs from that immediately outside of it by 1%.

The logarithmic behaviour in equation (2.39) within the boundary layer results from the turbulent shear stress proposed by *Prandtl* (1952):

$$\tau = -\rho\overline{v'_x v'_y} = \rho l^2 \left|\frac{\partial \overline{u}}{\partial z}\right| \frac{\partial \overline{u}}{\partial z} \tag{2.41}$$

where l is the so-called Prandtl mixing length and $\overline{u}$ is the fluid's horizontal speed $\overline{u} = \sqrt{\overline{v}_x^2 + \overline{v}_y^2}$. If we consider only z dependence for $\overline{u}$, let $\tau_L \equiv \frac{\tau}{\rho}\frac{1}{u*^2}$ and $\Upsilon \equiv \frac{\overline{u}}{u*}$, where $u*$

[1] The momentum, kinetic energy, and temperature boundary layer thicknesses, $\delta_{\rho u}$, δ_e, and δ_T, respectively, are analytically calculated as $\delta_{\rho u} = \int_0^h \frac{\rho u}{\rho_\delta u_\delta}\left(1 - \frac{u}{u_\delta}\right) dz$, $\delta_e = \int_0^h \frac{\rho u}{\rho_\delta u_\delta}\left[1 - \left(\frac{u}{u_\delta}\right)^2\right] dz$, and $\delta_T = \int_0^h \frac{\rho u}{\rho_\delta u_\delta}\left(\frac{T}{T_\delta} - 1\right) dz$.

is a velocity scale, and rearranging terms, we obtain:

$$\frac{d\Upsilon}{dz} = \frac{\sqrt{\tau_L}}{l}. \tag{2.42}$$

We then approximate the Prandtl mixing length to first order as $l = \kappa z$, where κ is the so-called Kármán constant. Therefore,

$$\frac{d\Upsilon}{dz} = \frac{\sqrt{\tau_L}}{\kappa z}. \tag{2.43}$$

Integrating the preceding equation gives:

$$\Upsilon = \frac{\sqrt{\tau_L}}{\kappa}\ln(z) + c \tag{2.44}$$

where c is an integration constant. At $z = \delta_u$, we have $c = \Upsilon(\delta_u) - \frac{\sqrt{\tau_L}}{\kappa}\ln(\delta_u)$, which then gives $\Upsilon(z) = \frac{\sqrt{\tau_L}}{\kappa}\ln\left(\frac{z}{\delta_u}\right) + \Upsilon(\delta_u)$. If we choose $u* = \overline{u}(\delta_u)$, then $\overline{u}(z) = \overline{u}(\delta_u) + \overline{u}(\delta_u)\frac{\sqrt{\tau_L}}{\kappa}\ln\left(\frac{z}{\delta_u}\right)$. Therefore,

$$\overline{u}(\delta_u) = \frac{\overline{u}(z)}{1 + \frac{\sqrt{\tau_L}}{\kappa}\ln\left(\frac{z}{\delta_u}\right)}. \tag{2.45}$$

which justifies equation (2.39). In the case when $z = h = \delta_u$, $\overline{\mathbf{u}}_\delta$ reduces to $\overline{\mathbf{u}}_h$.

Turbulent Kinetic Energy, $\overline{e}$

The boundary conditions for the turbulent kinetic energy are Dirichlet boundary conditions adapted from *Soetaert et al.* (2001) to take into account dynamic windspeed above the air-water interface in addition to the dynamic horizontal velocity of the water:

$$\overline{e}\Big|_{z=0} = c_{\overline{e},w}\frac{\rho_a}{\rho_0}\tau_{10}w_{10}^2 \tag{2.46}$$

$$\overline{e}\Big|_{z=L} = c_{\overline{e},L}\tau_L u_\delta^2 \tag{2.47}$$

where $c_{\overline{e},w}$ and $c_{\overline{e},L}$ are empirical constants.

Temperature, $\overline{T}$

The boundary conditions at both the air-water ($z = 0$) and water-sediment ($z = L$) interfaces are Neumann (flux) boundary conditions for the heat budget:

$$-\overline{K}_T \frac{\partial\left(\rho_0 c_p \overline{T}\right)}{\partial z}\Big|_{z=0} = I_0 - (Q_b + Q_e + Q_s) \tag{2.48}$$

$$-\overline{K}_T \frac{\partial\left(\rho_0 c_p \overline{T}\right)}{\partial z}\Big|_{z=L} = I_L \tag{2.49}$$

where Q_b is backradiation, Q_e is the latent heat of evaporation of water, Q_s is the sensible heat flux due to convection and conduction, and I_L is the light intensity at the water-sediment interface given by equation (2.19). The backradiation, latent heat of evaporation, and sensible heat flux are conventionally given by:

$$Q_b = 4\sigma T_{w_0}^3 \left(T_{w_0} - T_{a_{10}}\right) \tag{2.50}$$

where σ is the Stefan-Boltzmann constant, T_{w_0} is the temperature of the water at the interface, and $T_{a_{10}}$ is the temperature of the air, conventionally taken at 10 m above the air-water interface;

$$Q_e = c_e L_v \rho_a w_{10} \left(q_{w0} - q_{a_{10}}\right) \tag{2.51}$$

where c_e is an empirical constant, L_v is the specific latent heat of vaporization per mass of water, ρ_a is a reference air density, w_{10} is the wind conventionally taken at 10 m above the interface, and q_{w0} and $q_{a_{10}}$ are the specific humidities at the interface and 10 m above the interface, respectively. They are dimensionless quantities relating the amount of

water vapour mass, m_w, per total mass of humid air in a particular volume (*Gill* (1982)):

$$q = \frac{m_w}{m_w + m_a} \tag{2.52}$$

where m_a is the mass of dry air. The quantity $c_e \rho_a w_{10} \left(q_{w0} - q_{a_{10}}\right)$ is the evaporation rate (in units of mass $\cdot$ length^{-2} $\cdot$ time^{-1}); and finally,

$$Q_s = c_s \rho_a c_{pa} w_{10} \left(T_{w_0} - T_{a_{10}}\right) \tag{2.53}$$

where c_s is an empirical constant and c_{pa} is the specific heat capacity of air.

Salinity, $\overline{S}$

Soetaert et al. (2001) do not consider saline environments. However, *Gaspar et al.* (1990) only give a Neumann boundary condition for the air-water interface:

$$-\overline{K}_S \frac{\partial\left(\rho_0 \overline{S}\right)}{\partial z}\bigg|_{z=0} = \overline{S}_{pr} - \overline{S}_{ev} \tag{2.54}$$

where $\overline{S}_{pr}$ and $\overline{S}_{ev}$ are precipitation and evaporation fluxes, respectively.

By analogy with the boundary conditions for heat and momentum, it does not seem unreasonable to suggest a Neumann boundary condition for the water-sediment interface:

$$-K_{\overline{S}} \frac{\partial\left(\rho_0 \overline{S}\right)}{\partial z}\bigg|_{z=L} = \overline{S}_{sed} \tag{2.55}$$

where $\overline{S}_{sed}$ represents a salt exchange term between the water column and sediment.

2.2 The Biogeochemical Submodel

Let C be the concentration of a particular biogeochemical species. Then, its time average (in the sense of equation (2.2)) obeys the rate equation:

$$\frac{\partial \overline{C}}{\partial t} = \frac{\partial}{\partial z}\left(\overline{K}_C \frac{\partial \overline{C}}{\partial z}\right) - \frac{\partial}{\partial z}\left(\overline{V}_C \overline{C}\right) + \overline{r}_C \tag{2.56}$$

where $\overline{K}_C$ is the eddy diffusivity (related through $\overline{K}_C \frac{\partial \overline{C}}{\partial z} = -\overline{v_z' C'}$ and $\overline{K}_C \approx \overline{K}_u$, as before), $\overline{V}_C$ is the vertical advection rate of species $\overline{C}$ (for example, sinking or biological mobility), and $\overline{r}_c$ are reaction rates producing and/or consuming $\overline{C}$. The units of C are discussed in Chapter 3 - *Numerical Implementation*.

The present model only considers broad categories for phytoplankton, zooplankton, and detritus. The numerical modeling of a particular subspecies of plankton or detritus can be achieved using characteristic values for $\overline{V}_c$, along with appropriate expressions for the reaction terms $\overline{r}_c$.

The notation used herein to denote the time-averaged concentrations of phytoplankton, zooplankton, detritus, phosphate, nitrate, ammonium, ferrous iron, iron(III) hydroxide, and oxygen are [PHYTO], [ZOO], [DET], $[H_3PO_4]$, $\left[NO_3^-\right]$, $\left[NH_4^+\right]$, $\left[Fe^{2+}\right]$, $\left[Fe(OH)_3\right]$, and $[O_2]$, respectively. The overline denoting time-averaging has been omitted for brevity.

2.2.1 Reactions

In the present model, we consider five primary reactions (R1-R5) and two secondary reactions (R6-R7) for the production and degradation of organic matter (*Fossing et al.* (2004) and *Van Cappellen et al.* (1993)).

The composition of organic matter takes the form $(CH_2O)_a (NH_3)_b (H_3PO_4)_c (FeT)_d$, where a, b, c, and d are stoichiometric coefficients and T represent a form of iron bound to cell surface ligand.

Following the traditional and experimentally verified models of *Hudson et al.* (1990, 1993) and *Sunda et al.* (1995), the present model considers only unchelated[1] forms of iron available for nutrient uptake by phytoplankton. The cellular uptake of reduced chelated iron as proposed in *Shaked et al.* (2005) is not considered as this would require the additional dynamics of a chelating agent. As a first approximation, the present model considers the binding to cell surface ligand of available Fe^{2+} as the sole mechanism for iron uptake. However, contrary to *Hudson et al.* (1990, 1993) and *Sunda et al.* (1995), which permit the binding to cell surface ligand of unchelated Fe^{3+}, in addition to Fe^{2+}, and its subsequent cellular uptake, the approach of *Shaked et al.* (2005) is adopted in that it is always reduced Fe^{2+} (from both chelated and unchelated Fe^{3+}) at the cell surface that is bound to cell surface ligand to form FeT, which is then subsequently transported across the cell membrane. The binding of iron to produce FeT is taken to be instantaneous so that the cellular uptake rate of iron is effectively the uptake rate of Fe^{2+}. The introduction of FeT allows conceptual preservation of organic matter as being electrically neutral.

The production of organic matter occurs via two primary reactions

- Photosynthesis I (NH_4^+-Induced):

$$\begin{aligned} &a\mathrm{CO_2} + b\mathrm{NH_4^+} + c\mathrm{H_3PO_4} + d\mathrm{Fe^{2+}} + a\mathrm{H_2O} \\ &\qquad \xrightarrow[synthesis]{photo} \left(\mathrm{CH_2O}\right)_a \left(\mathrm{NH_3}\right)_b \left(\mathrm{H_3PO_4}\right)_c \left(\mathrm{FeT}\right)_d + a\mathrm{O_2} + b\mathrm{H^+} \end{aligned} \tag{R1}$$

- Photosynthesis II (NO_3^--Induced):

$$\begin{aligned} &a\mathrm{CO_2} + b\mathrm{NO_3^-} + c\mathrm{H_3PO_4} + d\mathrm{Fe^{2+}} + (a+b)\,\mathrm{H_2O} + b\mathrm{H^+} \\ &\qquad \xrightarrow[synthesis]{photo} \left(\mathrm{CH_2O}\right)_a \left(\mathrm{NH_3}\right)_b \left(\mathrm{H_3PO_4}\right)_c \left(\mathrm{FeT}\right)_d + (a+2b)\,\mathrm{O_2} \end{aligned} \tag{R2}$$

[1] A "chelated" compound is a central metal atom that contains a ligand bonded at two or more points, and the compound is typically organic. A "ligand" is an ion or molecule attached to a (usually larger) metal atom by coordinate bonding.

As a result of bacterial respiration, the degradation of organic matter can occur via three primary reactions:

- Oxidation (RO_2):

$$\begin{aligned}(CH_2O)_a\,(NH_3)_b\,(H_3PO_4)_c\,(FeT)_d + aO_2 + bH^+ \\ \xrightarrow{RO_2} aCO_2 + bNH_4^+ + cH_3PO_4 + dFe^{2+} + aH_2O\end{aligned} \tag{R3}$$

- Denitrification $\left(RNO_3^-\right)$:

$$\begin{aligned}(CH_2O)_a\,(NH_3)_b\,(H_3PO_4)_c\,(FeT)_d + \frac{4}{5}aNO_3^- + \left(\frac{4}{5}a + b\right)H^+ \\ \xrightarrow{RNO_3^-} aCO_2 + bNH_4^+ + cH_3PO_4 + dFe^{2+} + \frac{7}{5}aH_2O + \frac{2}{5}aN_2\end{aligned} \tag{R4}$$

  where the N_2 produced is lost directly to the atmosphere; and

- Reduction of Iron $\left(RFe(OH)_3\right)$:

$$\begin{aligned}(CH_2O)_a\,(NH_3)_b\,(H_3PO_4)_c\,(FeT)_d + 4aFe(OH)_3(s) + (8a + b)\,H^+ \\ \xrightarrow{RFe(OH)_3} aCO_2 + bNH_4^+ + cH_3PO_4 + (4a + d)\,Fe^{2+} + 11aH_2O\end{aligned} \tag{R5}$$

Two secondary (redox) reactions directly affecting the concentrations of nitrate, ammonium, iron, and oxygen available for primary production/degradation of organic matter are:

- Nitrification $\left(RNH_4^+\right)$:

$$NH_4^+ + 2O_2 \xrightarrow{RNH_4^+} NO_3^- + H_2O + 2H^+ \tag{R6}$$

- Iron Oxidation $\left(RFe^{2+}\right)$:

$$Fe^{2+} + \frac{1}{4}O_2 + \frac{5}{2}H_2O \xrightarrow{RFe^{2+}} Fe(OH)_3(s) + 2H^+ \tag{R7}$$

The present model does not consider appreciable variations in pH. Therefore, the rates of photosynthesis, oxidation, denitrification, nitrification, and iron oxidation and reduction are affected only by temperature, light intensity, and the various concentrations.

2.2.2 Kinetics

The kinetic equations of the above respiration reactions (equations R3-R5) are based on *Van Cappellen et al.* (1993) and *Boudreau* (1997) and take the following Monod forms:

$$\mathrm{RO_2} = k_{RO_2} \cdot \mathrm{e}^{(T-T_0)} \cdot [\mathrm{DET}] \cdot \frac{[\mathrm{O_2}]}{[\mathrm{O_2}] + k_{O_2}} \tag{2.57}$$

$$\mathrm{RNO_3^-} = k_{RNO_3^-} \cdot \mathrm{e}^{(T-T_0)} \cdot [\mathrm{DET}] \cdot \frac{\left[\mathrm{NO_3^-}\right]}{\left[\mathrm{NO_3^-}\right] + k_{NO_3^-}} \cdot \frac{k'_{O_2}}{k'_{O_2} + [\mathrm{O_2}]} \tag{2.58}$$

$$\mathrm{RFe(OH)_3} = k_{RFe(OH)_3} \cdot \mathrm{e}^{(T-T_0)}. \tag{2.59}$$

$$[\mathrm{DET}] \cdot \frac{\left[\mathrm{Fe(OH)_3}\right]}{\left[\mathrm{Fe(OH)_3}\right] + k_{Fe(OH)_3}} \cdot \frac{k'_{NO_3^-}}{k'_{NO_3^-} + \left[\mathrm{NO_3^-}\right]} \cdot \frac{k'_{O_2}}{k'_{O_2} + [\mathrm{O_2}]}, \tag{2.60}$$

whereas the nitrification and iron oxidation rates are written as:

$$\mathrm{RNH_4^+} = k_{RNH_4^+} \cdot \mathrm{e}^{(T-T_0)} \cdot \left[\mathrm{NH_4^+}\right] \cdot [\mathrm{O_2}] \tag{2.61}$$

$$\mathrm{RFe^{2+}} = k_{RFe^{2+}} \cdot \mathrm{e}^{(T-T_0)} \cdot \left[\mathrm{Fe^{2+}}\right] \cdot [\mathrm{O_2}] - \Phi\,(I) \cdot \left[\mathrm{Fe(OH)_3}\right]. \tag{2.62}$$

Here k_{RO_2}, $k_{RNO_3^-}$, $k_{RFe(OH)_3}$, $k_{RNH_4^+}$, and $k_{RFe^{2+}}$ are rate constants, k_{O_2}, $k_{NO_3^-}$, and $k_{Fe(OH)_3}$ are so-called Monod-type half-saturation constants, k'_{O_2} and $k'_{NO_3^-}$ are inhibition constants, and T_0 is a reference temperature. Inhibition is the suppression of one primary reaction by another primary reaction (*Boudreau* (1997)). For example, bacterial degradation of organic matter by oxygen is favoured over that of degradation by both

nitrate and iron; in the absence of oxygen, nitrate is the more-favoured oxidizing agent to that of iron.

$\Phi(I)$ is a function accounting for the photoreduction of $Fe(OH)_3(s)$ to Fe^{2+}. *Madsen et al.* (1986) discuss the photoreduction process, but they do not provide a mathematical expression for it. Therefore, based on their experimental data and conclusions, it is not unreasonable to suggest the following step function for the process:

$$\Phi = \begin{cases} k_{photo}, & I > 0 \\ 0, & I = 0 \end{cases} \tag{2.63}$$

where k_{photo} is an overall rate constant for photoreduction and I is the light intensity. *Madsen et al.* (1986) suggests that the value of the light intensity itself does not contribute to the rate of the photoreduction process.

Reduction of $Fe(OH)_3(s)$ to Fe^{2+} by microbial activity (*Shaked* (2005), *Madsen et al.* (1986)) is not considered in the present model.

The reaction terms appearing in equation (2.56) for each of the biogeochemical prognostic variables are (based on *Soetaert et al.* (2001), *Omlin et al.* (2001), *Edwards et al.* (2001)):

$$\begin{cases} r_{phyto} = U - G_{phyto} - L_{phyto} \\ r_{zoo} = \zeta\left(G_{phyto} + G_{det}\right) - L_{zoo} - L_{zoo,pr} \\ r_{det} = L_{phyto,zoo} + zoo_{exc} - det_{remin} \\ r_{H_3PO_4} = c\left(\gamma\left(G_{phyto} + G_{det}\right) + \mathrm{RO}_2 + \mathrm{RNO}_3^- + \mathrm{RFe(OH)}_3 - U\right) \\ r_{NO_3^-} = \mathrm{RNH}_4^+ - \frac{4}{5}a\mathrm{RNO}_3^- - bU_{NO_3^-} \\ r_{NH_4^+} = b\left(\mathrm{RO2} + \mathrm{RNO}_3^- + \mathrm{RFe(OH)}_3 + \gamma\left(G_{phyto} + G_{det}\right) - U_{NH_4^+}\right) - \mathrm{RNH}_4^+ \\ r_{Fe^{2+}} = d\left(\mathrm{RO2} + \mathrm{RNO}_3^- + \left(\frac{4a}{d} + 1\right)\mathrm{RFe(OH)}_3 - U\right) - \mathrm{RFe}^{2+} \\ r_{Fe(OH)_3} = \mathrm{RFe}^{2+} - 4a\mathrm{RFe(OH)}_3 \\ r_{O_2} = aU_{NH_4^+} + (a+2b)\,U_{NO_3^-} - \gamma\left(G_{phyto} + G_{det}\right) - a\mathrm{RO}_2 - 2\mathrm{RNH}_4^+ \\ \qquad - \frac{1}{4}\mathrm{RFe}^{2+} \end{cases} \tag{2.64}$$

where ζ and γ are empirical constants describing the growth efficiency of zooplankton and the zooplankton excretion fraction, respectively, and

- $U, U_{NO_3^-}, U_{NH_4^+} \equiv$ rate of uptake of nutrients (phosphorus, nitrogen, and iron) due to photosynthesis,

$$U = U_{NH_4^+} + U_{NO_3^-} \tag{2.65}$$

$$U_{NH_4^+} = k_U \cdot f_U \cdot \left(\frac{I}{I + k_I}\right) \cdot [\text{PHYTO}] \cdot \min\left(\frac{\left[\text{NH}_4^+\right]}{\left[\text{NH}_4^+\right] + k_{NH_4^+}}, \frac{[\text{H}_3\text{PO}_4]}{[\text{H}_3\text{PO}_4] + k_{H_3PO_4}}, \frac{\left[\text{Fe}^{2+}\right]}{\left[\text{Fe}^{2+}\right] + k_{Fe^{2+}}}\right) \tag{2.66}$$

$$U_{NO_3^-} = k_U \cdot f_U \cdot \left(\frac{I}{I + k_I}\right) \cdot [\text{PHYTO}] \cdot \min\left(\frac{\left[\text{NO}_3^-\right]}{\left[\text{NO}_3^-\right] + k_{NO_3^-}} \cdot \frac{k'_{NH_4^+}}{k'_{NH_4^+} + \left[\text{NH}_4^+\right]}, \frac{[\text{H}_3\text{PO}_4]}{[\text{H}_3\text{PO}_4] + k_{H_3PO_4}}, \frac{\left[\text{Fe}^{2+}\right]}{\left[\text{Fe}^{2+}\right] + k_{Fe^{2+}}}\right) \tag{2.67}$$

where k_U is an overall rate constant, $f_U = e^{\beta_U\left(\overline{T} - \overline{T}_0\right)}$ (a temperature-correction function, where $\overline{T}$ is the temperature at the location in question and $\overline{T}_0$ is a reference temperature (these temperatures are equivalent to T and T_0 introduced previously but for the fact that they reference the temperatures obtained as a result of the turbulent closure scheme), β_U is a constant), k_I, $k_{NO_3^-}$, $k_{NH_4^+}$, $k_{H_3PO_4}$, and $k_{Fe^{2+}}$ are Monod-type half-saturation constants ($k_{Fe^{2+}}$ reproducing the L_{Fe} iron-limiting parameter of *Denman et al.* (1998)), and $k'_{NH_4^+}$ is an inhibition constant reflecting the fact that NH_4^+ is preferably uptaken over NO_3^-. Recall that I is the light intensity as defined in equation (2.19).

Using minimum quantities for the uptake ensures continued organic matter synthesis. Uptaking the least-available nutrient contributes directly to the production of organic matter instead of it being removed from the system by way of other reactions and, therefore, halting further organic matter from being produced.

- $G_{phyto} \equiv$ rate of zooplankton grazing on phytoplankton,

$$G_{phyto} = k_G \cdot f_G \cdot \left(\frac{[\text{PHYTO}]^2}{\mu^2 + [\text{PHYTO}]^2 + \omega\,[\text{DET}]^2}\right) \cdot [\text{ZOO}] \tag{2.68}$$

where k_G is an overall rate constant, $f_G = e^{\beta_G\left(\overline{T} - \overline{T}_0\right)}$ (β_G is a constant), μ is a half-

saturation coefficient, and ω is the relative zooplankton palatability for detritus compared to phytoplankton. The expression $\frac{[\text{PHYTO}]^2}{\mu^2+[\text{PHYTO}]^2}$ follows the experimentally-observed Holling Type III function modeling of predator on prey hunger-feeding-satiation cycles,

- $L_{phyto} \equiv$ rate of natural death and decay of phytoplankton,

$$L_{phyto} = k_{L,phyto} \cdot f_U \cdot [\text{PHYTO}] \tag{2.69}$$

where $k_{L,phyto}$ is an overall rate constant. L_{phyto} is dependent on the same correction factor as the uptake (f_U) since natural death and decay of phytoplankton is directly correlated with their growth from the uptake of nutrients,

- $G_{det} \equiv$ rate of zooplankton grazing on detritus,

$$G_{det} = k_G \cdot f_G \cdot \left(\frac{\omega \, [\text{DET}]^2}{\mu^2 + [\text{PHYTO}]^2 + \omega \, [\text{DET}]^2} \right) \cdot [\text{ZOO}] \, , \tag{2.70}$$

- $L_{zoo} \equiv$ rate of natural death and decay of zooplankton,

$$L_{zoo} = k_{L,zoo} \cdot f_G \cdot [\text{ZOO}] \tag{2.71}$$

where $k_{L,zoo}$ is an overall rate constant. L_{zoo} is dependent on the same correction factor as the growth of zooplankton (f_G) since natural death and decay of zooplankton is directly correlated with their growth from grazing upon phytoplankton,

- $L_{zoo,pr} \equiv$ rate of death of zooplankton as a result of higher predation,

$$L_{zoo,pr} = k_{L,zoo,pr} \cdot f_G \cdot [\text{ZOO}]^2 \tag{2.72}$$

where $k_{L,zoo,pr}$ is an overall rate constant,

- $L_{phyto,zoo} \equiv$ rate of natural death and decay of total plankton,

$$L_{phyto,zoo} = L_{phyto} + L_{zoo}, \tag{2.73}$$

- $zoo_{exc} \equiv$ rate of zooplankton excretion,

$$zoo_{exc} = (1 - \zeta - \gamma) \cdot \left(G_{phyto} + G_{det}\right), \tag{2.74}$$

  Excretion by zooplankton results in the production of detritus. The degradation of this detritus will release nutrients back into the water column but oxygen will be consumed from the environment as the detritus is oxidized by bacteriological respiration.

- $det_{remin} \equiv$ rate of remineralization of detritus,

$$det_{remin} = k_d \cdot f_D \cdot [\mathrm{DET}] \tag{2.75}$$

  where k_d is an overall rate constant and $f_D = e^{\beta_D\left(\overline{T}-\overline{T}_0\right)}$ (β_D is a constant). Remineralization here is taken to mean the releasing back into the water column of the components as a result of the decomposition of dead and decaying organic matter.

2.2.3 Boundary Conditions

The biogeochemical prognostic rate equations are each supplemented with Neumann (flux) boundary conditions at both the air-water and water-sediment interfaces, except for oxygen at the air-water interface where the boundary condition is a mixed diffusive flux.

As a result of decoupling the water column from the atmosphere and sediment, imposed flux values are used to simulate quantitative exchanges of the respective prognostic variables across these interfaces.

Phytoplankton, Zooplankton, and Detritus

At both the air-water and water-sediment interfaces the Neumann boundary conditions are fixed total (diffusive + advective) fluxes:

$$-\overline{K}_u \frac{\partial \overline{C}}{\partial z}\bigg|_0 + \overline{V}_C \overline{C}\bigg|_0 = 0 \tag{2.76}$$

$$-\overline{K}_u \frac{\partial \overline{C}}{\partial z}\bigg|_L + \overline{V}_C \overline{C}\bigg|_L = F_{ws} \tag{2.77}$$

where F_{ws} is the flux from the water column to the sediment.

Phosphate, Nitrate, Ammonium, Ferrous Iron, and Ferric Iron

At both the air-water and water-sediment interfaces the Neumann boundary conditions are fixed diffusive fluxes:

$$-\overline{K}_u \frac{\partial \overline{C}}{\partial z}\bigg|_0 = F_{aw} \tag{2.78}$$

$$-\overline{K}_u \frac{\partial \overline{C}}{\partial z}\bigg|_L = F_{ws} \tag{2.79}$$

where F_{aw} and F_{ws} are the fluxes from the air into the water column and the water column to the sediment, respectively.

Without anthropogenic interference, normal circumstances would not bring any appreciable phosphate, nitrate, or ammonium fluxes at the air-water interface (flux = 0). However, some limnological environments immediately adjacent to farms and urbanized areas, for example, can experience run-off of fertilizer and waste (which can contain appreciable amounts of phosphorus and nitrogen) into the neighbouring limnological environments.

Oxygen

At the air-water interface the boundary condition is a mixed diffusive flux, while at the water-sediment interface the Neumann boundary condition is a fixed diffusive flux:

$$-\overline{K}_u \frac{\partial \overline{[\mathrm{O_2}]}}{\partial z}\bigg|_0 = f\left(w_{10}\right)\left(\mathrm{SatO_2} - \overline{[\mathrm{O_2}]}\right)\bigg|_0 \tag{2.80}$$

$$-\overline{K}_u \frac{\partial \overline{[\mathrm{O_2}]}}{\partial z}\bigg|_L = F_{ws} \tag{2.81}$$

where $f\left(w_{10}\right)$ is a coefficient that depends on the windspeed (conventionally taken at 10 m above the air-water interface), $\mathrm{SatO_2}$ is the saturated oxygen concentration (*Sarmiento et al.* (2006)), and F_{ws} is the flux from the water column to the sediment. The term $f\left(w_{10}\right)\left(\mathrm{SatO_2} - \overline{[\mathrm{O_2}]}\right)\Big|_0$ expresses the amount of atmospheric $\mathrm{O_2}$ dissolved at the top of the water column. Anthropogenic injection of oxygen at the air-water interface is neglected.

2.3 Summary of Model

A summary of the complete model is presented in Appendix B for easy reference.

Chapter 3

Numerical Implementation

The prognostic rate equations are approximated using the finite difference schemes of Crank-Nicolson (*Crank and Nicolson*, 1947), which is typically used to discretize parabolic (diffusion) partial differential equations, and Fiadeiro-Veronis (*Fiadeiro and Veronis*, 1977), which is used for discretizing mixed diffusion-advection partial differential equations.

The rate equations for the water's temperature, horizontal velocity, salinity, and turbulent kinetic energy, and the concentrations of phosphate, nitrate, ammonium, ferrous iron, ferric iron, and oxygen are all parabolic differential equations. The rate equations for the concentrations of phytoplankton, zooplankton, and detritus are diffusion-advection partial differential equations.

The corresponding numerical solutions to the non-linear rate equations of the present model are obtained using an iterative algorithm for a specified relative or absolute tolerance for the prognostic variables.

3.1 Crank-Nicolson Finite Differencing Scheme

Let $f(t,z)$ be a continuous and differentiable function in time and space satisfying $\frac{\partial f}{\partial t} \equiv R(t,z)$, where $R(t,z)$ represents diffusive $\frac{\partial}{\partial z}\left(K_f \frac{\partial f}{\partial z}\right)$, and possibly advective

$\frac{\partial}{\partial z}\left(V_f f\right)$ and reactive r_f, terms. The Crank-Nicolson scheme expresses the time derivative at the intermediate $n+\frac{1}{2}$ time-step as centre-differenced in time and evaluates $R\left(t,z\right)$ between its current (n) and next $(n+1)$ time-stepped values to obtain second-order accuracy in time:

$$\left.\frac{\partial f}{\partial t}\right|^{n+\frac{1}{2}} \approx \frac{f^{n+1}-f^{n}}{\Delta t} \approx \frac{1}{2}\left(R^{n}+R^{n+1}\right) \tag{3.1}$$

where Δt is the time-step. In the general case when $R\left(t,z\right)$ represents diffusive, advective, and reactive terms, the scheme gives:

$$\begin{aligned}\frac{f^{n+1}-f^{n}}{\Delta t} \approx & \frac{1}{2}\left[\frac{\partial}{\partial z}\left(K_f^{n+\frac{1}{2}}\left.\frac{\partial f}{\partial z}\right|^{n}\right)+\frac{\partial}{\partial z}\left(K_f^{n+\frac{1}{2}}\left.\frac{\partial f}{\partial z}\right|^{n+1}\right)\right] \\ & -\frac{1}{2}\left[\frac{\partial}{\partial z}\left(V_f^{n+\frac{1}{2}}\, f^{n}\right)+\frac{\partial}{\partial z}\left(V_f^{n+\frac{1}{2}}\, f^{n+1}\right)\right] \\ & +\frac{1}{2}\left(r_f^{n}+r_f^{n+1}\right)\end{aligned} \tag{3.2}$$

where $K_f^{n+\frac{1}{2}}=\frac{1}{2}\left(K_f^{n}+K_f^{n+1}\right)$, and $V_f^{n+\frac{1}{2}}=\frac{1}{2}\left(V_f^{n}+V_f^{n+1}\right)$.

With regards to spatial coordinates, finite differencing schemes represent each prognostic variable as having values defined only at a finite integer number of locations (nodes) fixed for the entire profile. Denoting the distance between adjacent nodes in an evenly spaced grid as Δz, a particular depth z can be written as $z=i\Delta z$, where i is the corresponding node of the discretized profile. The convention taken is that $i=0$ represents location at the air-water interface and $i=N-1$ represents location at the water-sediment interface, where N is the finite integer number of nodes.

To obtain second-order accuracy in space, the Crank-Nicolson scheme approximates the spatial derivative terms using centred-differencing:

$$\left.\frac{\partial}{\partial z}\left(K_f\frac{\partial f}{\partial z}\right)\right|_{z=i\Delta z} \approx \frac{1}{\Delta z}\left[K_{f;i+\frac{1}{2}}\left(\frac{f_{i+1}-f_i}{\Delta z}\right)-K_{f;i-\frac{1}{2}}\left(\frac{f_i-f_{i-1}}{\Delta z}\right)\right] \tag{3.3}$$

$$\left.\frac{\partial}{\partial z}\left(V_f f\right)\right|_{z=i\Delta z} \approx \frac{1}{\Delta z}\left(V_{f;i+\frac{1}{2}} f_{i+\frac{1}{2}} - V_{f;i-\frac{1}{2}} f_{i-\frac{1}{2}}\right) \tag{3.4}$$

where $K_{f;i\pm\frac{1}{2}} = \frac{1}{2}\left(K_{f;i} + K_{f;i\pm1}\right)$, $V_{f;i\pm\frac{1}{2}} = \frac{1}{2}\left(V_{f;i} + V_{f;i\pm1}\right)$, and $f_{i\pm\frac{1}{2}} = \frac{1}{2}\left(f_i + f_{i\pm1}\right)$[1], and the subscripts $i-1$, i, and $i+1$ denote the values of the corresponding quantities at the previous, current, and following nodes of the discretized profiles, respectively.

The system is then supplemented by appropriate Dirichlet (value), Neumann (gradient), or mixed boundary conditions at the interfaces.

The Crank-Nicolson scheme results in a semi-implicit system of equations that can be written in the form of a tridiagonal matrix system:

$$\begin{aligned}
&-\left(\alpha_i + \gamma_i\right) f_{i-1}^{n+1} + \left(1 + \alpha_i + \beta_i - \gamma_i + \delta_i\right) f_i^{n+1} - \left(\beta_i - \delta_i\right) f_{i+1}^{n+1} \\
&\qquad = \left(\alpha_i + \gamma_i\right) f_{i-1}^{n} + \left(1 - \alpha_i - \beta_i + \gamma_i - \delta_i\right) f_i^{n} + \left(\beta_i - \delta_i\right) f_{i+1}^{n} + \Delta t \cdot r_{f;i}^{n+\frac{1}{2}} \\
&\qquad \Rightarrow \boxed{\mathbf{A}\cdot\mathbf{f}^{n+1} = \mathbf{B}\cdot\mathbf{f}^{n} + \Delta t\cdot\mathbf{r}_f^{n+\frac{1}{2}}} \\
&\qquad \text{(see also Figure 2.1)}
\end{aligned} \tag{3.5}$$

where $\alpha_i \equiv \frac{\Delta t}{2(\Delta z)^2} K_{f;i-\frac{1}{2}}^{n+\frac{1}{2}}$, $\beta_i \equiv \frac{\Delta t}{2(\Delta z)^2} K_{f;i+\frac{1}{2}}^{n+\frac{1}{2}}$, $\gamma_i \equiv \frac{\Delta t}{4\Delta z} V_{f;i-\frac{1}{2}}^{n+\frac{1}{2}}$, and $\delta_i \equiv \frac{\Delta t}{4\Delta z} V_{f;i+\frac{1}{2}}^{n+\frac{1}{2}}$.

The matrix elements $(\mathrm{A,B})_{0,0;0,1}$ and $(\mathrm{A,B})_{\mathrm{N\text{-}1,N\text{-}2;N\text{-}1,N\text{-}1}}$ depend on the particular boundary conditions. Dirichlet boundary conditions, i.e. $f_{0;\mathrm{N\text{-}1}} = \text{constant}$, result in matrix elements $(\mathrm{A,B})_{0,0;\mathrm{N\text{-}1,N\text{-}1}} = 1$ and $(\mathrm{A,B})_{0,1;\mathrm{N\text{-}1,N\text{-}2}} = 0$. Neumann (flux) boundary conditions are implemented as: $\left. -K_f \frac{\partial f}{\partial z}\right|_{z=0} = \text{constant} \Rightarrow -K_{f;0}\left(\frac{f_1 - f_{-1}}{2\Delta z}\right) = \text{constant} \Rightarrow f_{-1} = f_1 + \frac{2\Delta z}{K_{f;0}}(\text{constant})$. Using this approach, it is possible to evaluate the above matrix system for $i = 0$ and obtain values for the matrix elements $(\mathrm{A,B})_{0,1}$. A similar approach can be used for the lower boundary.

The $n+1$ time-stepped values are then obtained by inverting the tridiagonal matrix

[1] While the general form of $f_{i\pm\frac{1}{2}}$ as appearing in the advective term is correct, a slight modification will be made in the following section, *Fiadeiro-Veronis Finite Differencing Scheme*, that controls the degrees of contribution by each of the f_{i-1}, f_i, and f_{i+1} quantities by means of a weighting factor.

A. However, a single inversion of **A** may or may not result in significant divergence from the exact solution, depending on non-linear contributions, for example in the diffusivity and reaction terms. An iterative approach is used to obtain an accurate solution: all $n+1$ terms are replaced by approximate, intermediate iterated values $(n+1, m)$, i.e. $f^{n+1,m}$, $K_f^{n+1,m}$, $V_f^{n+1,m}$, and $r_f^{n+1,m}$. The iteration is then initiated with $(n+1, 1) = n$ and continues until $\left|\mathbf{f}^{(n+1,m+1)} - \mathbf{f}^{(n+1,m)}\right| < \epsilon$ for all components in $\mathbf{f}$, where ϵ is a given tolerance. To be clear, the iterations are performed on the prognostic variables and not on functions that depend on them. For example, considering an arbitrary function $G \equiv G(f) \equiv G_f$:

$$G_f^{n+\frac{1}{2}} \approx G\left(\frac{1}{2}\left(f^n + f^{n+1}\right)\right) \neq \frac{1}{2}\left(G\left(f^n\right) + G\left(f^{n+1}\right)\right). \tag{3.6}$$

In other words, we consider the arguments of the function taken at the $n+\frac{1}{2}$ time-step and not the function approximated at $n+\frac{1}{2}$. With this approach, the iterations remain on the prognostic variables and do not contain iterations on auxiliary functions/quantities represented by G.

$$
\underbrace{\begin{pmatrix}
* & * & 0 & 0 & \cdots & 0 & 0 & 0 \\
-(\alpha_1+\gamma_1) & (1+\alpha_1+\beta_1-\gamma_1+\delta_1) & -(\beta_1-\delta_1) & 0 & \cdots & 0 & 0 & 0 \\
0 & -(\alpha_2+\gamma_2) & (1+\alpha_2+\beta_2-\gamma_2+\delta_2) & -(\beta_2-\delta_2) & \cdots & 0 & 0 & 0 \\
 & & & & \vdots & & & \\
0 & 0 & \cdots & -(\alpha_i+\gamma_i) & (1+\alpha_i+\beta_i-\gamma_i+\delta_i) & -(\beta_i-\delta_i) & \cdots & 0 \\
 & & & & \vdots & & & \\
0 & 0 & 0 & \cdots & -(\alpha_{\text{N-3}}+\gamma_{\text{N-3}}) & (1+\alpha_{\text{N-3}}+\beta_{\text{N-3}}-\gamma_{\text{N-3}}+\delta_{\text{N-3}}) & -(\beta_{\text{N-3}}-\delta_{\text{N-3}}) & 0 \\
0 & 0 & 0 & \cdots & 0 & -(\alpha_{\text{N-2}}+\gamma_{\text{N-2}}) & (1+\alpha_{\text{N-2}}+\beta_{\text{N-2}}-\delta_{\text{N-2}}+\delta_{\text{N-2}}) & -(\beta_{\text{N-2}}-\delta_{\text{N-2}}) \\
0 & 0 & 0 & \cdots & 0 & 0 & * & *
\end{pmatrix}}_{\mathbf{A}} \cdot \underbrace{\begin{pmatrix} f_0^{n+1} \\ f_1^{n+1} \\ f_2^{n+1} \\ f_3^{n+1} \\ \vdots \\ f_{i-1}^{n+1} \\ f_i^{n+1} \\ f_{i+1}^{n+1} \\ \vdots \\ f_{\text{N-4}}^{n+1} \\ f_{\text{N-3}}^{n+1} \\ f_{\text{N-2}}^{n+1} \\ f_{\text{N-1}}^{n+1} \end{pmatrix}}_{\mathbf{f}^{n+1}}
$$

$$
= \underbrace{\begin{pmatrix}
* & * & 0 & 0 & \cdots & 0 & 0 & 0 \\
(\alpha_1+\gamma_1) & (1-\alpha_1-\beta_1+\gamma_1-\delta_1) & (\beta_1-\delta_1) & 0 & \cdots & 0 & 0 & 0 \\
0 & (\alpha_2+\gamma_2) & (1-\alpha_2-\beta_2+\gamma_2-\delta_2) & (\beta_2-\delta_2) & \cdots & 0 & 0 & 0 \\
 & & & & \vdots & & & \\
0 & 0 & \cdots & (\alpha_i+\gamma_i) & (1-\alpha_i-\beta_i+\gamma_i-\delta_i) & (\beta_i-\delta_i) & \cdots & 0 \\
 & & & & \vdots & & & \\
0 & 0 & 0 & \cdots & (\alpha_{\text{N-3}}+\gamma_{\text{N-3}}) & (1-\alpha_{\text{N-3}}-\beta_{\text{N-3}}+\gamma_{\text{N-3}}-\delta_{\text{N-3}}) & (\beta_{\text{N-3}}-\delta_{\text{N-3}}) & 0 \\
0 & 0 & 0 & \cdots & 0 & (\alpha_{\text{N-2}}+\gamma_{\text{N-2}}) & (1-\alpha_{\text{N-2}}-\beta_{\text{N-2}}+\delta_{\text{N-2}}-\delta_{\text{N-2}}) & (\beta_{\text{N-2}}-\delta_{\text{N-2}}) \\
0 & 0 & 0 & \cdots & 0 & 0 & * & *
\end{pmatrix}}_{\mathbf{B}} \cdot \underbrace{\begin{pmatrix} f_0^{n} \\ f_1^{n} \\ f_2^{n} \\ f_3^{n} \\ \vdots \\ f_{i-1}^{n} \\ f_i^{n} \\ f_{i+1}^{n} \\ \vdots \\ f_{\text{N-4}}^{n} \\ f_{\text{N-3}}^{n} \\ f_{\text{N-2}}^{n} \\ f_{\text{N-1}}^{n} \end{pmatrix}}_{\mathbf{f}^{n}} + \Delta t \cdot \mathbf{r}_f^{n+\frac{1}{2}}
$$

Figure 3.1: Matrix Representation of Crank-Nicolson Scheme. The * terms are determined by the type of boundary conditions, i.e., Dirichlet or Neumann.

3.2 Fiadeiro-Veronis Finite Differencing Scheme

The conventional upwind/downwind schemes used for solving advection rate equations are only first-order accurate in space, compared with diffusion rate equations which are second-order accurate.[1] The Fiadeiro-Veronis scheme (*Fiadeiro and Veronis*, 1977) was devised for mixed diffusion-advection rate equations in order to maintain second-order accuracy in space in all instances whether the system is diffusion-dominant, advection-dominant, or neither. It approximates the advective term as:

$$\left.\frac{\partial}{\partial z}\left(V_f f\right)\right|_{z=i\Delta z} \approx \frac{1}{\Delta z}\left(V_{f;i+\frac{1}{2}} f_{i+\frac{1}{2}} - V_{f;i-\frac{1}{2}} f_{i-\frac{1}{2}}\right) \tag{3.7}$$

where $V_{f;i\pm\frac{1}{2}} = \frac{1}{2}\left(V_{f;i} + V_{f;i\pm1}\right)$, as before. However, the $f_{i\pm\frac{1}{2}}$ terms presented in the previous section, *Crank-Nicolson Finite Differencing Scheme*, are redefined as:

$$f_{i\pm\frac{1}{2}} \approx \begin{cases} \left(\dfrac{1 \pm \sigma_{i\pm\frac{1}{2}}}{2}\right) f_i + \left(\dfrac{1 \mp \sigma_{i\pm\frac{1}{2}}}{2}\right) f_{i\pm1}, & V_{f;i} > 0 \\ \left(\dfrac{1 \mp \sigma_{i\pm\frac{1}{2}}}{2}\right) f_i + \left(\dfrac{1 \pm \sigma_{i\pm\frac{1}{2}}}{2}\right) f_{i\pm1}, & V_{f;i} < 0 \end{cases} \tag{3.8}$$

where

$$\sigma_{i\pm\frac{1}{2}} = \coth\left(\frac{\left|V_{f;i\pm\frac{1}{2}}\right| \Delta z}{2K_{f;i\pm\frac{1}{2}}}\right) - \frac{2K_{f;i\pm\frac{1}{2}}}{\left|V_{f;i\pm\frac{1}{2}}\right| \Delta z}. \tag{3.9}$$

The blending coefficient $\sigma_{i\pm\frac{1}{2}}$ has the property that, given the value of the grid Peclet number, $Pe_{i\pm\frac{1}{2}} \equiv \frac{\left|V_{f;i\pm\frac{1}{2}}\right| \Delta z}{2K_{f;i\pm\frac{1}{2}}}$,

$$\sigma_{i\pm\frac{1}{2}} = \begin{cases} 0, & Pe_{i\pm\frac{1}{2}} \to 0 \quad \text{(diffusion dominated)} \\ 1, & Pe_{i\pm\frac{1}{2}} \to \infty \quad \text{(advection dominated)} \end{cases} . \tag{3.10}$$

[1] The Lax-Wendroff scheme is also conventionally used for advection rate equations. While this scheme is second-order accurate in space, it has the drawback that it does not guarantee non-oscillatory, monotonic solutions.

The quantities γ_i and δ_i in equation (3.5) of the Crank-Nicolson scheme are accordingly redefined to take into consideration $\sigma_{i\pm\frac{1}{2}}$.

If $\sigma_{i\pm\frac{1}{2}} = 0$, then pure central differencing is obtained as in the Crank-Nicolson scheme. If $\sigma_{i\pm\frac{1}{2}} = 1$, then pure backwards/forwards (upwind/downwind) differencing is obtained. The Fiadeiro-Veronis scheme remains second-order accurate in space even as the scheme switches between centred and backwards/forwards differencing.[1]

Lastly, the present model implements a diffusive time step[2] as opposed to an advective time step[3] since large-scale eddy diffusivity is the dominant mixing mechanism and occurs on a much quicker time scale compared to the typical sinking rates of plankton and detritus. The type of time-step, i.e., diffusive vs advective, refers to non-dimensionalizating the prognostic rate equations by a characteristic time scale. Choosing a timestep that is on the time scale of diffusion guarantees that the effects of diffusion will not underrepresent the contribution of eddies to the mixing process. The dynamics of eddy diffusivity might be missed altogether if larger timesteps are used would be the case with advective time scales.

3.3 Turbulent Length Scales

Although *Bougeault and Lacarrère* (1989) and *Gaspar et al.* (1990) define the turbulent primary length scales l_u and l_d (equations (2.30) and (2.31), respectively), neither present an algorithm how to numerically implement calculations of these length scales. The approach taken in the present model to calculate these length scales is as follows:

[1] *Fiadeiro and Veronis* (1977) derive their discretization scheme with the assumptions that K_f and V_f are constant. They propose, without proof, a generalization for non-constant K_f and V_f as presented in the present model. *Wright* (1992) demonstrates that the generalization proposed by *Fiadeiro and Veronis* (1977) generates a second order error $\frac{1}{2}\left[\frac{\partial}{\partial z}\left(\frac{V_f}{K_f}\right)\right]\Delta z^2$. Despite this, however, *Boudreau* (1997), and *Soetaert et al.* (2001) implement the proposed generalization of *Fiadeiro and Veronis* (1977) in their early diagenetic codes with successful results.

[2] $\Delta t \propto \frac{L^2}{K_f^*}$, where L is the characteristic macroscopic length scale (the depth of the lake), and K_f^* is the characteristic diffusivity.

[3] $\Delta t \propto \frac{L}{V_f^*}$, where V_f^* is the characteristic advective velocity.

Taking z_0 as a reference point for a particular depth/node, we

1. Let $z_0 \equiv i\Delta z$, where i is the node representing the depth z_0.

2. Let $l_u \equiv j\Delta z + \delta_u$, where j is the integral number of nodes in the upward direction away from the reference node i such that the integration of equation (2.30) up to j is the closest integration possible of integral nodes without overintegrating, and $\delta_u\,(>0)$ is the remainder of the distance required to makes the integration exact.

3. Let $l_d \equiv k\Delta z+\delta_d$, where k is the integral number of nodes in the downward direction away from the reference node i such that the integration of equation (2.31) up to k is the closest integration possible of integral nodes without overintegrating, and $\delta_d\,(>0)$ is the remainder of the distance required to makes the integration exact.

4. Rewrite equations (2.30) and (2.31), respectively, as

$$\overline{e}\,(i\Delta z) = \int_{i\Delta z}^{i\Delta z-(j\Delta z+\delta_u)} g\left(\alpha\left[\overline{T}\,(i\Delta z) - \overline{T}\,(z)\right] - \beta\left[\overline{S}\,(i\Delta z) - \overline{S}\,(z)\right]\right) dz \quad (3.11)$$

$$\overline{e}\,(i\Delta z) = \int_{i\Delta z}^{i\Delta z+(k\Delta z+\delta_d)} g\left(\alpha\left[\overline{T}\,(i\Delta z) - \overline{T}\,(z)\right] - \beta\left[\overline{S}\,(i\Delta z) - \overline{S}\,(z)\right]\right) dz. \quad (3.12)$$

These equations can also be written as:

$$\overline{e}\,(i\Delta z) = \int_{i\Delta z}^{i\Delta z-j\Delta z} g\left(\alpha\left[\overline{T}\,(i\Delta z) - \overline{T}\,(z)\right] - \beta\left[\overline{S}\,(i\Delta z) - \overline{S}\,(z)\right]\right) dz + g\Delta e_u \quad (3.13)$$

$$\overline{e}\,(i\Delta z) = \int_{i\Delta z}^{i\Delta z+k\Delta z} g\left(\alpha\left[\overline{T}\,(i\Delta z) - \overline{T}\,(z)\right] - \beta\left[\overline{S}\,(i\Delta z) - \overline{S}\,(z)\right]\right) dz + g\Delta e_d \quad (3.14)$$

where Δe_u and Δe_d are the remainders of the integrations needed to make the

integrals exact. Rearranging for Δe_u and Δe_d:

$$\Delta e_u = \frac{\overline{e}\left(i\Delta z\right)}{g} - \int_{i\Delta z}^{i\Delta z - j\Delta z} \left(\alpha\Big[\overline{T}\left(i\Delta z\right) - \overline{T}\left(z\right)\Big] - \beta\left[\overline{S}\left(i\Delta z\right) - \overline{S}\left(z\right)\right]\right) dz \quad (3.15)$$

$$\Delta e_d = \frac{\overline{e}\left(i\Delta z\right)}{g} - \int_{i\Delta z}^{i\Delta z + k\Delta z} \left(\alpha\Big[\overline{T}\left(i\Delta z\right) - \overline{T}\left(z\right)\Big] - \beta\left[\overline{S}\left(i\Delta z\right) - \overline{S}\left(z\right)\right]\right) dz. \quad (3.16)$$

Or, alternatively:

$$\begin{aligned}\Delta e_u &= \int_{i\Delta z - j\Delta z}^{i\Delta z - j\Delta z - \delta_u} \left(\alpha\Big[\overline{T}\left(i\Delta z\right) - \overline{T}\left(z\right)\Big] - \beta\left[\overline{S}\left(i\Delta z\right) - \overline{S}\left(z\right)\right]\right) dz \\ &\approx -\left(\alpha\left[\overline{T}\left(i\Delta z\right) - \overline{T}\left(i\Delta z - j\Delta z\right)\right] - \beta\left[\overline{S}\left(i\Delta z\right) - \overline{S}\left(i\Delta z - j\Delta z\right)\right]\right)\delta_u\end{aligned} \quad (3.17)$$

$$\begin{aligned}\Delta e_d &= \int_{i\Delta z + k\Delta z}^{i\Delta z + k\Delta z + \delta_d} \left(\alpha\Big[\overline{T}\left(i\Delta z\right) - \overline{T}\left(z\right)\Big] - \beta\left[\overline{S}\left(i\Delta z\right) - \overline{S}\left(z\right)\right]\right) dz \\ &\approx \left(\alpha\left[\overline{T}\left(i\Delta z\right) - \overline{T}\left(i\Delta z + k\Delta z\right)\right] - \beta\left[\overline{S}\left(i\Delta z\right) - \overline{S}\left(i\Delta z + k\Delta z\right)\right]\right)\delta_d.\end{aligned} \quad (3.18)$$

These approximations are as accurate as the discretization schemes; the finer the discretization, the more accurate the approximations.

Equating the two expressions respectively for each of Δe_u and Δe_d and solving for

δ_u and δ_d give:

$$\delta_u \approx \frac{-1}{\left(\alpha\left[\overline{T}\left(i\Delta z\right)-\overline{T}\left(i\Delta z-j\Delta z\right)\right]-\beta\left[\overline{S}\left(i\Delta z\right)-\overline{S}\left(i\Delta z-j\Delta z\right)\right]\right)}\times \left[\frac{\overline{e}\left(i\Delta z\right)}{g}-\int_{i\Delta z}^{i\Delta z-j\Delta z}\left(\alpha\left[\overline{T}\left(i\Delta z\right)-\overline{T}\left(z\right)\right]-\beta\left[\overline{S}\left(i\Delta z\right)-\overline{S}\left(z\right)\right]\right)dz\right] \tag{3.19}$$

$$\delta_d \approx \frac{1}{\left(\alpha\left[\overline{T}\left(i\Delta z\right)-\overline{T}\left(i\Delta z+k\Delta z\right)\right]-\beta\left[\overline{S}\left(i\Delta z\right)-\overline{S}\left(i\Delta z+k\Delta z\right)\right]\right)}\times \left[\frac{\overline{e}\left(i\Delta z\right)}{g}-\int_{i\Delta z}^{i\Delta z+k\Delta z}\left(\alpha\left[\overline{T}\left(i\Delta z\right)-\overline{T}\left(z\right)\right]-\beta\left[\overline{S}\left(i\Delta z\right)-\overline{S}\left(z\right)\right]\right)dz\right]. \tag{3.20}$$

δ_u and δ_d must be > 0 by construction.

5. Integration (using the trapezoidal algorithm) is done until either encountering a physical boundary or until there is a change in sign in Δe_u or Δe_d, accordingly, as a result of over-integrating. Once the change in sign in integration is encountered, the correct values of j and k are determined, and δ_u and δ_d can be computed, which immediately yield l_u and l_d. In the case where it is determined that $j, k = 1$ already over-integrate Δe_u or Δe_d, respectively, the value of the buoyancy length scale l_b (2.31) is calculated and used accordingly for l_u, l_d.

6. The locations within the water column where adjacent stable and unstable density stratifications intersect are treated as physical boundaries. The former are characterized by positive density gradients and are, therefore, directly proportional to the so-called buoyancy length scale, l_b, as in equation (2.34). The latter are characterized by either negative or zero density gradients and, therefore, can persist throughout the entire water column. For example, in the extreme case where the

entire water column exhibits an unstable density stratification, l_u and l_d will at all depths persist until reaching the air-water and water-sediment interfaces, respectively.

7. The parametrization of the dissipation rate of turbulent kinetic energy, ε in equation (2.29), does not permit its corresponding turbulent length scale, l_ε, to equal zero, since l_ε is the only denominator term in that equation. Equation (2.33) defines l_ε in terms of l_u and l_d; if either l_u or l_d are zero, then l_ε is zero. In the present model, there is a potential problem that $l_\varepsilon = 0$ at the air-water and water-sediment interfaces, since the model implies that $l_u = 0$ and $l_d = 0$, respectively, at these interfaces. Therefore, numerical overflows in these cases are avoided by artificially imposing l_u at the air-water interface to have the value of l_u at the node immediately below this interface, and l_d at the sediment-water interface to have the value of l_d at the node immediately above that interface.

3.4 Parameter Estimates

The parameters of the present model rely on empirical experiments to determine the ranges of typical and acceptable values. Once particular values are chosen for most of these parameters, they remain constant for the duration of a simulation. However, some parameters are functions of prognostic variables or other parameters and, as such, might not remain constant for the duration of a simulation. A presentation of these dynamic parameters follows.

3.4.1 Thermal Expansion and Saline Contraction Coefficients

The thermal expansion and saline contraction coefficients, $\alpha \equiv -\frac{1}{\rho}\left(\frac{\partial \rho}{\partial T}\right)_{S,p}$ and $\beta \equiv \frac{1}{\rho}\left(\frac{\partial \rho}{\partial S}\right)_{T,p}$, respectively, are calculated using a polynomial fit for the density of water, ρ, that is based on empirical observations as detailed by *Gill* (1982). This calculation of

ρ was defined by the Joint Panel on Oceanographic Tables and Standards (UNESCO, 1981). It is expressed as (in units of kg·m^{-3}):

$$\begin{aligned}\rho(T,S) =& \rho_w(T) \\ &+ S\Big[0.824493 - \left(4.0899\times10^{-3}\right)T + \left(7.6438\times10^{-5}\right)T^2 \\ &\quad - \left(8.2467\times10^{-7}\right)T^3 + \left(5.3875\times10^{-9}\right)T^4\Big] \\ &+ S^{\frac{3}{2}}\left[-5.72466\times10^{-3} + \left(1.0227\times10^{-4}\right)T - \left(1.6546\times10^{-6}\right)T^2\right] \\ &\quad + \left(4.8314\times10^{-4}\right)S^2\end{aligned} \tag{3.21}$$

where

$$\begin{aligned}\rho_w(T) =& 999.842594 \\ &+ \left(6.793952\times10^{-2}\right)T \\ &- \left(9.095290\times10^{-3}\right)T^2 \\ &+ \left(1.001685\times10^{-4}\right)T^3 \\ &- \left(1.120083\times10^{-6}\right)T^4 \\ &+ \left(6.536332\times10^{-9}\right)T^5\end{aligned} \tag{3.22}$$

is the density of pure water (salinity = 0), T is the temperature in degrees Celsius, and S is the salinity in practical salinity units or psu.

Gill (1982) continues with a polynomial formula for ρ to include pressure dependence (the above fits are for a pressure of one standard atmosphere), but as the present model does not consider variations in pressure, this section is omitted.

3.4.2 Specific Heat Capacity of Water

Calculation of the specific heat capacity of water, c_p, as a function of temperature and salinity are taken from *Gill* (1982) (in units of J·kg^{-1}·K^{-1}):

$$\begin{aligned} c_p(T,S) =& c_p(T) \\ &+ S\Big[-7.6444 + (0.107276)\,T - \left(1.3839 \times 10^{-3}\right) T^2\Big] \\ &+ S^{\frac{3}{2}}\Big[0.7709 - \left(4.0772 \times 10^{-3}\right) T + \left(5.3539 \times 10^{-5}\right) T^2\Big] \end{aligned} \tag{3.23}$$

where

$$\begin{aligned} c_p(T) =& 4217.4 \\ &- (3.720283)\,T \\ &+ (0.1412855)\,T^2 \\ &- \left(2.654387 \times 10^{-3}\right) T^3 \\ &+ \left(2.093236 \times 10^{-5}\right) T^4 \end{aligned} \tag{3.24}$$

is the specific heat capacity of pure water (salinity = 0), T is the temperature in degrees Celsius, and S is the salinity in practical salinity units or psu.

As was the case for the density, ρ, above, the pressure is taken to be a constant at one standard atmosphere.

3.4.3 Latent Heat of Vaporization

The latent heat of vaporization, $L_v(T)$, is calculated from *Gill* (1982) (in units of J·kg^{-1}):

$$L_v(T) = 2.5008 \times 10^6 - \left(2.3 \times 10^3\right) T \tag{3.25}$$

where T is the temperature in degrees Celsius.

3.4.4 Specific Humidity

The specific humidity of air, q, is calculated from *Gill* (1982) using the ideal gas law relation:

$$\rho_a = \frac{p}{RT_v} \tag{3.26}$$

where ρ_a is the density of moist air, p is the pressure in Pascals, $R = 287.04$ J kg^{-1} K^{-1} is the gas constant for dry air ($q = 0$), and $T_v \equiv T\,(1 + 0.6078q)$, with the temperature, T, in units of degrees Kelvin. T_v, also referred to as the *virtual temperature*, is the temperature needed in order for dry air to have the same density as moist air for a given pressure. The number 0.6708 comes from $\frac{m_a}{m_w} - 1$, where m_a and m_w are the molecular masses of dry air and water, respectively.

3.4.5 Wind Drag Coefficient

The wind drag coefficient (in dimensionless units) is calculated using *Soetaert et al.* (2001):

$$\tau_{10} = \frac{(0.81 + 0.064w_{10})}{1000} \tag{3.27}$$

where w_{10}, the windspeed 10 m above the air-water interface, is in units of metres/second.

3.4.6 Oxygen Exchange Coefficient; Oxygen Saturation

The oxygen exchange coefficient (in units of metres/second) is calculated using *Soetaert et al.* (2001):

$$f\,(w_{10}) = 0.78\sqrt{w_{10}} - 0.317w_{10} + 0.0372w_{10}^2 \tag{3.28}$$

where w_{10}, the windspeed 10 m above the air-water interface, is in units of metres/second.

The oxygen saturation (in units of grams/metre cubed) is calculated using *Sarmiento et al.* (2006):

$$\mathrm{SatO_2} = k_{SatO_2} \cdot \exp\,(l) \tag{3.29}$$

where

$$\begin{aligned} l =& A_0 + A_1 T_s + A_2 T_s^2 + A_3 T_s^3 + A_4 T_s^4 + A_5 T_s^5 \\ &+ S\left(B_0 + B_1 T_s + B_2 T_s^2 + B_3 T_s^3\right) + C_0 S^2 \end{aligned} \tag{3.30}$$

and

$$T_s = \ln\left[(298.15 - T) / (273.15 + T)\right] \tag{3.31}$$

with T being the temperature in degrees Celsius, S the salinity in practical salinity units, and k_{SatO_2}, A_0-A_5, B_0-B_3, and C_0 empirical constants. These constants are available in *Sarmiento et al.* (2006).

3.4.7 Biogeochemical Fluxes

Due to the decoupling of the present model from the sediment, no parametrizations are possible for any of the flux terms. They must be supplied either from empirical data or imposed with artificial values.

3.5 Biogeochemical Concentration Units

The composition of organic matter is taken to be the constant Redfield ratio, 106C : 16N : 1P : 0.05Fe (atomic stoichiometry relative to P) (*Reynolds* (2006)). If an organism's molecular stoichiometric ratio is the Redfield ratio, then its ash-free dry mass is approximately 50% carbon, 8.5% nitrogen, 1.2% phosphorous, and 0.1% iron, or 41C : 7N: 1P : 0.1Fe by weight (relative to P) (*Reynolds* (2006)). Therefore, the concentrations for phytoplankton, zooplankton, and detritus are represented in units of grams of total ash-free dry mass per cubic metre. Adopting the Redfield ratio fixes the value of a, b, c, and d in the rate equations.

For the sole purpose of maintaining consistency, the concentrations of phosphate, nitrate, ammonium, ferrous iron, ferric iron, and oxygen follow the convention for organic

matter and are expressed in units of grams per cubic metre of the respective quantities.

3.6 Verification of Computer Code

3.6.1 Turbulent Length Scales

Verification of the algorithm for computing the turbulent length scales l_u and l_d (section 3.3) was done by artificially creating numerous scenarios of stable, unstable, and mixed stable-unstable density stratifications. For simplicity, salinity was taken to be zero. Some of these results are presented below.

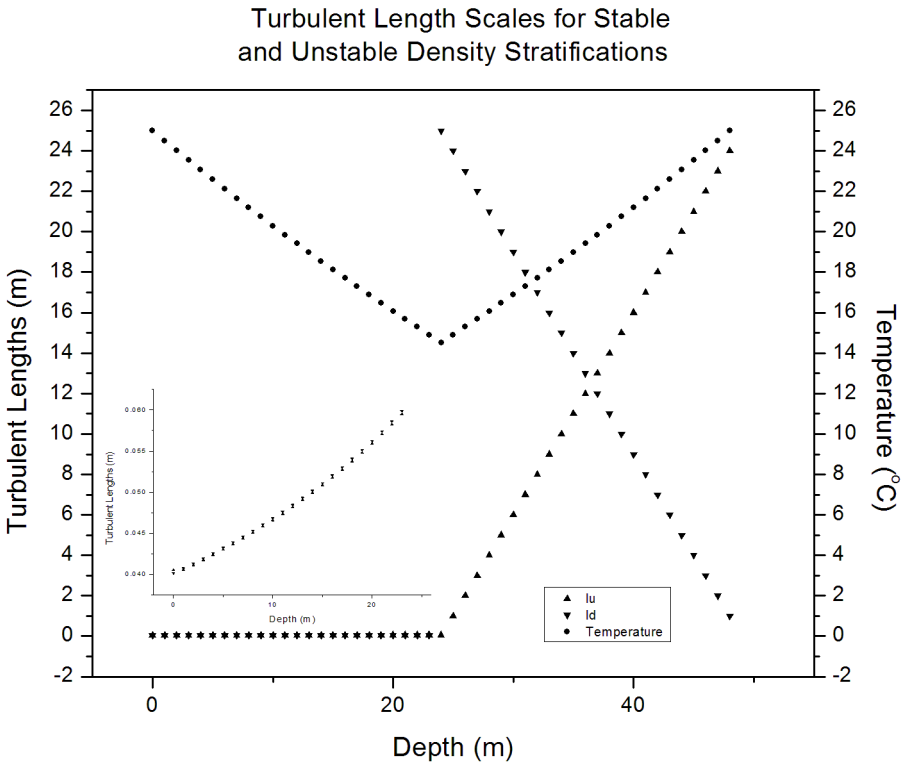

Figure 3.2: Turbulent Length Scales for Stable and Unstable Density Stratifications.

The sub-graph in the lower left-hand corner of Figure 3.2 is a blow-up of the data for the first 25 m. The Turbulent Lengths scale (i.e., the y-axis) for this subgraph goes from

0.040 m to 0.060 m. This subgraph is meant to show that the data are non-zero in this region and are on the same order of magnitude as the so-called buoyancy length scale as defined in Chapter 2. The V-shaped temperature profile is used to illustrate the stable (\) and unstable (/) density stratifications. In the stable case, l_u and l_d both coincide with the buoyancy length scale l_b. In the unstable case, l_u and l_d persist to the respective boundaries, as represented by the X.

3.6.2 Steady-State Profiles

In order to ascertain that the computer code has been implemented correctly for the Crank-Nicolson and Fiadeiro-Veronis finite differencing schemes, steady-state profiles for the diffusive-only transport of heat $\left(\frac{\partial \overline{T}}{\partial t} = \frac{\partial}{\partial z}\left(\overline{K}_T \frac{\partial \overline{T}}{\partial z}\right) + r_T\right)$ and mixed diffusive-advective transport of heat $\left(\frac{\partial \overline{T}}{\partial t} = \frac{\partial}{\partial z}\left(\overline{K}_T \frac{\partial \overline{T}}{\partial z}\right) - \frac{\partial}{\partial z}\left(\overline{V}_T \overline{T}\right) + r_T\right)$ were determined analytically using the computer program *Maple* and simulated numerically. The differences were negligible, i.e., less than 1%. The term r_T comes from equation (2.19) describing the attenuation of light intensity as a function of depth. All parameters were kept constant and the biogeochemical concentrations were all set to zero, which simplifies the expression for the light attenuation. An artificial advection term was added to the temperature equation so as to test the Fiadeiro-Veronis algorithm.

Diffusion-Only Transport of Heat

At the air-water interface a Dirichlet boundary condition was used, i.e. $\overline{T}\Big|_{z=0} =$ constant. At the water-sediment interface a Neumann (diffusive flux) boundary condition was used, i.e. $-\overline{K}_T \frac{\partial \overline{T}}{\partial z}\Big|_{z=L} = \frac{I_L}{\rho_0 c_p}$. The steady-state temperature profile is then:

$$\overline{T}(z) = a_D \exp(-k_1 z) + b_D z + c_D \tag{3.32}$$

where a_D, b_D, and c_D are constants. Simulations were performed using 11, 51, 101, 501, and 1001 nodes for the discretized temperature profile. The largest relative errors in each of the simulated results were approximately 0.001, 0.00006, 0.00002, 0.000003, and 0.000002, respectively.

Diffusion-Advection Transport of Heat

At the air-water interface a Dirichlet boundary condition was used, i.e. $\overline{T}\Big|_{z=0} =$ constant. At the water-sediment interface a Neumann (total flux) boundary condition was used, i.e. $\left(-\overline{K}_T \frac{\partial \overline{T}}{\partial z} + \overline{V_T}\ \overline{T}\right)\Big|_{z=L} = \frac{I_L}{\rho_0 c_p}$. The steady-state temperature profile is then:

$$\overline{T}(z) = a_{DA}\exp(-k_1 z) + b_{DA}\exp(d_{DA} z) + c_{DA} \tag{3.33}$$

where a_{DA}, b_{DA}, c_{DA}, and d_{DA} are constants. Simulations were performed using 11, 51, 101, 501, and 1001 nodes for the discretized temperature profile. The largest relative errors in each of the simulated results were approximately 0.1, 0.007, 0.003, 0.002, and 0.002, respectively.

Chapter 4

Classification of Trophic States

In order to numerically classify the trophic states of limnological environments, i.e., the continuous spectrum between oligotrophy and eutrophy, the *Self-Consistent Trophic State Index* (SCTSI) is proposed. This index is used as a guide to identify and probe biogeochemical and physical scenarios that possibly contribute to the eutrophication process.

In defining an index-based classification scheme for the trophic states of limnological environments, we require that the index satisfy the following two *a priori* specific requirements:

i. That the variables used to determine the trophic states of limnological environments be independent from any one particular model; and

ii. That the index not be arbitrarily defined.

These two requirements aim to address specific shortcomings of the currently-used so-called *Trophic State Index* (TSI) of *Carlson* (1977), defined immediately below.

4.1 The Trophic State Index (TSI)

The so-called *Trophic State Index* (TSI) proposed by *Carlson* (1977) is a single numerical value between 0 and 100, inclusive, that represents the continuum of the possible trophic states (oligotrophic to eutrophic) of limnological environments.

The TSI is an arbitrarily-chosen logarithmic-based scale that uses the doubling of algal biomass as the criterion for the divisions between trophic states. However, *Carlson* (1977) does not rely on direct empirical measurements of algal biomass in order to calculate the TSI; three empirically-measurable parameters that are correlated with algal biomass are used to calculate a TSI: the depth at which a Secchi disk is no longer visible to the naked eye (SD),[1] the chlorophyll *a* concentration (Chl),[2] or the total phosphorus concentration (TP):

$$\begin{aligned} \mathrm{TSI(SD)} &= 10\left(6 - \frac{\ln \mathrm{SD}}{\ln 2}\right) \\ \mathrm{TSI(Chl)} &= 10\left(6 - \frac{2.04 - 0.68 \ln \mathrm{Chl}}{\ln 2}\right) \\ \mathrm{TSI(TP)} &= 10\left(6 - \frac{\ln \frac{48}{\mathrm{TP}}}{\ln 2}\right). \end{aligned} \tag{4.1}$$

Carlson (1977) does not provide a formula for calculating a single, overall TSI value that encompasses all three parameters, for example, by averaging the three individual TSI values. In other words, one is free to choose from any of the above formulas to calculate a TSI. The trophic classification scheme based on the above TSI equations is tabulated by *Carlson* (1977):

[1] A so-called Secchi disk is a simple circular disk usually containing alternating black and white patterns. It is used to measure water transparency by submerging it from the air-water interface and measuring the depth at which the patterns can no longer be visible with the naked eye from the air-water interface.

[2] Chlorophyll *a* is a substance found in plant species required in order for photosynthesis to occur.

TSI (−)	**Secchi Disk** (m)	**Surface Chlorophyll** $(\mathrm{mg/m^3})$	**Surface Phosphorus** $(\mathrm{mg/m^3})$
0	64	0.04	0.75
10	32	0.12	1.5
20	16	0.34	3
30	8	0.94	6
40	4	2.6	12
50	2	6.4	24
60	1	20	48
70	0.5	56	96
80	0.25	154	192
90	0.12	427	384
100	0.062	1183	768

The TSI values of 0 and 100 represent the oligotrophic and eutrophic extremes, respectively. The TSI of equation (4.1) is calculated using $\mathrm{mg/m^3}$, as tabulated.

4.2 The Self-Consistent Trophic State Index (SCTSI)

Two difficulties exist with the TSI of *Carlson* (1977):

1. In defining the TSI, there is an incorrect assumption that a doubling in algal biomass results in halving Secchi disk transparency; and

2. The use of nutrient concentrations (i.e., phosphorus) to calculate an index value violate our first *a priori* requirement in defining an acceptable index-based trophic state classification scheme.

The difficulty in the first point arises largely from artificial construction of the TSI. Without any serious justifications, *Carlson* (1977) states i) that the doubling of algal

biomass concentration will be the criterion for the division of trophic states, ii) that the doubling of algal biomass would half the Secchi disk transparency "[b]ecause of the reciprocal relationship," and iii) that he "felt that the zero point on the scale should be located at a Secchi disk (SD) value greater than any yet reported" based on "[t]he next greatest integer on the $\log_2$ scale" (to that reported by *Hutchinson* (1957)), which is at 64 m.

What the TSI reflects, first and foremost, is that the doubling of algal biomass concentration to represent divisions of trophic states is completely arbitrary. Why not a tripling or quadrupling of algal biomass concentration? Moreover, the TSI calculation based on Secchi disk transparency does not take into consideration the light attenuation by other particulate matter, for example, detritus. This flaw is reinforced by the results of *Carlson* (1977) that graphically demonstrate that there is no direct one-to-one correlation between changes in algal biomass concentration and Secchi disk transparency in the sense that not every increase or decrease in algal biomass concentration results in a similar decrease or increase in Secchi disk transparency.

The second point presents a difficulty because certain nutrients (in this case, phosphorus) might not necessarily be involved in the reaction process producing algal biomass. Algal biomass growth is nutrient-limited in that it can exclusively utilize either phosphorus, nitrogen, or iron in the photosynthetic process. For example, phosphorus and iron can be overly abundant compared to nitrogen, yet nitrogen would act as the limiting nutrient in its utilization to promote algal biomass growth. In this case, phosphorus and iron concentration levels can potentially remain fairly constant since they will not participate in the uptake process. To this effect, *Carlson* (1977) graphically demonstrates that significant fluctuations in Secchi disk transparency and surface chlorophyll *a* concentrations do not necessarily correlate with changes in phosphorus concentrations. Given such adaptability by phytoplankton, the problem would not be addressed by simply incorporating other nutrients in the calculation of a TSI value.

The motivations for defining a new index *ab initio*, i.e., the *Self-Consistent Trophic State Index* (SCTSI), are the eliminations of the above-mentioned arbitrariness and difficulties in the TSI. We define the SCTSI to be a single numerical value in the continuum between 0 and 100, inclusive; this range of values represents the continuum of possible trophic states of limnological environments. We define the following ranges to represent distinct trophic states: $0 - 24 \equiv$ oligotrophic, $25 - 49 \equiv$ meso-oligotrophic, $50 \equiv$ mesotrophic, $51 - 74 \equiv$ meso-eutrophic and $75 - 100 \equiv$ eutrophic. The SCTSI is calculated as the fractional attenuation of light by the primary biomass concentration ([PB]):

$$\boxed{\mathrm{SCTSI} = 100 \times \frac{\int_0^L \left(k_2 \cdot [\mathrm{PB}]\right) dz'}{\int_0^L \left(k_1 + k_2 \cdot [\mathrm{BGC}]\right) dz'}} \tag{4.2}$$

where L is the depth of the water column, [BGC] is the sum concentration of all biogeochemical particulate matter (i.e., phytoplankton, zooplankton, detritus, and iron(III) hydroxide), and k_1 and k_2 are light attenuation coefficients as before. The denominator represents the total light-attenuating factor, namely attenuation due to molecular (k_1) and particulate (k_2) scattering and absorption, and is taken from equation (2.19).

The SCTSI represents the *potential* for light attenuation as opposed to actual attenuation. This avoids the difficulty in calculating an index value when there is no incident light at the air-water interface, for example, during the night. In this way, it is always possible to calculate an index value.[1]

With the above-proposed SCTSI, we also propose a way to directly connect the theoretical calculation of an index value with empirical measurements. For example, consider that disks are suspended every so-many metres throughout the water column along a wire stretching from the air-water interface to the water-sediment interface.

[1] Traditionally, the Secchi disk transparency is crudely measured using the naked eye, thereby limiting measurements to the daytime. However, the potential use of lasers instead of the naked eye would make measurements at any time of the day or night feasible.

These disks would act as detectors or filtration devices capturing particulate matter. The primary biomass can be extracted and an empirical calculation of the SCTSI can be performed. Moreover, the number and spacing of the disks could correspond to the numerical discretization scheme of the water column into nodes. This approach has the potential to introduce intermediate state conditions throughout the water column analogous to Dirichlet and Neumann boundary conditions.

When attempting to understand the tropic state using the SCTSI, it is important to not consider its value in isolation as a single snapshot in time. Eutrophication is a process, and so a time-evolution of the index is necessary to establish the overall tendency of the system and trophic state. This differs from the schemes implemented by *Carlson* (1977) and *Wetzel* (2001) where empirical measurements of biogeochemical species concentrations are not considered as a function of time and only measurements at one particular time are used to classify the environment into a trophic state. The tedious nature of sample collecting makes classificatory schemes based on empirical measurements grossly inefficient, which can potentially lead to incorrect classifications. Not only is the SCTSI capable of reproducing the experimentally-based classificatory scheme, but any change in the system can yield immediate results to indicate a possible change in trophic state. The inefficiencies of the *Carlson* (1977) and *Wetzel* (2001) schemes can be demonstrated by a simple example: empirical measurements are taken, the trophic state is determined to be oligotrophic, then minutes later anthropogenic runoff from a nearby farm injects into the ecosystem manure and detergent rich in phosphorus and nitrogen. Empirically, a whole new sampling is required as there is it likely that the trophic state will tend towards eutrophic. With the SCTSI, modelling the behaviour computationally is straightforward by changing the boundary conditions. The new state is immediately calculated, which can be corroborated by empirical measurements.

It may be argued that there are limitations of using the SCTSI in that it does not identify the formation of an anoxic region towards the lower portions of the water column

nor a reduction in animal populations. However, this is not a limitation or a problem of the SCTSI but rather of intentional design. Since eutrophication is a process, we manually examine whether or not an anoxic region is forming and there is a reduction in animal populations by simply looking at the respective concentration profiles. If a change is noticeable from one time step to the next, then it is safe to conclude the trophic state. Therefore, an index value calculated at any one particular point in time should only be regarded as a predisposition towards a particular trophic state. This is where empirical schemes like *Carlson* (1977) and *Wetzel* (2001) break down in efficiency in that they mandate subsequent field measurements.

Chapter 5

Results and Discussion

The reaction-transport model of Chapters 2 and 3 and the *Self-Consistent Trophic State Index* of Chapter 4 were used to numerically simulate different biogeochemical and physical scenarios in an attempt to provide insights into the eutrophication process of limnological environments. This investigation was motivated by the desire to phenomenologically understand the mechanisms that cause and sustain freshwater eutrophication and to determine if it is possible to predict when freshwater eutrophication will occur.

Phenomenological investigation is different from so-called parameter investigations of a model. In particular, parameter investigations are largely concerned with how different values for a model's parameters affect the model (for example, model output). In other words, the model itself becomes the subject of investigation with the aims of clarifying the limits of the model. On the other hand, a phenomenological investigation takes known, accepted values for its parameters and uses the model to identify trends and behaviours within a particular context. In the present context, we take acceptable parameter values from the literature and consider how the prognostic variables evolve in time.

5.1 Biogeochemical Interactions, Physical Forcing Mechanisms, and the Eutrophication Process

The effects that excessive nutrient loading have on the eutrophication process were examined in the absence and presence of physical forcing mechanisms, namely the effects that solar heating and wind-induced turbulence (the two physical forcing mechanisms) have on the eddy diffusivity and in turn how changes in the eddy diffusivity affect the biogeochemical reactions. The simulations were first performed in the absence of physical forcing (i.e., turbulent kinetic energy was kept constant at the minimum value imposed by the turbulence closure scheme) and then repeated with physical forcing present (i.e., dynamic turbulent kinetic energy). Solar insolation followed a diurnal cycle so that the environment experienced a natural and continuous transition between daytime and nightime. Each simulation was run for a period of 3 simulated months for the period of July-August-September (90 days) for which lakes are statistically correlated with eutrophic states (i.e., empirically, it is during this time that a limnological environment has the greatest chance of becoming eutrophic).

In the case where there was no physical forcing by solar heating nor wind-induced turbulence, temperature profile changes that were induced by the diurnal cycle were permitted to affect the coupling to the biogeochemical submodel, e.g., uptake of nutrients by phytoplankton, grazing of zooplankton on phytoplankton, remineralization of detritus, etc. However, solar heating represented as temperature gradients contributing to the production of turbulent kinetic energy were not permitted to alter the turbulent kinetic energy. In this case, the resulting eddy diffusivity was effectively constant given that there was no turbulent mixing and redistribution of heat throughout the water column. Moreover, the timescale of changes in the temperature profile due to changes in the diurnal solar insolation were much larger than the timescale of the biogeochemical kinetics and dynamics.

The resulting profiles have been self-normalized in order to facilitate a correlation-based analysis, i.e., each profile was normalized with its repsective maximum value. Furthermore, the number of nodes in the following graphs has been deliberately chosen so that the profiles appear coarse for three reasons:

1. To permit a much easier correlation analysis;

2. To mimic empirical measurement efforts; and

3. To improve computational efficiency without sacrificing accuracy. For example, the distance between nodes can be reduced from 10 m to 1 cm, which would provide extremely smooth curves, but at a *significant* computational price without providing additional information.

The parameter values chosen were those from the literature as referenced in the previous Theory chapter, namely from *Boudreau* (1997), *Edwards* (2001), *Gaspar et al.* (1990), *Gill* (1982), *Imboden* (1995), *Madsen et al.* (1986), *Omlin et al.* (2001), *Sarmiento* (2006), *Soetaert* (2001), and *Van Cappellen* (1993). With regards to the results presented here, we have the following parameter values: $c_k = 0.5$ (-), $c_\varepsilon = 0.1$ (-), $g = 9.8$ m/s^2, $I_0 = 1000$ W/m^2, $k_1 = 0.31$ m^{-1}, $k_2 = 0.026$ $\left([\,] \cdot \mathrm{m}\right)^{-2}$, $k_D = 0.1$ d^{-1}, $k_G = 0.3$ $\left([\,] \cdot \mathrm{d}\right)^{-1}$, $k_I = 34$ W/m^2, $k_{L,phyto} = 0.03$ d^{-1}, $k_{L,zoo} = 0.029$ d^{-1}, $k_{L,zoo,pr} = 1$ $\left([\,] \cdot \mathrm{d}\right)^{-1}$, $k'_{O_2} = 10$ μMO_2, $k'_{NO_3^-} = 10$ μMNO_3^-, $k_{RFe^{2+}} = 0.1$ d^{-1}, $k_{RFe(OH)_3} = 0.01$ d^{-1}, $k_{RNH_4^+} = 0.1$ d^{-1}, $k_{RNO_3^-} = 0.01$ d^{-1}, $k_{RO_2} = 0.01$ d^{-1}, $k_{Fe^{2+}} = 0.0001$ [ ], $k_{Fe(OH)_3} = 0.1$ [ ], $k_{H_3PO_4} = 0.0019$ [ ], $k_{NH_4^+} = 0.5$ [ ], $k_{NO_3^-} = 0.1$ [ ], $k_{O_2} = 0.4$ [ ], $k_{photo} = 0$ d^{-1}, $k_U = 1.1$ d^{-1}, $Pr_t = 1$ (-), $\alpha = 69\text{x}10^{-6}$ K^{-1}, $\beta_D = 0.046$ $(^\circ C)^{-1}$, $\beta_G = 0.08$ $(^\circ C)^{-1}$, $\beta_U = 0.046$ $(^\circ C)^{-1}$, $\gamma = 0.33$ (-), $\zeta = 0.25$ (-), $\mu = 0.035$ gC/m^3, $\rho_0 = 1025$ kg/m^3, $\Omega = 7.3\text{x}10^{-5}$ rad/s. All concentrations denoted by [ ] are in g/m^3 of the respective quantity. In the case of oxygen, the concentration is for O_2. Also, the natural settling velocities of phytoplankton and detritus were 5 m/d and 100 m/d, respectively.

Parameter choices global in scope were: 1) latitude of 45° in order to exhibit an appreciable Coriolis effect, 2) depth of 100 m for the lake, and 3) a constant wind (15 m/s) for the entire duration of the simulation run. A depth of 100 m has been encountered on numerous occasions in the literature. This depth is also sufficient in order to maintain two distinct zones in the case of wind-induced turbulence, as the effects of wind would only manifest within the upper region of the water column. This would allow one to determine whether the effects of wind-induced turbulence on eutrophication are shallow or deep. Additionally, when wind was introduced into the system, it was present and constant for the entire duration of the simulation run. The reason for doing this is discussed below. The initial conditions for the profiles was as follows: (1) horizontal velocity of water was set to a uniform profile of 0, (2) temperature of the water was a linear decline from 25 degrees Celsius at the air-water interface to 23 degrees celsius at the water-sediment interface, (3) turbulent kinetic energy was set to a uniform profile of its minimum value, $1\text{x}10^{-6}$ m^2/s^2, (4) all nutrients were pooled together and set at a uniform profile of 12 mg/m^3, (5) phytoplankton was set at a uniform profile of 2.6 mg/m^3, (6) zooplankton was set at a uniform profile of 0, (7) detritus was set at a uniform profile of 2.6 mg/m^3, and (8) oxygen was set to a uniform profile of 10 mg/m^3. These values were chosen in order to correspond to a TSI value of 40 according to *Carlson* (1977), which is a mesotrophic state. In the SCTSI scheme, the mesotrophic state is defined by a value of 50. Therefore, the concentrations for phytoplankton and detritus were set equal in order to achieve this. Lastly, the simulation timestep, i.e., the timestep used to propagate the solution forward in time and the interval of time between successive solutions in time, was 3 minutes. This timestep is sufficient to account for diffusive and advective mixing timescales (so as not to under represent the contributions of diffusive and advective mixing, which would occur if too large a timestep were to be used) and reasonable in computational efficiency.

5.1.1 Excessive Nutrient Loading in the Absence of Physical Forcing

The most trivial, but most important, biogeochemical interactions leading to eutrophication are those involving excessive nutrient loading of either phosphorus, nitrogen, or iron. The triviality of nutrient loading comes from the fact that since eutrophication is the result of plankton growth, providing plankton with abundant nourishment will lead to growth. However, nutrient loading is the result of external input into the environment. Unless this external input is sustained, the eutrophic state can then only possibly persist within a closed system of limit cycles between existing nutrients, plankton, and detritus, i.e., as detritus decays, nutrients are released into the environment so that living plankton can then uptake them and proliferate, then once these plankton die and decay they release nutrients and the process repeats indefinitely. The existence of limit cycles have been demonstrated by *Edwards* (2001). However, investigation using the present model was unable to reproduce either the limit cycles of *Edwards* (2001) or to produce limit cycles in general, which will be discussed shortly. The system always exhibited a long-term tendency for the phytoplankton to be completely eliminated from the water column. The amount of nutrients loaded into the system only seemed to affect the amount of time that it took to reach this end result.

We collapse phosphate, nitrate, ammonium, ferrous and ferric iron into a single "nutrient" pool. Two cases are then possible for simulations: (1) the system begins with an excess of nutrients and no further nutrients are ingested into the system, and (2) the system always has excess nutrients.

Remarkably, the results are all identical in that regardless of initial conditions and transient behaviour indicating a growth in phytoplankton, all phytoplankton eventually advected completely out of the water column and into the sediment. This result is shown in the following graph:

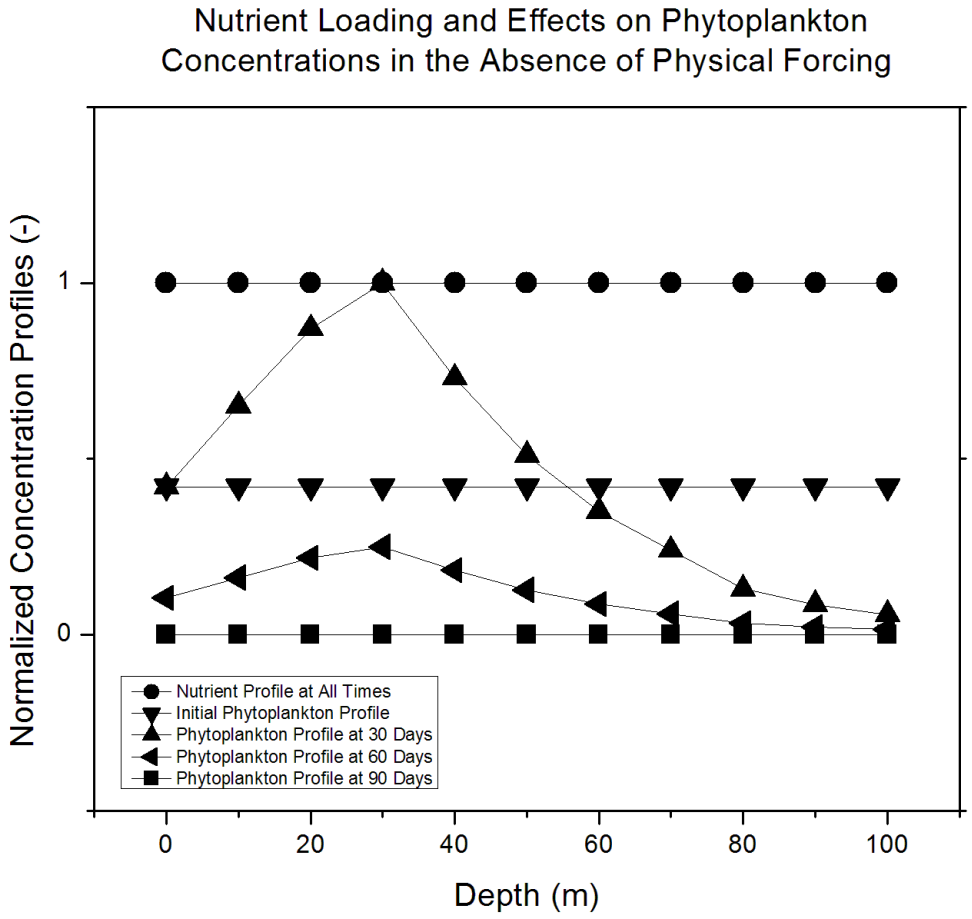

Figure 5.1: The effects of nutrient loading on the concentration of phytoplankton in the absence of physical forcing mechanisms.

The initial increase in phytoplankton concentrations as depicted in the previous graph suggests that there might be an increase in the value of the SCTSI. To better understand the dynamics of the lake, we consider a plot of the SCTSI as a function of time.

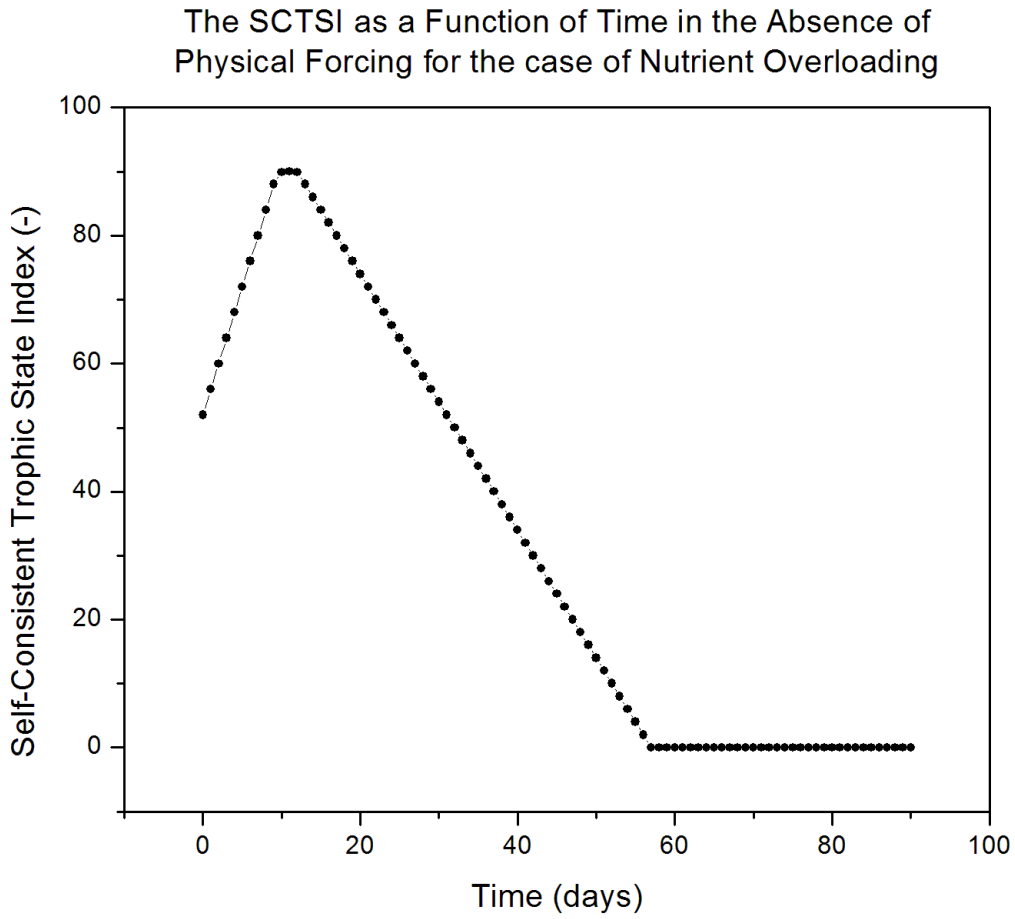

Figure 5.2: The Self-Consistent Trophic State Index as a function of time in the absence of physical forcing mechanisms for the case of nutrient overloading.

We see that there is a direct correlation in the increase and decrease of the value for the SCTSI to the increase and decrease of phytoplankton concentrations, as expected. However, there is one region that warrants special attention as it suggests that the SCTSI can produce erroneous values for the trophic state: 60 days. At this point, Figure 5.2 indicates an index value of 0, yet Figure 5.1 shows a non-zero phytoplankton concentration profile. Technically, a non-zero phytoplankton profile must have a corresponding non-zero index value. There are two reasons why this is not the case for the current situation: 1) numerical implementation approximating the cut-off for zero concentration

(i.e., at what small value of x do you say a concentration of 10^{-x} is effectively 0?), and 2) the overabundance of other particulate species (e.g., detritus) compared to phytoplankton. In this case, the ratio defining the SCTSI can be orders of magnitude smaller than the phytoplankton concentration profiles. In this latter case, the SCTSI can actually be used as a dynamical scale to gauge when a concentration should be effectively set to 0.

5.1.2 Excessive Nutrient Loading in the Presence of Physical Forcing

The physical forcing mechanisms considered are wind-induced turbulence and solar heating. In the cases involving solar heating, unlike in the previous section, the changes in temperature were permitted to directly affect the production of turbulent kinetic energy. However, the results were comparable to the previous section in that persistent eutrophic states were not observed.

The turbulence closure scheme used in the present model, which has been repeatedly tested and verified in the literature to be accurate, introduces the concept of a minimum value for the so-called turbulent kinetic energy. The sum of random fluctuating components of the velocity field (i.e., the sum that defines turbulent kinetic energy) must maintain a particular threshold in order to couple properly to eddy diffusivity since large bodies of water are never stagnant and this characterization must be maintained at all times. The manner in which turbulent kinetic energy scales in order to be in accordance with observation leads to a minimum value for the turbulent kinetic energy that is orders of magnitude larger than the molecular diffusivities of plankton, detritus, nutrients, etc. In other words, the mere presence of a turbulence closure scheme effectively imposes eddy diffusivity as *the* diffusivity for the biogeochemical species.

Models such as *Edwards* (2001) which do not incorporate a turbulence closure scheme rely on *molecular* diffusion as the mechanism responsible for diffusive transport. Such models are unrealistic for the reason that limnological environments are not strictly

stagnant. Artificially replacing the molecular diffusion coefficients in these models by a value of the eddy diffusivity corresponding to a constant minimum value for the turbulent kinetic energy completely destroyed limit cycle behaviour. The proposed explanation is straightforward: the diffusion becomes too great to sustain the species within the region of interaction. Therefore, under the conditions that Edwards proposes, namely using the parameter values chosen for biogeochemical interactions that produced limit cycles, it was not possible to produce nor sustain any sort of limit cycles. Possible alternate candidates for creating a persistent eutrophic state within the context of nutrient loading are: (1) external input of nutrients into the environment, and/or (2) quasi limit cycle behaviour due to dynamic eddy diffusivity. The latter can be thought of as an external driving frequency forcing the system to resonate. However, since the behaviour is not a true limit cycle (it is not possible to obtain an analytical solution to the system and no limit cycles were discovered through trial and error), the persistent eutrophic state is characterized by repetitive increases and decreases in plankton population, but without regard for exact repetitive values as what defines true limit cycles.

With regards to wind-induced turbulence, the observance of a persistent eutrophic state was possible. Initial conditions were irrelevant in that so long as there is some phytoplankton present in the system, then given the correct penetration depth of the wind to provide large-scale mixing, and the persistence of this wind, eutrophication was possible. The following graph (Fig. 5.3) shows a non-zero phytoplankton concentration profile at the end of 90 days with an SCTSI value of 91. Therefore, at the end of the simulation run, a eutrophic lake was produced. The profile for phytoplankton concentration is similar to the case of no physical forcing of the previous section, the main difference being that this profile persists and remains prominent.

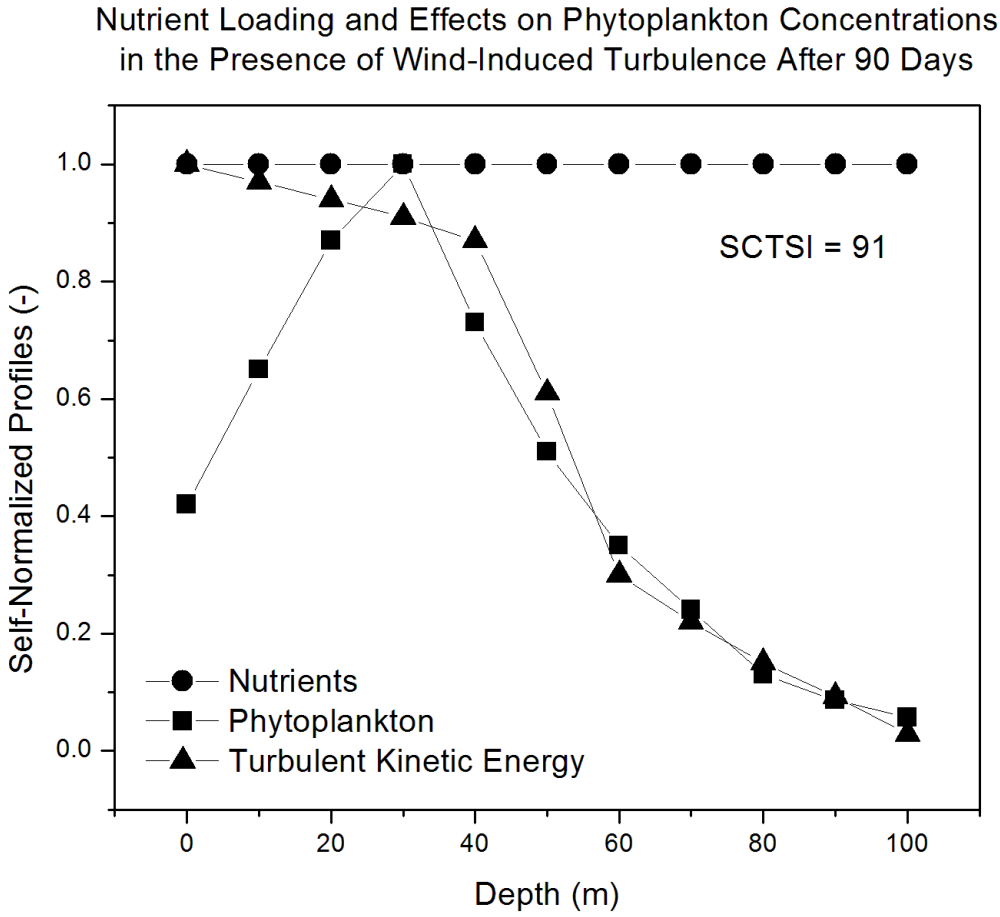

Figure 5.3: The effects of nutrient loading on the concentration of phytoplankton in the presence of wind-induced turbulence.

The following snapshot of multiple phytoplankton profiles demonstrates the existence of a wind-induced turbulent mixing zone, indicated by the profiles coinciding with each other at a depth of approximately 55m.

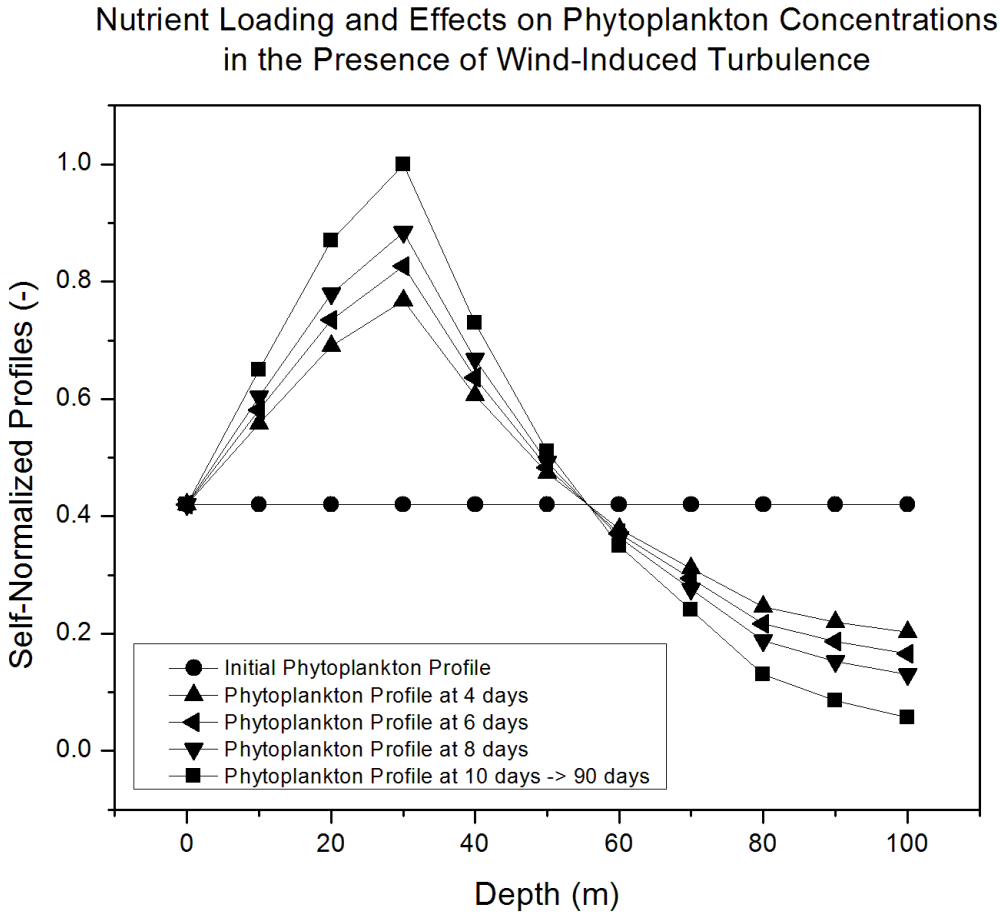

Figure 5.4: The effects of nutrient loading on the concentration of phytoplankton in the presence of wind-induced turbulence. Multiple superimposed phytoplankton profiles.

The overabundance of phytoplankton is readily observed when turbulent mixing layers are present in the water column. Turbulent mixing restricts phytoplankton from advecting towards the sediment and instead redistributes it from lower portions of the water column to upper portions. This redistribution permits the phytoplankton to continue to grow by providing it access to greater light intensity for photosynthetic production. Further access to nutrients does not appear necessary in order to stimulate additional growth. Turbulent mixing and redistribution of phytoplankton with a limited supply of nutrients only serves to accelerate the uptake of those nutrients by ensuring that more

phytoplankton gain access to the available nutrients. However, this is not the case when there is no competition among phytoplankton to uptake nutrients. When excessive nutrients are available for uptake, the determining factor whether or not phytoplankton will grow is access to more light.

The peak in the profile where the greatest concentration of phytoplankton occurs is determined mostly by two factors: (1) strength of the wind, and (2) natural settling velocity of phytoplankton. Stronger wind creates greater turbulent kinetic energy and greater penetration depth into the water column of this wind-induced turbulence. An increase in turbulent kinetic energy also results in an increase in the eddy diffusivity, resulting in less prominent peaks in the profile and instead exhibiting a more uniform distribution of the phytoplankton throughout the mixing layer. In these cases, the diffusive timescale is often much smaller than the advective timescale represented by the natural settling velocity of the phytoplankton. In cases where enough wind is present in order to induce a mixing layer, but mild enough to allow the phytoplankton to still exhibit their natural tendency to settle, a more prominent peak in the concentration profile will be identifiable. On the other hand, the choice of settling velocity creates competition between diffusive and advective transport, which would affect where the peak in the profile would occur. Also, given that the present model uses a general category for 'phytoplankton' changing the natural settling velocity of the phytoplankton could artificially mimic different species of phytoplankton. For example, a negative settling velocity, i.e., movement of phytoplankton towards the air-water interface, could mimic the flagellum present on some phyoplankton that allows them to propel themselves throughout the water column. A negative settling velocity could also represent the alterations in the phytoplankton's physical form so as to make itself more buoyant. In such cases, this velocity could be temperature or light-intensity dependent, as these would be the natural reasons for why phytoplankton would migrate upwards.

As in the previous section, we consider the SCTSI as a function of time:

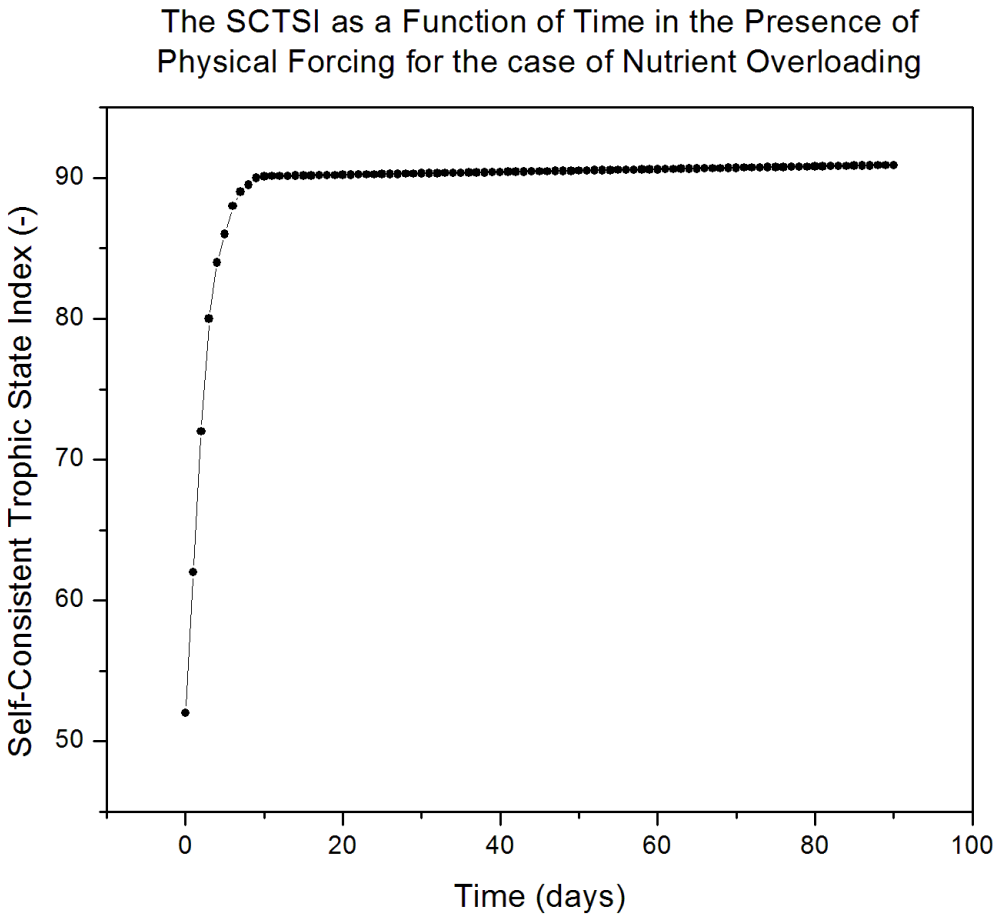

Figure 5.5: The Self-Consistent Trophic State Index as a function of time in the presence of wind-induced turbulence for the case of nutrient overloading.

In this case, we have a very prominent spike of the index value that stabilizes very quickly. The turbulent kinetic energy up to 40 m (i.e., the penetration depth of the wind) is an important region to understand the SCTSI values of Figure 5.4. In most cases, the competition for light absorption that defines the SCTSI will be between phytoplankton and detritus. On short turbulent timescales (i.e., eddy diffusivity), once detritus is close to the 40 m boundary, it has a tendency to advect out of this upper region and sink toward the sediment, eventually advecting out of the water column. On the other hand, the production of phytoplankton occurs much more quickly than the production of new

detritus in the upper region. Even though phytoplankton will advect out of the 40 m zone in the same manner as the detritus, hence leading to a similar profile distribution as in the non-physical forcing scenario, its replenishment in the upper 40 m region is sufficient to increase and maintain overall growth. Unlike photosynthesis that stimulates phytoplankton growth, there are no mechanisms to stimulate detrital growth. Therefore, the ratio defining the SCTSI becomes very quickly skewed towards 1, i.e., a eutrophic state.

Superimposing the two graphs for the SCTSI we have:

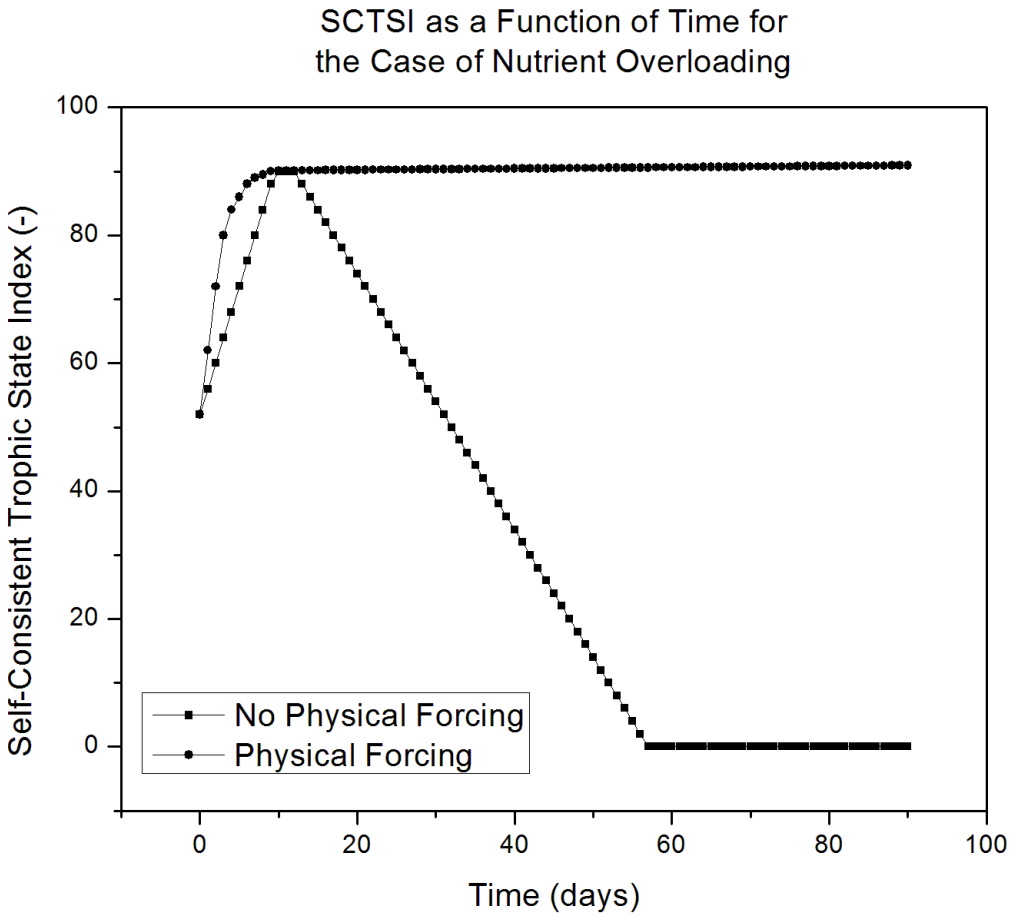

Figure 5.6: The Self-Consistent Trophic State Index as a function of time in the absence and presence of wind-induced turbulence for the case of nutrient overloading.

These plots suggest that biogeochemical interactions are largely responsible for inducing a eutrophic state, but that long-term maintenance of this state is only possible in the presence of physical forcing mechanisms that create a mixing zone in the upper portions of the water column via eddy diffusivity.

Preliminary investigations suggest that solar heating has virtually no effect in producing or sustaining eutrophication as its contribution to mixing, i.e., eddy diffusivity, is negligible. Despite the existence of diurnal cycles, contributions to solar-induced turbulence arise from temperature gradients of the water column and not changes in temperature alone. A distinct thermocline region can manifest throughout the entirety of limnological environments, in contrast to oceanic environments where a thermocline can persist anywhere from approximately 200 m - 1000 m. For limnological environments where depths of 100 m are reasonable, the change in temperature for the thermocline is typically on the order of a few degrees. However, when comparing to oceanic environments, what would be considered a thermocline in the limnological case would by no means be considered the thermocline in the oceanic case. In the oceanic case, a distinct thermocline typically manifests only after 100 m depth:

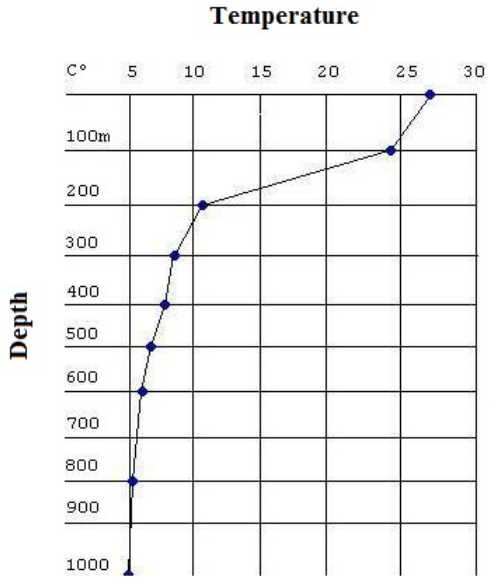

Figure 5.7: Typical oceanic thermocline profile.

This profile comes from the International Geophysical Year (an international scientific project) and published in the *Atlantic Ocean Atlas*, which is part of the *Woods Hole Oceanographic Institution Atlas Series*, Vol. 1. (Woods Hole: Woods Hole Oceanographic Institution, 1960).

From the above profile, the temperature gradient of an oceanic environment is much greater than in a typical limnological environment and can exhibit a temperature change of 15 °C for the thermocline. Within the limnological context, the "thermocline" stratification seems to play a meaningful role only insofar as it confines zooplankton to regions of constant density stratifications. Given that temperature is almost constant up to a depth of 100 m, its contribution to the production of turbulent kinetic energy is effectively negligible, i.e., $\frac{\partial \overline{T}}{\partial z} \approx 0$. Therefore, solar heating from the thermocline is not a sufficient source for the production of turbulent kinetic energy and eddy diffusivity in limnological environments.

On the other hand, wind-induced turbulence has significant contributions to the production of turbulence. The sheer stresses produced at the furthest depth of penetration by the wind can create a significant barrier to confine the ecosystem to this upper portion of the water column. In such cases, the biogeochemical species remain concentrated in this upper region and as a result, algal growth is stimulated leading to eutrophication. This correlates to the observed phenomenon that in the absence of wind-induced turbulence, regardless of the initial starting conditions, everything will eventually advect out of the water column and into the sediment, i.e., the steady-state solution is the trivial solution. We compare this to the steady-state solutions of *Edwards* (2001). Had *Edwards* (2001) instead used the minimum value of the turbulent kinetic energy imposed by the turbulence closure scheme, as opposed to using molecular diffusivity, then the steady-state limit cycles would be destroyed because everything would advect out of the region of interaction, i.e., eddy diffusivity is much larger than molecular diffusivity.

Since limnological environments where eutrophication occur are not stagnant bodies

of water, and therefore not governed by molecular diffusion, a more detailed investigation into periodic behaviour of the appearance and disappearance of eutrophication might support the proposal that local and global atmospheric phenomenon, namely wind, instead of biogeochemical interactions, are the main causes of eutrophication. Therefore, producing and sustaining eutrophication without considering turbulence, and specifically, wind-induced turbulence, seems to not be possible.

5.2 Nutrient Limitation

An avenue of investigation encountered in the literature with regards to reaction-transport modelling of biogeochemical quantities is the effects of competition between two or more nutrients involved in a particular process. While this avenue of investigation was not the focus of research herein, a handful of random scenarios were tested just to observe the effects that competition between phosphorus, nitrogen, and iron have on the eutrophication process in the framework elaborated above. Investigation into nutrient limitation dynamics warrants its own research endeavours and so the following remarks are cursory in nature.

When one nutrient required for organic matter synthesis (i.e., phytoplankton growth) approaches complete consumption from the environment, it is still possible for the eutrophic state to persist since nutrients can be injected back into the environment by the degradation of organic matter through oxidation, denitrification, or iron reduction, thereby allowing phytoplankton to still undergo the photosynthetic process.

Traditionally, the literature considers the Redfield ratio for phytoplankton composition to consist of only phosphorus and nitrogen as limiting nutrients. When the ratio is extended to include iron, even though it's amount in the ratio is significantly smaller, if it is the limiting nutrient, then it is possible to have overabundance of either phosphorus or nitrogen in the eutrophic state leading one to conclude incorrectly that eutrophication

is caused by the presence of only these two latter nutrients, as demonstrated by *Carlson* (1977). The over-reliance on phosphorus and nitrogen to the exclusion of iron persists to the present day as exhibited by *Soetaert* (2001) and *Omlin et al.* (2001). However, since iron can be present and abundant in limnological environments, its presence and limiting nature can be masked if there is an interplay and correlation between phosphorus-iron or nitrogen-iron as the limiting nutrient. Therefore, this would allow for approximately correct modelling of phosphorus and nitrogen cyclings, but erroneous conclusions as to what is causing the eutrophic state specifically. *Carlson* (1977) demonstrated that it is erroneous to assume a 1:1 correlation between eutrophic states and a particular nutrient. Despite that phosphorus concentrations are often exclusively identified with trophic states in the literature, empirical data presented by *Carlson* (1977) demonstrates that phosphorus concentrations can remain constant while Chlorophyll *a* and Secchi disk transparency values change. This would suggest that it is possible to have eutrophic states in both cases of abundance and non-abundance of phosphorus, since other nutrients, namely nitrogen and iron, are available for uptake by phytoplankton instead of phosphorus. In cases where only phosphorus and nitrogen are considered for the uptake of nutrients by phytoplankton, the actual dynamics could be due to an unconsidered contribution by iron, the effects of which are erroneously attributed to phosphorus or nitrogen. Therefore, the presence of iron as a limiting nutrient can lead to both of the following eutrophic scenarios: (i) abundance of phosphorus, non-abundance of nitrogen, or (ii) abundance of nitrogen, non-abundance of phosphorus.

The introduction of iron into the system presents a new problem, however: the consideration of pH. The rates of iron reduction and iron oxidation are dependent on pH. Varying the pH will change the rates of these reactions. Changes in these rates is important because the uptake of iron by phytoplankton can only be in its soluble form. High pH values induce iron precipitation; the higher the pH, the faster the precipitation. The opposite is also true: lower pH values dissolve iron into a form that can be uptaken

by phytoplankton. Therefore, changes in the pH value have a direct effect on whether or not iron is a limiting nutrient. The present model does not consider pH because it is possible to artificially model a particular pH value by imposing certain values for the parameters controlling the reaction kinetics. In order to appropriately incorporate pH into the model, other species that directly affect pH, such as carbonates, will have to be considered. Therefore, as a first approximation, the present model works strictly within a controlled environment that has a neutral pH.

Investigation into the effects that nutrient limitation has on the eutrophication process found that there were virtually no changes to the scenarios and results presented above. In the absence of physical forcing, the long-term state of the lake tended to oligotrophic. In the presence of physical forcing, a persistent eutrophic state was observed. When the nutrients are distinguished from each other, there are four possible routes that phytoplankton can uptake nourishment. If one of these routes is exhausted, then phytoplankton would simply uptake a different nutrient. For the phytoplankton, the situation is virtually identical as the case of nutrient overloading in that nutrients are always available. Investigation into the propagation in time of the individual nutrient concentration profiles and an examination of their cyclings was beyond the scope of the present research.

Chapter 6

Conclusions and Future Work

A one-dimensional numerical reaction-transport model of limnological dynamics was developed. The model developed is a coupled system of partial differential equations representing prominent physical and biogeochemical processes and interactions in limnological environments. The prognostic variables considered are temperature, horizontal velocity, salinity, and turbulent kinetic energy of the water column, and the concentrations of phytoplankton, zooplankton, detritus, phosphate (H_3PO_4), nitrate $\left(NO_3^-\right)$, ammonium $\left(NH_4^+\right)$, ferrous iron $\left(Fe^{2+}\right)$, iron(III) hydroxide $\left(Fe\left(OH\right)_3\left(s\right)\right)$, and oxygen ($O_2$) suspended within the water column. Turbulence is modelled using a classical $k-\varepsilon$ closure scheme.

The model was used to demonstrate how it is possible to investigate limnological trophic states by considering the problem of eutrophication as an example. A phenomenological investigation of processes leading to and sustaining eutrophication were examined. The specific scenario of nutrient loading, i.e., phytoplankton do not encounter scarcity in uptaking nourishment, was examined in the absence and presence of solar heating and wind-induced turbulence representing physical forcing mechanisms and the cause of large-scale turbulent mixing and eddy diffusivity.

A new indexing system that identifies different trophic states, the so-called *Self-*

Consistent Trophic State Index (SCTSI), was proposed. This index does not rely on empirical measurements that are then compared to existing tables for classifying limnological environments into particular trophic states. Rather, the index is calculated using dynamic properties of only the limnological environment being considered and examines how those properties affect the sustainability of the ecosystem. Specifically, the index is calculated from a ratio of light attenuation by the ecosystem's primary biomass to that of total light attenuation by all particulate species and molecular scattering throughout the entire water column.

The index was used as a guide to probe the effects and relevance of nutrient loading in the absence and presence of physical forcing on eutrophication. This research was motivated by the desire to answer three fundamental questions related to eutrophication:

1. *What mechanisms cause and sustain freshwater eutrophication?*

2. *Is it possible to predict when freshwater eutrophication will occur?*; and

3. *Can a single variable be used to reasonably characterize eutrophication?*

Preliminary findings suggest that the presence of a prominent turbulent mixing zone in the upper portions of the water column in conjunction with nutrient loading are required in order to produce and sustain a eutrophic state, which is characterized most prominently by a significant increase in and presence of phytoplankton. In the absence of a turbulent mixing zone, all simulated cases exhibited the trend towards a trivial steady-state where all phytoplankton would eventually die off or advect out of the water column into the sediment. On the other hand, the constant presence of a turbulent mixing zone ensured that phytoplankton that otherwise would have advected to the sediment are instead constantly redistributed to the upper portions of the water column.

While being motivated to know if it is possible to predict when eutrophication will occur, a conclusive answer to this question is, unfortunately, not forthcoming from the results of the research presented here. However, there are indications on how future

research could address this question: for a given set of initial conditions, a specific constant value for the wind speed would be chosen. Then, a long-term simulation would be performed just as has been done in this thesis. The trophic state as a function of time would be recorded. Then, a new simulation would be performed where the same initial conditions are again used but the wind speed is slightly changed. The idea is to repeat this process from a wind speed of 0, i.e., when no eutrophication will occur, up until a persistent eutrophic state is observed. It must be kept in mind that each particular initial condition might not share the same transition value. However, it might also be possible that the system has an attractor, in which case different initial conditions could approach the same solution. Given the complexity of the system, this would have to be determined statistically by performing numerous simulation runs and observing the time evolution of the trophic state in each case and comparing. Additional research could also investigate the effects of dynamic or stochastic wind speeds on the trophic states.

The empirical methods used in the literature permit the classification of trophic states, but the methods employed are laborious, inefficient, and inelegant. Moreover, the TSI of *Carlson* (1977) by design uses several subversions in order to create several index values that are statistical in nature and that do not necessarily correlate with each other. Despite its drawbacks, the TSI scheme has been proven successful in some trophic state classifications. However, the limitations of the TSI are successfully overcome by the SCTSI and does not suffer from any of its drawbacks and especially allows the classification of any arbitrary lake without recourse to approximations with other existing lakes that have been empirically tabulated. Nonetheless, the SCTSI has the potential to be refined.

The literature (e.g., *Wetzel* (2001)) defines two regions within the water column in relation to the production and degradation of an ecosystem's primary biomass: (1) trophogenic zone, and (2) tropholytic zone. The trophogenic zone is where photosynthesis and large-scale production of the biomass occurs and is restricted to the upper portions

of the water column. The tropholytic zone is the region in the water column where degradation of the biomass dominates. The boundary for these two zones (denoting the boundary depth as z^*) can be determined mathematically by examining the reaction rates of the primary biomass:

$$H = \left| \int_0^{z^*} r_{pb}\, dz - \int_0^{z^*+\delta} r_{pb}\, dz \right| \leq \epsilon \tag{6.1}$$

where ϵ is the tolerance.

Within the present framework, the SCTSI could then be refined by either performing the integration restricted to the trophogenic zone:

$$\text{SCTSI} = 100 \times \frac{\int_0^{z^*} \left(k_2 \cdot [\text{PB}]\right) dz'}{\int_0^{z^*} \left(k_1 + k_2 \cdot [\text{BGC}]\right) dz'} \tag{6.2}$$

or a ratio of the SCTSI values of the trophogenic zone and the entire water column:

$$\text{SCTSI} = 100 \times \frac{\int_0^{z^*} \left([\text{PB}]\right) dz'}{\int_0^{L} \left([\text{PB}]\right) dz'} \cdot \frac{\int_0^{L} \left(1 + \frac{k_2}{k_1} \cdot [\text{BGC}]\right) dz'}{\int_0^{z^*} \left(1 + \frac{k_2}{k_1} \cdot [\text{BGC}]\right) dz'}. \tag{6.3}$$

Investigations into refining the SCTSI in either of these ways would allow determination as to whether or not the turbulent mixing zone and trophogenic zone are synonymous.

Additional extensions to the model could include:

1. Coupling the water column to sediment and atmospheric models. This would allow proper couplings between these subenvironments instead of relying on artificial flux boundary conditions for the exchange of quantities. However, the coupling to the sediment might present one potential problem in that the sediment reaction-transport models fall under the category of 'stiff' systems. The biogeochemical

reactions are modelled in these systems on timescales much larger than the interactions would occur in the water column. Therefore, there is the problem of computational stability that would need to be addressed when coupling the two models.

2. The incorporation of flocs and the flocculation process. With regards to eutrophication, these particulate species would be another source for light attenuation and, therefore, affect the SCTSI value.

3. Allowing for variations in pH. Changes in pH would affect reaction kinetics. This would also require incorporating into the model additional chemical species such as calcium, sulfur, and magnesium.

There is also the possibility of testing different turbulence closure schemes.

Appendix A

Derivation of Hydrodynamic Equations

For a more in-depth treatment, please refer to the classical textbooks on the subject *Landau and Lifshitz* (1986) and *Monin and Yaglom* (1971).

A.1 The Continuity Equation

We equate the total mass flux per unit time out of an arbitrary volume element dV to that of the total mass decrease per unit time inside this volume element:

$$\oint_S \rho \mathbf{v} \cdot dS = -\frac{d}{dt} \int_V \rho dV \tag{A.1}$$

where the left-hand side is the mass flux per unit time across the surface enclosing the volume element dV and the minus sign denotes a decrease inside dV. We take the convention that outward fluxes across the surface bounding dV to be positive. Then,

using the divergence theorem, we can convert the surface integral into a volume integral:

$$\oint_S \rho \mathbf{v} \cdot dS = \int_V \nabla \cdot (\rho \mathbf{v})\, dV = -\frac{d}{dt} \int_V \rho dV \tag{A.2}$$

Upon rearranging terms and invoking the *transport theorem*, which allows us to bring the time derivative within the integral, and observing that the equality is valid for any arbitrary volume element dV, we get the continuity equation:

$$\boxed{\frac{\partial \rho}{\partial t} + \nabla \cdot (\rho \mathbf{v}) = 0}. \tag{A.3}$$

We now consider the case of a biogeochemical species whose concentration (in moles per unit volume of fluid) is C and apply the principle of conservation to this situation, for which the physical quantity conserved is the total number of moles of a given chemical element. In this case, the density $\rho \mathbf{v}$ is the concentration C. We introduce a current density $\mathbf{J}_Q$ which has contributions $\mathbf{v}C$ due to macroscopic transport through the surface delimiting dV, and diffusive transport, $\mathbf{J}_D$:

$$\mathbf{J}_Q = \mathbf{J}_D + \mathbf{v}C. \tag{A.4}$$

Finally, there is also the case where biogeochemical reactions convert the identity of the species in the fluid. In this case, we let r denote the reaction rate (number of moles transformed per unit time per unit volume). The principle of conservation of the number of moles is written as follows:

$$\frac{\partial C}{\partial t} + \nabla \cdot \mathbf{J}_D + \nabla \cdot (\mathbf{v}C) - r = 0 \tag{A.5}$$

There is an empirical law (constitutive) expressing the diffusive transport of molecules. Experience confirms that this transport is proportional to the gradient concentration.

The proportionality coefficient is called the diffusion coefficient K. Therefore, we have:

$$\mathbf{J}_D = -K\nabla C \tag{A.6}$$

Making this substitution into the preceding equation and rearranging terms gives:

$$\boxed{\frac{\partial C}{\partial t} + \nabla \cdot (\mathbf{v}C) = \nabla \cdot (K\nabla C) + r} \tag{A.7}$$

A.2 The Navier-Stokes Equation

The Navier-Stokes equation is the equation that results from applying the conservation of momentum (Newton's second law of motion) to a volume of fluid:

$$\begin{aligned} \frac{d\mathbf{p}}{dt} &= -\int_S p\mathbf{n}dS + \int_V \rho\mathbf{F}_b dV \\ \frac{d}{dt}\left(\int_V \rho\mathbf{v}dV\right) &= -\int_S p\mathbf{n}dS + \int_V \rho\mathbf{F}_b dV \end{aligned} \tag{A.8}$$

where $\mathbf{p}$ denotes the momentum of the volume of fluid, S is the surface bounding the volume of fluid, p is the pressure, $\mathbf{n}$ is the normal to S, and $\mathbf{F}_b$ represents the body forces per unit mass acting on the volume of fluid. By considering the fluid inviscid, the only internal forces considered are those due to the pressure. Using the *transport theorem* for differentiating over a volume on the left-hand side, converting from a total derivative to partial derivatives, and using the divergence theorem on the right-hand side, we transform the preceding equation into:

$$\int_V \left(\frac{\partial(\rho\mathbf{v})}{\partial t} + \nabla \cdot (\rho\mathbf{v}\mathbf{v})\right) dV = \int_V \left(-\nabla p + \rho\mathbf{F}_b\right) dV \tag{A.9}$$

Since this relation is valid for any arbitrary volume V, we have:

$$\boxed{\frac{\partial(\rho\mathbf{v})}{\partial t} + \nabla\cdot(\rho\mathbf{v}\mathbf{v}) = \nabla(\eta\nabla\mathbf{v}) - \nabla p + \rho\mathbf{F}_b}. \tag{A.10}$$

A.3 Turbulent Kinetic Energy, $\overline{e}$

Recall the definition of turbulent kinetic energy:

$$\overline{e} \equiv \frac{1}{2}\sum_i \overline{v_i' v_i'} \tag{A.11}$$

where i denotes the respective components in a particular coordinate system. We develop the rate equation for e by applying Reynolds' decomposition to the Navier-Stokes equation and manipulating to obtain an expression for $\frac{\partial\left(\overline{v_i' v_i'}\right)}{\partial t}$.

Substituting the Reynolds' decomposition of the velocity field, pressure, and source/sink terms into the Navier-Stokes equation gives:

$$\frac{\partial\left[\rho\left(\overline{\mathbf{v}}+\mathbf{v}'\right)\right]}{\partial t} + \nabla\cdot\left[\rho\left(\overline{\mathbf{v}}+\mathbf{v}'\right)\left(\overline{\mathbf{v}}+\mathbf{v}'\right)\right] = \nabla\cdot\left(\eta\nabla\left(\overline{\mathbf{v}}+\mathbf{v}'\right)\right) - \nabla\left(\overline{p}+p'\right) + ... \tag{A.12}$$

The buoyancy term is considered later. Currently, it is left out and it's possible inclusion is represented by '...' which encompasses other terms dependent on context. The time-averaged form of this equation is:

$$\frac{\partial(\rho\overline{v}_i)}{\partial t} + \overline{\mathbf{v}}\cdot\nabla(\rho\overline{v}_i) = \nabla\cdot(\eta\nabla\overline{v}_i) - \nabla\overline{p} - \nabla\cdot\left(\rho\overline{v_i'\mathbf{v}'}\right) \tag{A.13}$$

where $-\rho\overline{v_i'\mathbf{v}'}$ are the Reynolds' stress terms. Then, subtracting equation $(A.13)$ from equation $(A.12)$ gives:

$$\frac{\partial(\rho v_i')}{\partial t} + \overline{\mathbf{v}}\cdot\nabla\left(\rho v_i'\right) + \mathbf{v}'\cdot\nabla(\rho\overline{v_i}) + \mathbf{v}'\cdot\nabla\left(\rho v_i'\right) = \nabla\cdot\left(\eta\nabla v_i'\right) - \nabla p' + \nabla\cdot\left(\rho\overline{v_i'\mathbf{v}'}\right). \tag{A.14}$$

Next, we multiply equation ($A.14$) by the fluctuating velocity component v_i':

$$\begin{aligned} v_i'\frac{\partial\left(\rho v_i'\right)}{\partial t} + v_i'\overline{\mathbf{v}}\cdot\nabla\left(\rho v_i'\right) + v_i'\mathbf{v}'\cdot\nabla\left(\rho\overline{v_i}\right) + v_i'\mathbf{v}'\cdot\nabla\left(\rho v_i'\right) \\ = v_i'\nabla\cdot\left(\eta\nabla v_i'\right) - v_i'\nabla p' + v_i'\nabla\cdot\left(\rho\overline{v_i'\mathbf{v}'}\right). \end{aligned} \tag{A.15}$$

Adding equation ($A.15$) to itself, time-averaging, and assuming incompressibility of the fluid, i.e. $\nabla\cdot\mathbf{v}=0$, gives:

$$\begin{aligned} \frac{\partial\left(\overline{v_i'v_i'}\right)}{\partial t} =& -\overline{\mathbf{v}}\cdot\nabla\left(\overline{v_i'v_i'}\right) - 2\overline{v_i'\mathbf{v}'}\cdot\nabla\overline{v_i} - 2\overline{v_i'\mathbf{v}'\cdot\nabla v_i'} \\ &+ \nabla\cdot\left[\frac{\eta}{\rho_0}\nabla\left(\overline{v_i'v_i'}\right)\right] + 2\sum_{i,j}\frac{\partial}{\partial x_i}\left[\frac{\eta}{\rho_0}\frac{\partial}{\partial x_j}\left(\overline{v_i'v_j'}\right)\right] - \frac{\eta}{\rho_0}\left[\sum_{i,j}\overline{\left(\frac{\partial v_i'}{\partial x_j}+\frac{\partial v_j'}{\partial x_i}\right)^2}\right] \\ &- \frac{2}{\rho_0}\nabla\cdot\overline{\mathbf{v}'p'} - \nabla\cdot\overline{v_i'v_i'\mathbf{v}'}. \end{aligned} \tag{A.16}$$

Rearranging terms and dividing through by 2 gives:

$$\begin{aligned} \frac{\partial\left(\frac{\overline{v_i'v_i'}}{2}\right)}{\partial t} =& -\nabla\cdot\left(\frac{\overline{v_i'v_i'\mathbf{v}'}}{2} + \frac{\overline{\mathbf{v}'p'}}{\rho_0}\right) - \overline{v_i'\mathbf{v}'}\cdot\nabla\overline{v_i} \\ &- \frac{1}{2}\overline{\mathbf{v}}\cdot\nabla\left(\overline{v_i'v_i'}\right) - \overline{v_i'\mathbf{v}'\cdot\nabla v_i'} \\ &+ \nabla\cdot\left[\frac{1}{2}\frac{\eta}{\rho_0}\nabla\left(\overline{v_i'v_i'}\right)\right] + \sum_{i,j}\frac{\partial}{\partial x_i}\left[\frac{\eta}{\rho_0}\frac{\partial}{\partial x_j}\left(\overline{v_i'v_j'}\right)\right] - \frac{1}{2}\frac{\eta}{\rho_0}\left[\sum_{i,j}\overline{\left(\frac{\partial v_i'}{\partial x_j}+\frac{\partial v_j'}{\partial x_i}\right)^2}\right]. \end{aligned} \tag{A.17}$$

Resolving only the z component and making the substitution $\overline{e} \equiv \frac{\overline{v_i' v_i'}}{2}$ gives:

$$\begin{aligned}\frac{\partial \overline{e}}{\partial t} =& -\frac{\partial}{\partial z}\left(\overline{v_z' e} + \frac{\overline{v_z' p'}}{\rho_0}\right) - \overline{v_z' \mathbf{v}'} \cdot \frac{\partial \overline{\mathbf{v}}}{\partial z} \\ & - \overline{v_z}\frac{\partial \overline{e}}{\partial z} - \overline{v_z' \mathbf{v}'} \cdot \frac{\partial \overline{\mathbf{v}'}}{\partial z} \\ & + \nabla \cdot \left[\frac{1}{2}\frac{\eta}{\rho_0}\nabla\left(\overline{v_i' v_i'}\right)\right] + \sum_{i,j}\frac{\partial}{\partial x_i}\left[\frac{\eta}{\rho_0}\frac{\partial}{\partial x_j}\left(\overline{v_i' v_j'}\right)\right] - \frac{1}{2}\frac{\eta}{\rho_0}\left[\sum_{i,j}\overline{\left(\frac{\partial v_i'}{\partial x_j} + \frac{\partial v_j'}{\partial x_i}\right)^2}\right].\end{aligned} \tag{A.18}$$

By definition, $\overline{\mathbf{v}'} = 0$. Also, if we make the approximation that $\overline{v_z} \cong 0$, then we have:

$$\begin{aligned}\frac{\partial \overline{e}}{\partial t} =& -\frac{\partial}{\partial z}\left(\overline{v_z' e} + \frac{\overline{v_z' p'}}{\rho_0}\right) - \overline{v_z' \mathbf{u}'} \cdot \frac{\partial \overline{\mathbf{u}}}{\partial z} \\ & + \nabla \cdot \left[\frac{1}{2}\frac{\eta}{\rho_0}\nabla\left(\overline{v_i' v_i'}\right)\right] + \sum_{i,j}\frac{\partial}{\partial x_i}\left[\frac{\eta}{\rho_0}\frac{\partial}{\partial x_j}\left(\overline{v_i' v_j'}\right)\right] - \frac{1}{2}\frac{\eta}{\rho_0}\left[\sum_{i,j}\overline{\left(\frac{\partial v_i'}{\partial x_j} + \frac{\partial v_j'}{\partial x_i}\right)^2}\right].\end{aligned} \tag{A.19}$$

where $\mathbf{u} = (v_x, v_y)$. The last term in the preceding equation is the rate of dissipation of the turbulent kinetic energy:

$$\varepsilon \equiv \frac{1}{2}\frac{\eta}{\rho_0}\left[\sum_{i,j}\overline{\left(\frac{\partial v_i'}{\partial x_j} + \frac{\partial v_j'}{\partial x_i}\right)^2}\right]. \tag{A.20}$$

We can safely identify its appearance in the equation as a dissipative term because the quantity itself is always positive and within the equation it is preceded by a negative sign. Therefore, it will always reduce turbulent kinetic energy. Making this substitution

into the equation gives:

$$\begin{aligned}\frac{\partial \overline{e}}{\partial t} =& -\frac{\partial}{\partial z}\left(\overline{v_z' e} + \frac{\overline{v_z' p'}}{\rho_0}\right) - \overline{v_z' \mathbf{u}'} \cdot \frac{\partial \overline{\mathbf{u}}}{\partial z} - \varepsilon \\ &+ \nabla \cdot \left[\frac{1}{2}\frac{\eta}{\rho_0}\nabla\left(\overline{v_i' v_i'}\right)\right] + \sum_{i,j}\frac{\partial}{\partial x_i}\left[\frac{\eta}{\rho_0}\frac{\partial}{\partial x_j}\left(\overline{v_i' v_j'}\right)\right].\end{aligned} \tag{A.21}$$

Given that turbulent transport is orders of magnitude greater than molecular transport, the last two terms of the preceding equation are negligible in comparison and can be dropped. The only other term left to consider is the buoyancy term. This term could have been added at the outset of equation (A.13) as $\delta_{i3} b = \delta_{i3}\overline{b} + \delta_{i3} b'$. The Kronecker delta is used to resolve the so-called Boussinesq approximation in only the z coordinate (where i = {1, 2, 3} corresponds to coordinates {x, y, z}, respectively). The algebra on b follows in the preceding equations is straightforward, leaving only the turbulent correlated term $\overline{v_z' b'}$. Therefore, inserting this into the equation gives:

$$\boxed{\frac{\partial \overline{e}}{\partial t} = -\frac{\partial}{\partial z}\left(\overline{v_z' e} + \frac{\overline{v_z' p'}}{\rho_0}\right) - \overline{v_z' \mathbf{u}'} \cdot \frac{\partial \overline{\mathbf{u}}}{\partial z} + \overline{v_z' b'} - \varepsilon}. \tag{A.22}$$

Appendix B

Summary of Model

Variable and parameter definitions can be found in the ***List of Symbols*** at the beginning of the thesis.

B.1 Prognostic Rate Equations

$$
\begin{cases}
\dfrac{\partial \overline{\mathbf{u}}}{\partial t} = \dfrac{\partial}{\partial z}\left(\overline{K}_u \dfrac{\partial \overline{\mathbf{u}}}{\partial z}\right) + f\left(\hat{\mathbf{z}} \times \overline{\mathbf{u}}\right) \\
\dfrac{\partial \overline{e}}{\partial t} = \dfrac{\partial}{\partial z}\left(\overline{K}_u \dfrac{\partial \overline{e}}{\partial z}\right) + \overline{K}_u \dfrac{\partial \overline{\mathbf{u}}}{\partial z} \cdot \dfrac{\partial \overline{\mathbf{u}}}{\partial z} + g\alpha \overline{K}_u \dfrac{\partial \overline{T}}{\partial z} - g\beta \overline{K}_u \dfrac{\partial \overline{S}}{\partial z} - \varepsilon \\
\dfrac{\partial \overline{T}}{\partial t} = \dfrac{\partial}{\partial z}\left(\overline{K}_u \dfrac{\partial \overline{T}}{\partial z}\right) - \dfrac{1}{\rho_0 c_p} \dfrac{\partial I}{\partial z} \\
\dfrac{\partial \overline{S}}{\partial t} = \dfrac{\partial}{\partial z}\left(\overline{K}_u \dfrac{\partial \overline{S}}{\partial z}\right) \\
\dfrac{\partial \mathrm{C}_{*,1}}{\partial t} = \dfrac{\partial}{\partial z}\left(\overline{K}_u \dfrac{\partial \mathrm{C}_{*,1}}{\partial z}\right) - \dfrac{\partial}{\partial z}\left(\overline{V}_{C_{*,1}} \mathrm{C}_{*,1}\right) + r_{C_{*,1}} \\
\dfrac{\partial \mathrm{C}_{*,2}}{\partial t} = \dfrac{\partial}{\partial z}\left(\overline{K}_u \dfrac{\partial \mathrm{C}_{*,2}}{\partial z}\right) + r_{C_{*,2}}
\end{cases}
$$

$$\mathrm{C}_{*,1} = \overline{[\mathrm{PHYTO}]}, \overline{[\mathrm{ZOO}]}, \overline{[\mathrm{DET}]}, \overline{\left[\mathrm{Fe(OH)_3}\right]}$$

$$\mathrm{C}_{*,2} = \overline{[\mathrm{H_3PO_4}]}, \overline{\left[\mathrm{NO_3^-}\right]}, \overline{\left[\mathrm{NH_4^+}\right]}, \overline{\left[\mathrm{Fe^{2+}}\right]}, \overline{[\mathrm{O_2}]}$$

$$\overline{K}_u = c_k l_k \sqrt{\overline{e}}$$

$$\varepsilon = \frac{c_\varepsilon \overline{e}^{\frac{2}{3}}}{l_\varepsilon}$$

$$l_k = \min\left(l_u, l_d\right)$$

$$l_\varepsilon = \sqrt{l_u l_d}$$

$$\overline{e}\left(z_0\right) = \int_{z_0}^{z_0 - l_u} g\left(\alpha\left[\overline{T}\left(z_0\right) - \overline{T}\left(z\right)\right] - \beta\left[\overline{S}\left(z_0\right) - \overline{S}\left(z\right)\right]\right) dz$$

$$\overline{e}\left(z_0\right) = \int_{z_0}^{z_0 + l_d} g\left(\alpha\left[\overline{T}\left(z_0\right) - \overline{T}\left(z\right)\right] - \beta\left[\overline{S}\left(z_0\right) - \overline{S}\left(z\right)\right]\right) dz$$

$$I\left(z\right) = I_0 e^{\left(-\int_0^z \left(k_1 + k_2 \cdot [\mathrm{BGC}]\right) dz'\right)}$$

B.2 Biogeochemical Reactions

- Photosynthesis I ($\mathrm{NH_4^+}$-Induced):

$$\begin{aligned} &a\mathrm{CO_2} + b\mathrm{NH_4^+} + c\mathrm{H_3PO_4} + d\mathrm{Fe^{2+}} + a\mathrm{H_2O} \\ &\quad \xrightarrow[synthesis]{photo} \left(\mathrm{CH_2O}\right)_a \left(\mathrm{NH_3}\right)_b \left(\mathrm{H_3PO_4}\right)_c \left(\mathrm{FeT}\right)_d + a\mathrm{O_2} + b\mathrm{H^+} \end{aligned} \tag{R1}$$

- Photosynthesis II (NO_3^--Induced):

$$\begin{aligned} &a\mathrm{CO_2} + b\mathrm{NO_3^-} + c\mathrm{H_3PO_4} + d\mathrm{Fe^{2+}} + (a+b)\,\mathrm{H_2O} + b\mathrm{H^+} \\ &\xrightarrow[synthesis]{photo} (\mathrm{CH_2O})_a\,(\mathrm{NH_3})_b\,(\mathrm{H_3PO_4})_c\,(\mathrm{FeT})_d + (a+2b)\,\mathrm{O_2} \end{aligned} \tag{R2}$$

- Oxidation (RO_2):

$$\begin{aligned} &(\mathrm{CH_2O})_a\,(\mathrm{NH_3})_b\,(\mathrm{H_3PO_4})_c\,(\mathrm{FeT})_d + a\mathrm{O_2} + b\mathrm{H^+} \\ &\xrightarrow{\mathrm{RO_2}} a\mathrm{CO_2} + b\mathrm{NH_4^+} + c\mathrm{H_3PO_4} + d\mathrm{Fe^{2+}} + a\mathrm{H_2O} \end{aligned} \tag{R3}$$

- Denitrification $\left(\mathrm{RNO_3^-}\right)$:

$$\begin{aligned} &(\mathrm{CH_2O})_a\,(\mathrm{NH_3})_b\,(\mathrm{H_3PO_4})_c\,(\mathrm{FeT})_d + \frac{4}{5}a\mathrm{NO_3^-} + \left(\frac{4}{5}a + b\right)\mathrm{H^+} \\ &\xrightarrow{\mathrm{RNO_3^-}} a\mathrm{CO_2} + b\mathrm{NH_4^+} + c\mathrm{H_3PO_4} + d\mathrm{Fe^{2+}} + \frac{7}{5}a\mathrm{H_2O} + \frac{2}{5}a\mathrm{N_2} \end{aligned} \tag{R4}$$

- Reduction of Iron $\left(\mathrm{RFe(OH)_3}\right)$:

$$\begin{aligned} &(\mathrm{CH_2O})_a\,(\mathrm{NH_3})_b\,(\mathrm{H_3PO_4})_c\,(\mathrm{FeT})_d + 4a\mathrm{Fe(OH)_3(s)} + (8a+b)\,\mathrm{H^+} \\ &\xrightarrow{\mathrm{RFe(OH)_3}} a\mathrm{CO_2} + b\mathrm{NH_4^+} + c\mathrm{H_3PO_4} + (4a+d)\,\mathrm{Fe^{2+}} + 11a\mathrm{H_2O} \end{aligned} \tag{R5}$$

- Nitrification $\left(\mathrm{RNH_4^+}\right)$:

$$\mathrm{NH_4^+} + 2\mathrm{O_2} \xrightarrow{\mathrm{RNH_4^+}} \mathrm{NO_3^-} + \mathrm{H_2O} + 2\mathrm{H^+} \tag{R6}$$

- Iron Oxidation $\left(\mathrm{RFe^{2+}}\right)$:

$$\mathrm{Fe^{2+}} + \frac{1}{4}\mathrm{O_2} + \frac{5}{2}\mathrm{H_2O} \xrightarrow{\mathrm{RFe^{2+}}} \mathrm{Fe(OH)_3(s)} + 2\mathrm{H^+} \tag{R7}$$

B.3 Biogeochemical Reaction Kinetics

$$\mathrm{RO_2} = k_{RO_2} \cdot \overline{[\mathrm{DET}]} \cdot \frac{\overline{[\mathrm{O_2}]}}{\overline{[\mathrm{O_2}]} + k_{O_2}}$$

$$\mathrm{RNO_3^-} = k_{RNO_3^-} \cdot \overline{[\mathrm{DET}]} \cdot \frac{\overline{\left[\mathrm{NO_3^-}\right]}}{\overline{\left[\mathrm{NO_3^-}\right]} + k_{NO_3^-}} \cdot \frac{k'_{O_2}}{k'_{O_2} + \overline{[\mathrm{O_2}]}}$$

$$\mathrm{RFe(OH)_3} = k_{RFe(OH)_3} \cdot \overline{[\mathrm{DET}]} \cdot \frac{\overline{\left[\mathrm{Fe(OH)_3}\right]}}{\overline{\left[\mathrm{Fe(OH)_3}\right]} + k_{Fe(OH)_3}} \cdot \frac{k'_{NO_3^-}}{k'_{NO_3^-} + \overline{\left[\mathrm{NO_3^-}\right]}} \cdot \frac{k'_{O_2}}{k'_{O_2} + \overline{[\mathrm{O_2}]}}$$

$$\mathrm{RNH_4^+} = k_{RNH_4^+} \cdot \overline{\left[\mathrm{NH_4^+}\right]} \cdot \overline{[\mathrm{O_2}]}$$

$$\mathrm{RFe^{2+}} = k_{RFe^{2+}} \cdot \overline{[\mathrm{Fe^{2+}}]} \cdot \overline{[\mathrm{O_2}]} - \Phi\left(I\right) \cdot \overline{\left[\mathrm{Fe(OH)_3}\right]}$$

B.4 Biogeochemical Reaction Rates

$$
\begin{cases}
r_{phyto} = U - G_{phyto} - L_{phyto} \\
r_{zoo} = \zeta\left(G_{phyto} + G_{det}\right) - L_{zoo} - L_{zoo,pr} \\
r_{det} = L_{phyto,zoo} + zoo_{exc} - det_{remin} \\
r_{H_3PO_4} = c\left(\gamma\left(G_{phyto} + G_{det}\right) + \mathrm{RO}_2 + \mathrm{RNO}_3^- + \mathrm{RFe(OH)}_3 - U\right) \\
r_{NO_3^-} = \mathrm{RNH}_4^+ - \frac{4}{5}a\mathrm{RNO}_3^- - bU_{NO_3^-} \\
r_{NH_4^+} = b\left(\mathrm{RO2} + \mathrm{RNO}_3^- + \mathrm{RFe(OH)}_3 + \gamma\left(G_{phyto} + G_{det}\right) - U_{NH_4^+}\right) - \mathrm{RNH}_4^+ \\
r_{Fe^{2+}} = d\left(\mathrm{RO2} + \mathrm{RNO3} + \left(\frac{4a}{d} + 1\right)\mathrm{RFe(OH)}_3 - U\right) - \mathrm{RFe}^{2+} \\
r_{Fe(OH)_3} = \mathrm{RFe}^{2+} - 4a\mathrm{RFe(OH)}_3 \\
r_{O_2} = aU_{NH_4^+} + (a+2b)\,U_{NO_3^-} - \gamma\left(G_{phyto} + G_{det}\right) - a\mathrm{RO}_2 - 2\mathrm{RNH}_4^+ \\
\qquad\qquad - \frac{1}{4}\mathrm{RFe}^{2+}
\end{cases}
$$

$$U = U_{NH_4^+} + U_{NO_3^-}$$

$$U_{NH_4^+} = k_U \cdot f_U \cdot \left(\frac{I}{I + k_I}\right) \cdot [\text{PHYTO}] \cdot \min\left(\frac{\left[\text{NH}_4^+\right]}{\left[\text{NH}_4^+\right] + k_{NH_4^+}}, \frac{[\text{H}_3\text{PO}_4]}{[\text{H}_3\text{PO}_4] + k_{H_3PO_4}}, \frac{\left[\text{Fe}^{2+}\right]}{[\text{Fe}^{2+}] + k_{Fe^{2+}}}\right)$$

$$U_{NO_3^-} = k_U \cdot f_U \cdot \left(\frac{I}{I + k_I}\right) \cdot [\text{PHYTO}] \cdot \min\left(\frac{\left[\text{NO}_3^-\right]}{\left[\text{NO}_3^-\right] + k_{NO_3^-}} \cdot \frac{k'_{NH_4^+}}{k'_{NH_4^+} + \left[\text{NH}_4^+\right]}, \frac{[\text{H}_3\text{PO}_4]}{[\text{H}_3\text{PO}_4] + k_{H_3PO_4}}, \frac{\left[\text{Fe}^{2+}\right]}{[\text{Fe}^{2+}] + k_{Fe^{2+}}}\right)$$

$$G_{phyto} = k_G \cdot f_G \cdot \left(\frac{\overline{[\text{PHYTO}]}^2}{\mu^2 + \overline{[\text{PHYTO}]}^2 + \omega\overline{[\text{DET}]}^2}\right) \cdot \overline{[\text{ZOO}]}$$

$$L_p = k_{L,phyto} \cdot f_U \cdot \overline{[\text{PHYTO}]}$$

$$G_{det} = k_G \cdot f_G \cdot \left(\frac{\omega\overline{[\text{DET}]}^2}{\mu^2 + \overline{[\text{PHYTO}]}^2 + \omega\overline{[\text{DET}]}^2}\right) \cdot \overline{[\text{ZOO}]}$$

$$L_{zoo} = k_{L,zoo} \cdot f_G \cdot \overline{[\text{ZOO}]}$$

$$L_{zoo,pr} = k_{L,zoo,pr} \cdot f_G \cdot \overline{[\text{ZOO}]}^2$$

$$L_{phyto,zoo} = L_{phyto} + L_{zoo}$$

$$zoo_{exc} = (1 - \zeta - \gamma) \cdot \left(G_{phyto} + G_{det}\right)$$

$$det_{remin} = k_d \cdot f_D \cdot \overline{[\text{DET}]}$$

$$f_i = e^{\beta_i\left(\overline{T} - \overline{T}_0\right)} \quad ; \quad i = U, G, D$$

References

Bougeault, P., Lacarrère, P. (1989) Parametrization of Orography-Induced Turbulence in a Meso-Beta Scale Model. *Monthly Weather Review*, *117*, 1872-1890.

Boudreau, B.P. (1997) *Diagenetic Models and Their Implementation. Modelling Transport and Reactions in Aquatic Sediments.* Springer-Verlag Berlin Heidelberg, Germany.

Bryan, K., Cox, M.D. (1972) An Approximate Equation of State for Numerical Models of Ocean Circulation. *Journal of Physical Oceanography*, Volume 2, 510-514.

Carlson, R.E. (1977) A trophic state index for lakes. *Limnology and Oceanography*, 22:2, 361-369.

Crank, J., Nicolson, P. (1947) A practical method for numerical evaluation of solutions of partial differential equations of the heat conduction type. *Proc. Camb. Phil. Soc.*, 43(1): 5067.

Cummings, N. W. (1926) Evaporation from Lakes. *In partial fulfillment of the requirements for the degree of Doctor of Philosophy*, California Institute of Technology, Pasadena, California.

Denman, K.L., Peña, M.A., Haigh, S.P. (1998) Simulations of Marine Ecosystem Response to Climate Variation with a One Dimensional Coupled Ecosystem/Mixed Layer Model. *Biotic Impacts of Extratropical Climate Change in the Pacific*, Pro-

ceedings ‘Aha Huliko‘a Hawaiian Winter Workshop, University of Hawaii at Manoa, June 25-29, 1998.

Edwards, A. (2001) Adding Detritus to a Nutrient-Phytoplankton-Zooplankton Model: A Dynamical-Systems Approach. *Journal of Plankton Research*, Volume 23, Number 4, pages 389-413.

Ferziger, J.H., Perić, M. (2002) *Computational Methods for Fluid Dynamics. Third, Revised Edition*. Springer-Verlag Berlin Heidelberg New York.

Fiadeiro, M.E., Veronis, G. (1977) On Weighted-Mean Schemes for the Finite-Difference Approximation to the Advection-Diffusion Equation. *Tellus* **29**.

Fossing, H., Berg, P., Thamdrup, B., Rysgaard, S., Sørensen, H.M., Nielson, K. (2004) A model set-up for an oxygen and nutrient flux model for Aarhus Bay (Denmark). National Environment Research Institute, Denmark. 65 pp. - NERI Technical Report No. 483.

Friedrich, H., Levitus, S. (1972) An Approximation to the Equation of State for Sea Water, Suitable for Numerical Ocean Models. *Journal of Physical Oceanography*, Volume 2, 514-517.

Gaspar, P., Grégoris, Y., Lefevre, J-M. (1990) A Simple Eddy Kinetic Energy Model for Simulations of the Oceanic Vertical Mixing: Tests at Station Papa and Long-Term Upper Ocean Study Site. *Journal of Geophysical Research*, 95:179-193.

Gill, A. (1982) *Atmosphere-Ocean Dynamics*. Academy Press, Inc.

Goldman, C.R. (1966) *Primary Productivity in Aquatic Environments. Proceedings of an I.B.P. PF Symposium. Pallanza, Italy, April 26 - May 1, 1965*. University of California Press (Berkeley and Los Angeles).

Harris, G.P. (1986) *Phytoplankton Ecology. Structure, Function and Fluctuation.* Chapman and Hall Ltd.

Holland, H.D. (1984) *The Chemical Evolution of the Atmosphere and Oceans.* Princeton University Press.

Hutchinson, G.E. (1957) *A treatise on limnology, v. 1.* Wiley.

Imberger, J. (1998) *Coastal and Estuarine Studies. Physical Processes in Lakes and Oceans.* American Geophysical Union.

Imboden, D.M., Wüest, A. (1995) Physics and Chemistry of Lakes. Second Edition. *Springer-Verlag*, pp. 83-138 (Mixing Mechanisms in Lakes).

Janssen, P. (2004) *The Interaction of Ocean Waves and Wind.* Cambridge University Press.

Kalff, J. (2002) *Limnology. Inland Water Ecosystems.* Prentice-Hall, Inc.

Kolmogorov, A. N. (1941a) The local structure of turbulence in incompressible viscous fluid for very large Reynolds numbers. *Proceedings of the USSR Academy of Sciences* 30: 299-303. (Russian), translated into English by Kolmogorov, Andrey Nikolaevich (July 8 1991).

— (1941b) Dissipation of energy in locally isotropic turbulence. *Proceedings of the USSR Academy of Sciences* 32: 16-18. (Russian), translated into English by Kolmogorov, Andrey Nikolaevich (July 8 1991).

Kraus, E.B., Businger, J.A. (1994) *Atmosphere-Ocean Interaction. Second Edition.* Oxford University Press, Inc., New York.

Landau, L.D., Lifshitz, E.M. (1986) *Theoretical Physics. Volume 6: Fluid Mechanics.* Pergamon Press.

Lillibridge III, J.L. (1988) Computing the Seawater Expansion Coefficients Directly from the 1980 Equation of State. *Journal of Atmospheric and Oceanic Technology*, Volume 6, 59-66.

Madsen, E.L., Morgan, M.D., Good, R.E. (1986) Simultaneous Photoreduction and Microbial Oxidation of Iron in a Stream in the New Jersey Pinelands. *Limnology and Oceanography*, Volume 31, Number 4, 832-838.

Monin, A.S., Yaglom, A.M. (1971) *Statistical Fluid Mechanics. Volume 1.* MIT Press.

Ockendon, H., Ockendon, J.R. (2004) *Waves and Compressible Flow.* Springer.

Oertel, H. (2004) *Prandtl's Essentials of Fluid Mechanics. Second Edition.* Springer.

Okuda, S., Imberger, J., Kumagai, M. (1995) *Coastal and Estuarine Studies. Physical Processes in a Large Lake: Lake Biwa, Japan.* American Geophysical Union.

Omlin. M., Reichert, P., Forster, R. (2001) Biogeochemical Model of Lake Zürich: Model Equations and Results. *Ecological Modelling*, 141 (2001) 77-103.

Prandtl, L. (1952) *Essentials of Fluid Dynamics With Applications to Hydraulics, Aeronautics, Meteorology and Other Subjects. Authorized Translation.* Hafner Publishing Company, New York.

Reynolds, C.S. (2006) *The Ecology of Phytoplankton.* Cambridge University Press.

Sarmiento, J.L., Gruber, N. (2006) *Ocean Biogeochemical Dynamics.* Princeton University Press.

Schlichting, H. (1979) *Boundary-Layer Theory. Seventh Edition* (translated by Kestin, J). McGraw-Hill, New York.

Shaked, Y., Kustka, A.B., Morel, F.M.M. (2005) A General Kinetic Model for Iron Acquisition by Eukaryotic Phytoplankton. *Limnology and Oceanography*, Volume 50, Number 3, 872-882.

Soetaert, K. (2001) Numerical Modelling of the Shelf Break Ecosystem: Reproducing Benthic and Pelagic Measurements. *Deep-Sea Research Part II*, 48, 3141-3177.

Stumm, W., Morgan J.J. (1996) *Aquatic Chemistry. Chemical Equilibria and Rates in Natural Waters. Third Edition.* John Wiley & Sons, Inc.

— (1990) *Aquatic Chemical Kinetics. Reaction Rates of Processes in Natural Waters.* John Wiley & Sons, Inc.

Therry, G., Lacarrère, P. (1983) Improving the Eddy Kinetic Energy Model for Planetary Boundary Layer Description. *Boundary-Layer Meteorology*, **25** (1983) 63-88.

Toba, Y. (2003) *Ocean-Atmosphere Interactions.* Terra Scientific Publishing Company (TERRAPUB) / Kluwer Academic Publishers.

Van Cappellen, P., Gaillard, J-F., Rabouille, C. (1993) Biogeochemical transformations in sediments: Kinetic models of early diagenesis. *NATO ASI Series*, Vol. 14, 401-445.

Versteeg, H.K., Malalasekera, W. (1995) *An Introduction to Computational Fluid Dynamics. The Finite Volume Method.* Pearson Prentice Hall.

Weiss, R.F. (1970) The solubility of nitrogen, oxygen and argon in water and seawater. *Deep-Sea Research*, Vol. 17, pp. 721-735, Pergamon Press.

Wetzel, R.G. (2001) *Limnology. Lake and River Ecosystems. Third Edition.* Academic Press.

Williams, P.J. le B., Thomas, D.N., Reynolds, C.S. (2002) *Phytoplankton Productivity. Carbon Assimilation in Marine and Freshwater Ecosystems.* Blackwell Science Ltd.

WRIGHT, D.G. (1992) Finite Difference Approximations to the Advection-Diffusion Equations. *Tellus A*, Volume 44, Issue 3, p. 261-269.

YOUNG, A.D. (1989) *Boundary Layers*. BSP Professional Books.